

THE SEARCH FOR PREBIOTIC ORGANIC MOLECULES IN THE OUTER GALAXY

by

SAMANTHA KAJ BLAIR

(Under the Direction of Loris Magnani)

ABSTRACT

This study was conducted to determine the distribution and abundance of two key prebiotic organic molecules, H_2CO and HCN , in outer Galaxy giant molecular clouds. Both H_2CO and HCN most likely played important roles in the formation of amino acids on the early Earth. By determining the distribution of these molecules in the outer Galaxy, the current definition of a Galactic Habitable Zone, the region where conditions are conducive to the formation of life, may be better constrained. We searched for H_2CO in a sample of 69 molecular clouds at distances ranging from 12 to 23.5 kpc from the Galactic Center, and in a subset of these clouds, 46 of 69, we searched for HCN . The H_2CO ($2_{12}-1_{11}$) spectral line at 140.8 GHz was detected in 65% of the clouds, and the HCN ($J=1-0$) spectral line at 88.6 GHz was detected in 67% of the clouds. The H_2CO ($1_{01}-1_{11}$) spectral line at 4.83 GHz and the H_2CO ($3_{12}-2_{11}$) spectral line at 225.6 GHz were also detected towards a subset of the clouds. A multi-transition study was conducted for H_2CO using a statistical equilibrium code in the large velocity gradient (LVG) approximation to better estimate abundances of H_2CO . We conclude that H_2CO and HCN are found readily in the outer Galaxy, and that the widespread distribution of these molecules may indicate that the outer Galaxy could possibly be hospitable to the formation of life

INDEX WORDS: Prebiotic molecules, H₂CO, HCN, Habitable Zone, Molecular Clouds

THE SEARCH FOR PREBIOTIC ORGANIC MOLECULES IN THE OUTER GALAXY

by

SAMANTHA KAJ BLAIR

B.S., Auburn University, 1997

M.S., Auburn University, 2000

A Dissertation Submitted to the Graduate Faculty of The University of Georgia in Partial

Fulfillment of the Requirements for the Degree

DOCTOR OF PHILOSOPHY

ATHENS, GEORGIA

2008

© 2008

Samantha Kaj Blair

All Rights Reserved

THE SEARCH FOR PREBIOTIC ORGANIC MOLECULES IN THE OUTER GALAXY

by

SAMANTHA KAJ BLAIR

Major Professor: Loris Magnani

Committee: Jean-Pierre Caillault
Henning Meyer

Electronic Version Approved:

Maureen Grasso
Dean of the Graduate School
The University of Georgia
December 2008

DEDICATION

To my mother, Eugenia Anne Bates-Yielding, my father, George Blair Jr., my uncle, Bobby Lee Blair, and the Big Guy Upstairs.

ACKNOWLEDGEMENTS

I would like to first thank Dr. Loris Magnani for his leadership, friendship, and for passing his knowledge on to me. He was patient, kind, funny, supportive, inspirational, and really stood up for me when the cards were on the table. I do not think that I could have had a better advisor and friend through these last five years. I would like to thank my parents for their undying support, love, and motivation throughout this whole ordeal.

I would like to thank my committee, Dr. J.P. Caillault and Dr. Henning Meyer, for reading this dissertation and sitting through my defense. I would like to thank Dr. Bill Dennis, Dr. Gary Love, Dr. Howard Lee, Dr. Uwe Happek, and Dr. Steven Lewis for their patient tutelage, without which I could not have succeeded.

Thanks to Jan Brand and Jan Wouterloot for collaborating with us, providing technical insight, and for the 225.6 GHz H₂CO observational data.

To Roger Lugo, thanks for pushing me in the right direction and for believing in me. I would like to thank Jason Perry, a dear friend who was there for me whenever I needed it. Thanks also to Sarah Dunning for inspirational posters and small gestures of kindness to keep me going.

This project would not have been possible without support from NASA grant NNG05GQ21G. I would like to thank Dr. Lucy Ziurys and the Arizona Radio Observatory staff, especially Sean Keel, for their assistance during the course of the 140.8 GHz H₂CO and HCN observations. I would finally like to acknowledge the Arecibo Radio Telescope for providing telescope time for our 4.85 GHz H₂CO observations.

TABLE OF CONTENTS

	Page
ACKNOWLEDGEMENTS	v
LIST OF TABLES.....	vii
LIST OF FIGURES.....	ix
CHAPTER	
1 INTRODUCTION.....	1
1.1 Background and History of the Search for Life in the Galaxy	1
1.2 Building Blocks of Life	9
1.3 Molecular Clouds	10
1.4 Outline of Dissertation.....	18
2 THE OUTER GALAXY AND THE FAR OUTER GALAXY	19
2.1 The Molecular Cloud Distribution in the Outer Galaxy.....	19
2.2 Metallicity in the Outer Galaxy.....	31
3 BASIC BIOLOGY	38
3.1 The Basic Building Blocks of Life.....	38
3.2 Sugars	43
3.3 The Importance of H ₂ CO and HCN Observations	44
4 OBSERVATIONS.....	50
4.1 Review of Previous of H ₂ CO and HCN	50

4.2	The Excitation of H ₂ CO.....	51
4.3	The H ₂ CO Observations	56
4.4	The Excitation of HCN.....	73
4.5	The HCN Observations.....	73
4.6	Correlation Between H ₂ CO and HCN in the Outer Galaxy.....	78
5	THE H ₂ CO AND HCN ANALYSES.....	83
5.1	Derivation and Calculation of the Column Density of the H ₂ CO Transitions..	83
5.2	The Total Column Density of H ₂ CO using Simplistic Assumptions	89
5.3	The Total Column Density of HCN using Simplistic Assumptions	90
5.4	Large Velocity Gradient Code Abundance Calculations for H ₂ CO.....	100
6	CONCLUSIONS AND FUTURE WORK.....	108
	REFERENCES.....	111
	APPENDICES	120
A	SPECTRA OF H ₂ CO OBSERVATIONS	120
B	SPECTRA OF HCN OBSERVATIONS.....	151

LIST OF TABLES

	Page
Table 2-1: Abundance gradient calculations from various studies.....	33
Table 2-2: Comparison of chemical abundances of C, O, and N in at different distances from the Galactic Center.....	37
Table 4-1: Observations at 140.8 GHz of Outer Galaxy Giant Molecular Clouds.....	58
Table 4-2: H ₂ CO (1 ₁₁ -1 ₁₀) Observations at 4.83 GHz of Outer Galaxy Giant Molecular Clouds.....	67
Table 4-3: H ₂ CO (3 ₁₂ -2 ₁₁) Observations at 225.6 GHz of Outer Galaxy Giant Molecular Clouds.....	70
Table 4-4: Molecular clouds with more than one H ₂ CO transition observed.....	72
Table 4-5: HCN (1-0) Observations of Outer Galaxy Giant Molecular Clouds.....	76
Table 5-1: Calculation of column density of the 4.83 GHz line of H ₂ CO in units of cm ⁻²	86
Table 5-2: Column density values for the 140.8 GHz transition of H ₂ CO.....	86
Table 5-3: Calculation of column density of the 225.6 GHz line of H ₂ CO in units of cm ⁻²	88
Table 5-4: Total H ₂ CO column density values using the 140.8 GHz transition.....	91
Table 5-5: Fractional abundance of H ₂ CO to H ₂ in outer Galaxy GMCs.....	93
Table 5-6: Column density values for the 88.6 GHz transition of HCN.....	95
Table 5-7: Total HCN column density values using the 88.6 GHz transition.....	96
Table 5-8: Fractional abundance of HCN to H ₂ in outer Galaxy GMCs.....	98

LIST OF FIGURES

	Page
Figure 1-1: Galactic distribution of H ₂ (solid line) and HI (dashed line) as a function of galactocentric distance.	4
Figure 1-2: Distribution of dark clouds in the galaxy from a study of photographic plates by Lundmark (1926).....	16
Figure 2-1: Spiral arms of the Milky Way Galaxy.	20
Figure 2-2: Distribution of molecular clouds from three CO (1-0) surveys.	23
Figure 3-1: The twenty standard amino acids.	40
Figure 4-1: Structure of the H ₂ CO molecule adapted from Rohlfs and Wilson (2006).....	53
Figure 4-2: Diagram of energy levels in formaldehyde; adapted from Rohlfs and Wilson (2006).....	54
Figure 4-3: Histogram of the galactocentric distribution of the observed clouds.	60
Figure 4-4: Diagram of all sources observed at 140.8 GHz.....	61
Figure 4-5: Diagram of all sources observed at 140.8 GHz.....	62
Figure 4-6: Typical spectrum for the H ₂ CO (2 ₁₂ -1 ₁₁) transition.....	64
Figure 4-7: Histogram of observations at 140.8 GHz in terms of Galactic longitude.....	66
Figure 4-8: Typical spectrum of H ₂ CO (1 ₁₁ -1 ₁₀) line.....	68
Figure 4-9: Typical spectrum for the H ₂ CO (3 ₁₂ -2 ₁₁) 225.6 GHz line.....	71
Figure 4-10: The structure of HCN.....	74

Figure 4-11: Energy level diagram showing the hyperfine splitting of the HCN J=1-0
Transition.....75

Figure 4-12: Diagram of all sources observed in the HCN (1-0) transition at 88.6 GHz..... 79

Figure 4-13: Typical HCN (1-0) spectra..... 80

Figure 4-14: The correlation between W(HCN) and W(H₂CO)..... 81

Figure 5-1: LVG model calculations of line strength ratios at different molecular gas densities
compared to measured values for sources detected in both the 4.83 GHz and the 140.8
GHz line at a temperature of 10 K and velocity gradient of 5 km/s/pc. 104

Figure 5-2: 2 LVG model calculations of line strength ratios at different molecular gas densities
compared to measured values for sources detected in both the 4.83 GHz and the 140.8
GHz line at a temperature of 20 K and a velocity gradient of 5 km/s/pc..... 105

Figure 5-3: 3 LVG model calculations of line strength ratios at different molecular gas densities
compared to measured values for sources detected in both the 4.83 GHz and the 140.8
GHz line at a temperature of 10 K and a velocity gradient of 2 km/s/pc..... 106

Figure 5-4: LVG model calculations of line strength ratios at different molecular gas densities
compared to measured values for sources detected in both the 4.83 GHz and the 140.8
GHz line at a temperature of 20 K and a velocity gradient of 2 km/s/pc..... 107

CHAPTER 1

INTRODUCTION

1.1 BACKGROUND AND HISTORY OF THE SEARCH FOR LIFE IN THE GALAXY

A question that man has asked repeatedly throughout the ages has been ‘are we alone in the cosmos?’ Technological advances in multi-wavelength astronomical techniques during the last three decades have allowed scientists to address this question systematically. We now know what the basic structure of the Galaxy is and have identified virtually all the baryonic component. This has allowed us to identify regions suitable for life as we know it (the region at the Sun’s distance from the Galactic Center), and regions not so suitable for life (the Galactic Center).

The search for life in the universe has taken many forms over the years. In the 1960’s, Frank Drake was the first scientist to search for extraterrestrial life using radio astronomy (www.setileague.org). In 1961, he developed the Drake Equation that estimates how many intelligent civilizations could potentially exist in our galaxy. The equation is written as

$$N = R^* \times f_p \times n_e \times f_l \times f_i \times f_c \times L$$

where N is the number of intelligent civilizations, R^* is the average rate of star formation in the galaxy, f_p is the fraction of stars that have planets, n_e is the average number of planets that could support life per star that has planets, f_l is the fraction of planets that actually develop life, f_i is the fraction of planets that develop intelligent life, f_c is the fraction of civilizations that develop the ability to communicate via detectable signals, and L is the length of time it takes for the

intelligent civilizations to develop sufficiently to send signals into space (www.setileague.org). Because of the great uncertainty in many of these parameters, the Drake equation can be considered primarily an organizational tool to focus our attention on what questions need to be addressed if we are to determine how prevalent intelligent life is in the Galaxy. Given the original parameters Drake used in his calculation, he estimated that there are about 10 intelligent civilizations in our Galaxy. Others have used different assumptions for parameters like R^* and L , and have estimated that there could be anywhere from a few to 5,000 intelligent civilizations in our galaxy (www.seti.org). The SETI (Search for Extraterrestrial Intelligence) Institute in Mountain View, California was created in 1984 to continue searching for signs of intelligent civilizations, and is still actively pursuing this objective.

In recent years, the new interdisciplinary science of astrobiology has attempted to address some of the issues raised by Frank Drake and systematically study the origin, development and distribution of life in the Galaxy. The Galaxy, which has a diameter of 50 kpc and a mass of 10^{12} solar masses¹, is divided into the Galactic Bulge that contains the Galactic Center, the disk, which is subdivided into the Young disk, the Intermediate disk, and the Old disk, the Halo, and the Spiral arm region (Elmegreen 1998).

The Galactic Bulge and the Halo contain spherically distributed Population II stars (older, metal-poor stars)² in globular clusters and as variable RR Lyrae stars, with the stars in the Halo having a lower metallicity than those in the Galactic Bulge. The Galactic bulge has a scale height of roughly 2 kpc and diameter of about 4 kpc, while the Halo has a scale height of greater than 2 kpc and a diameter of up to 200 kpc (Elmegreen 1998).

¹1 solar mass is equal to 2×10^{33} grams.

²Astronomers refer to all elements beyond helium as “metals.” “Metallicity” is the abundance of metals with respect to hydrogen.

The entire disk has a diameter of 50 kpc and has a scale height ranging from 0.3 to 0.6 kpc thick. The Young disk, scale height 0.2 kpc, is composed of Population I stars (younger, metal-rich) that have spectral types³ A-FV and A-KIII. The Intermediate disk, scale height of 0.4 kpc, has Population I stars which includes our Sun in addition to spectral types like GKMV and PN⁴ stars. Finally, the Old disk, scale height of 0.7 kpc, contains Population I K-MV stars, subgiants (II), red giants (III), long-period variables and RR Lyraes (Elmegreen 1998).

The Spiral arm regions have scale heights of 0.12 kpc and contain significant quantities of gas and dust as well as Population I stars, open clusters, Type I Cepheid variables and variable T Tauri stars (Elmegreen 1998).

The Galactic Bulge and Halo are virtually gas and dust free, while the other regions of the Galaxy, including the Galactic Center, contain both components. Figure 1-1 below illustrates the distribution of molecular gas, H₂ (solid line) versus atomic gas HI (dotted line) from the Galactic Center out to galactocentric distance $R_G = 14$ kpc. At the Galactic Center the H₂ surface density is the highest at $150 M_\odot/\text{pc}^2$ and then drops off dramatically at around $R_g = 1$ kpc. The H₂ then begins to increase at $R_G = 4 - 5$ kpc to $10 M_\odot/\text{pc}^2$ in the region known as the Molecular Ring. From 5 kpc out to the edge of the Galaxy, H₂ gradually declines to levels just above a few tenths M_\odot/pc^2 . In contrast, the atomic gas follows a much different distribution. The surface density of HI at $R_G = 1$ kpc from the Galactic Center is a little greater than a few tenths M_\odot/pc^2 , and steadily increases to roughly $2.5 M_\odot/\text{pc}^2$ between 3 and 4 kpc. Around the Solar Circle, HI increases to about $3 M_\odot/\text{pc}^2$ and levels off out to greater than $R_G = 14$ kpc. (Scoville 1987).

³A spectral type is a classification scheme used to identify stars based on their spectra where the letter (OBAFGKM) represents where the star is on the main sequence early-type for O and late-type for M. Each category is further subdivided into luminosity classes I-V representing stars at different stages of evolution.

⁴ PN stars are the central stars in Planetary Nebulae.

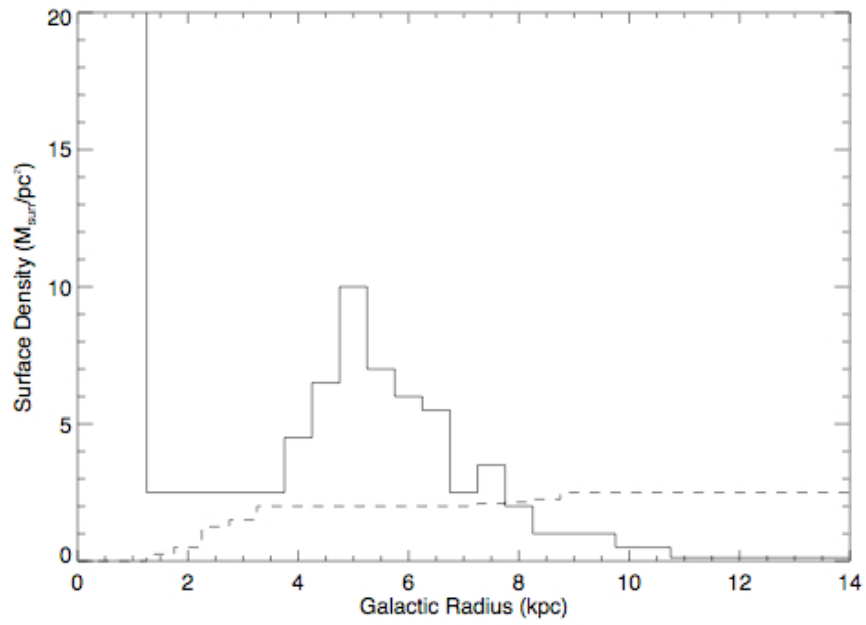


Figure 1-1 Galactic distribution of H₂ (solid line) and HI (dashed line) as a function of galactocentric distance. The y-axis is the mass surface density in units of solar masses per square parsec. Adapted from Scoville (1987).

With this knowledge of the distribution of stars and gas in the Galaxy, the question of which regions would be most suitable for life can be addressed. Balazs (1986), assumed that the passage of a star system containing an advanced civilization through the dense environment of a spiral arm would be deadly to higher lifeforms because of higher radiation fields and supernovae. Thus, according to Balazs, favorable Galactic environments for the formation of long-lived civilizations would preclude the passage of the system through spiral arms. With this criterion he developed a definition for the region of the Galaxy suitable for the development of intelligent life. Using the density wave theory of C.C. Lin (Lin and Shu 1964) to predict the motion of the spiral arm pattern, he proposed that the “belt of intelligent life” was located along the co-rotation circle, the region where the angular velocity of the Galactic disk is equal to that of the density wave rotation. This co-rotation circle includes our Sun. An object in the co-rotation circle would not move through a spiral arm. Thus, Balazs used parameters like pitch angle and angular velocity of the spiral pattern to suggest that the belt was an annulus about 0.5 kpc thick in the radial direction at a distance of 8.0 kpc from the Galactic center (Balazs 1986).

The “belt of life” concept was further explored by Marochnik and Mukhin (1988), where they estimated the number of potential technological civilizations in the Galaxy. They developed the idea of a Galactic anthropic principle that stated that civilizations like ours could only form in “belts of life,” effectively Galactic Habitable Zones. Like Balazs, they estimated that the lifetime of a civilization is dictated by the length of time the solar system spends between spiral arms, on the order of 4.6×10^9 years (Marochnik and Mukhin 1988). The authors postulated that the corotation ring zone thickness is on the order of 0.3 kpc, presumably with the Sun at the midpoint of the ring at 8.5 kpc from the Galactic center. They speculated that the ratio of the number of “upper-level” civilizations (i.e., similar to ours) to “lower-level” or less advanced

civilizations, to be on the order of 0.7 based on probabilities of the number of stars with planetary systems in the co-rotation zone, and the lifetimes of solar systems with intelligent life. They conclude that our presence was probably an accident of Nature (Marochnik and Mukhin 1988).

In addition to the search for intelligent life, the search for signs of less complex life forms is also important, though tremendously more difficult to detect on a Galactic scale. The concept of a galactic habitable zone for intelligent life can be extended to lower life forms to address which regions of the Galaxy are potentially habitable, in general.

In contrast to the Galactic habitable zones, there are a number of “dead zones” in the Galaxy and more broadly in the Universe that are strictly unfavorable for the formation of life (Brownlee and Ward 2000). Metal poor regions like globular clusters, the Galactic bulge, small galaxies and elliptical galaxies are not favorable for terrestrial planet formation and regions like the centers of galaxies are too energetic for life as we know it to emerge. Solar systems that contain hot Jupiters, or Jupiter size planets in highly eccentric orbits, prove to be too unstable for the formation of Earth-like terrestrial planets. Conversely, a number of regions have been delineated that may have the capacity to harbor life. Brownlee and Ward (2000) defined the habitable zone (HZ) around a given star as the region in a planetary system where Earth-like planets may exist. It is the region where the central star can maintain a surface temperature suitable for water to remain liquid. This definition was first introduced in the late 1950’s as the Circumstellar Habitable Zone (CHZ) (Gonzalez et al. 2001), and was expanded upon as climate models were improved (Kasting 1993). The concept uses the Earth as a baseline for other regions of the Galaxy, but introduces problems like the need for advanced plant life for efficient chemical weathering (a cooling effect), a factor that influences the width of the CHZ. James Kasting

redefined the HZ as “the region around a star in which an Earth-like planet (of comparable mass) and having an atmosphere containing nitrogen, water and carbon dioxide is climatically suitable for surface dwelling, water-dependent life” and they surmise that the zone lies between 0.95 and 1.15 AU from the Sun (Kasting 1993). The HZ can also be divided into the animal habitable zone (AHZ) and the microbial habitable zone (MHZ). With the discovery of extremophiles, the MHZ is certainly a broader region than the AHZ, both spatially and temporally. The MHZ extends to the edge of the solar system while the AHZ is confined to the region containing Earth. The MHZ temporally ranges from planet formation to present day while the AHZ is restricted to the biological evolutionary time scale, on the order of a few billion years (Brownlee and Ward 2000).

Around the Sun, there are several regions that may be suitable for the formation of life. One of the criteria for harboring life is the presence of liquid water and another is the availability of the raw materials for life, namely organic compounds. Mars is a good candidate in that it has frozen water and there is evidence that water has flowed on the surface in the past. Because Mars may have been warmer, wetter, and had a thicker atmosphere in the past, life may have formed on the surface and then perhaps moved subsurface (Bibring 2005, Weiss et al. 2000). One of the goals of any mission to Mars would be to look for biomarkers, traces of biogenic material like lipids (molecules, like steroids, that are insoluble in water but soluble in organic solvents), on the surface. The recent successful landing of the Phoenix Mars Lander, which contains several instruments for measuring biosignatures, will hopefully answer some of our queries about the existence of past or present life on Mars.

One of Jupiter’s moons, Europa, is also thought to have a liquid water ocean beneath the icy surface layer. It is suspected that there may be enough energy from tidal flexing to supply

sufficient heat to support at least microbial life. Another necessary component for life would be raw materials like organic compounds. Titan, the largest moon of Saturn, has a thick atmosphere with an abundance of hydrocarbons and large pools of hydrocarbon sludge on the surface. These examples illustrate the fact that we may have other favorable environments for life in our own solar neighborhood that differ significantly from the Earth's environment.

Extending these ideas to the Galaxy leads to the concept of the Galactic Habitable Zone (GHZ). This idea, pioneered by Balazs, Marochnik and Mukhin and called the "belt of life", was described earlier and represents a broader variation on the themes described above (Balazs 1987, Marochnik and Mukhin 1988). Gonzalez, Brownlee, and Ward (2001) defined the GHZ as "the region in the Milky Way where an Earth-like planet can retain liquid water on its surface and provide a long-term habitat for animal-like aerobic life." No longer focusing exclusively on intelligent life, Gonzalez, Brownlee, and Ward (2001) examined where in the Galaxy the metallicity, supernova frequency, and stellar lifetimes conspire to produce a favorable environment for the formation of complex multi-cellular life. They approximated that to form a habitable terrestrial planet, a star would need a metallicity of at least half of that of the Sun. They also stressed the importance of long-lived radioisotopes like ^{40}K , ^{235}U , ^{238}U , and ^{232}Th as sources of radiogenic heating that helps to stabilize a habitable climate through the carbon cycle⁵. They determined that the thin disk region of the Galaxy is the most likely region for Earth-like planets to form because the inner disk planets would be too large given the higher metallicity, and the outer disk planets too small as the metallicity decreases with increasing distance from the Galactic Center. These authors also determined the GHZ – at the current time

⁵The carbon cycle is the biogeochemical cycle where carbon is exchanged between the biosphere, geosphere, hydrosphere, and atmosphere of Earth (<http://earthobservatory.nasa.gov/Features/CarbonCycle/>).

– to be a narrow annulus at approximately the Sun’s galactocentric distance 8.5 kpc⁶. Finally, Lineweaver, Fenner, and Gibson (2004) modeled the above astrophysical parameters and included considerations on the timescale for the development of life, 3-4 Gyr, to conclude that the GHZ is 7 – 9 kpc from the Galactic center and widening with time. It is somewhat striking, in an echo of pre-Copernican thought, that these early attempts at determining the Galaxy’s GHZ always place the Sun squarely in the middle of the habitable region.

In an effort to explore and further constrain the definition of the GHZ proposed by Gonzalez, Brownlee and Ward, we conducted a survey of H₂CO and HCN, key building blocks of life, in Giant Molecular Clouds in the Outer Galaxy at $R_g > 16$ kpc. We believe that the regions of the outer Galaxy are favorable for the formation of life and will elaborate on this theme throughout this thesis. We now discuss the building blocks of life and the distribution of molecular clouds in the Galaxy.

1.2 BUILDING BLOCKS OF LIFE

Living systems are comprised of organic molecules; thus, for life to develop, these molecules, or constituents thereof, must be available in the environment. If organic molecules are not present in the environment *ab initio*, then they must either be manufactured or brought in from regions where they are present. Organic molecules are used to produce the primary building blocks of life: amino acids. The 20 proteinogenic amino acids are necessary for the synthesis of proteins, molecules without which life as we understand it would not be possible. Other important biological molecules are: DNA and RNA, deoxyribonucleic acid and ribonucleic acid, respectively, which contain the genetic code; carbohydrates which are built of sugars and

⁶The authors originally used a galactocentric distance R_G for the Sun of 10 kpc. However, the IAU recommended that $R_g \approx 8.5$ kpc be adopted.

provide energy; and the lipids like fats and oils to name a few, that are components of biological membranes. A more detailed explanation of the functions of the various biological molecules will be provided in chapter 3.

In the 1950's, Stanley Miller demonstrated that reactions in a mixture of CH_4 , NH_3 , H_2O , and H_2 gases subjected to electrical discharge produced amino acids, aldehydes, and various other organic compounds (Miller 1953, Miller 1955). Specifically, the simplest amino acid, glycine, can be formed from a reaction of H_2CO with NH_3 and HCN (Oro 1959, Miller 1992). Moreover, molecules like DNA and RNA are composed of several molecular components like sugars, and sugars can be synthesized from smaller molecules like H_2CO . To date, over 130 molecules have been identified in both the interstellar medium and in circumstellar disks around newly formed stars, and many of these are organic molecules including H_2CO and HCN (Thaddeus 2006). Interstellar clouds thus contain the organic molecules necessary for the chemical evolution of life. However, given the radial metallicity gradient in the Galaxy, it is very likely that the molecular abundances will vary significantly from the Galactic Center to the edge of the molecular disk.

1.3 MOLECULAR CLOUDS

The Interstellar Medium (ISM) is defined as the gas and dust that permeates the regions between the stars. Stars are both formed from and replenish this material through stellar wind, planetary nebulae, and supernovae. The gas and dust in the ISM are well mixed and the gas-to-dust ratio by mass is typically 100 in our Galaxy. The gas, by mass, is primarily neutral and can take atomic or molecular forms. The atomic gas can be in very different temperature and density regimes called phases (Cox 2005). These phases are mostly in pressure equilibrium with each

other and form a widespread layer within which the stars and the molecular gas are contained. The molecular gas behaves very differently from the atomic gas (HI⁷). Instead of being distributed in widespread fashion throughout the Galactic disk, the molecular gas is concentrated into discrete entities whimsically referred to as “clouds”.

Molecular clouds in general can be divided into large and small entities by mass. The large clouds are known as Giant Molecular Clouds (GMCs). GMCs have been studied primarily by observing them in the CO (J=1-0) transition at 115 GHz and their large scale distribution has been established by Galactic plane surveys (Blitz 1990). GMCs are typically not observed in H₂ because it has no dipole moment and a small moment of inertia. The lack of dipole rotational or vibrational transitions causes the opacity of the H₂ lines to be small, and the small moment of inertia leads to widely spaced rotational levels that are rarely excited (Lacy et al. 1994). GMCs are some of the largest objects in the Galaxy with dimensions up to 50 pc, masses from 10³ – 10⁶ M_⊙, temperatures around 10 K in regions not actively forming stars, and average densities of order 10² cm⁻³ (Goldsmith 1987). GMCs contain most of the molecular gas mass of the Galaxy, they are the primary star forming clouds, and almost always have clusters of OB stars associated with them (Blitz 1991). However, the properties of GMCs vary depending on their location in the Galaxy, a topic that will be discussed in Chapter 2.

Early CO surveys revealed that the dense molecular gas in the inner Galaxy was located in the “molecular ring”, an annulus between 4 and 8 kpc if one uses a solar distance, R_o, of 10 kpc from the Galactic center (Blitz 1991). With the currently accepted value of R_o, ~8.5 kpc, the molecular ring is at 3.5-7 kpc. Three later molecular cloud surveys gave the most extensive information on the distribution of GMCs to date: the Massachusetts-Stony Brook survey, the

⁷HI, or atomic hydrogen, produces the 21cm line during the spin-flip transition. For the distribution of Galactic HI, see figure 1.

Columbia-Cerro Tololo survey, and the Bell Laboratories survey (Friberg and Hjalmarson 1990, Dame et al. 1987, Stark et al. 1988). The Massachusetts-Stony Brook survey was designed to detect all clouds of size >20 pc inside the Solar Circle. The survey contains 40,000 CO spectra from Galactic longitude 8° to 90° and latitude -1° to $+1^\circ$. This survey identified a spiral arm population of clouds associated with HII regions that have temperatures >10 K which suggested that the HII regions⁸ are typically associated with the larger and warmer molecular clouds (Friberg and Hjalmarson 1990).

The Columbia-Cerro Tololo survey focused on massive clouds and cloud complexes, and contains 31,000 CO spectra along the entire Galactic plane between latitudes 10° and 30° (Dame et al. 1987). The survey outlined the Sagittarius spiral arm. The Columbia-Cerro Tololo group moved to Harvard in the late 80's and continued improving their survey. The most recent survey by Dame et al. (2001) corroborated the data from the Massachusetts-Stony Brook survey finding that the HII regions were associated with larger mass clouds. Dame et. al. (2001) also identified 17 large complexes, collected more spectra (488,000), has greater resolution (3.4 times higher), and greater sensitivity (10 times higher per unit solid angle) than the Dame et al. (1987) survey. This survey resolved the molecular Galaxy into hundreds of GMC's located predominately along the spiral arms. The authors verified that the CO-to-H₂ mass conversion factor was comparable to that calculated for the whole Galaxy by comparing the observed CO map with the predicted molecular map (Dame et al. 2001).

The Bell laboratories survey is comprised of more than 70,000 ¹³CO spectra and 4,000 CO spectra and covers longitudes of -5° to 120° and latitudes -1° to 1° . This study was designed to search for clouds in the first quadrant ($0^\circ < l < 90^\circ$) with masses $>10^3 M_\odot$. Stark et. al. (1987)

⁸HII regions are ionized regions of hydrogen around early-type stars. HII regions are typically a few pcs in size and have temperatures of $\sim 10^4$ K.

determined that there are large areas devoid of GMCs, presumably interarm regions, an observation also recorded in the Columbia survey. Within these voids, the Bell laboratories survey detected a population of smaller molecular clouds (Friberg and Hjalmarson 1990).

Several other important results emerged from these surveys regarding physical parameters of GMCs and molecular clouds in general (Friberg and Hjalmarson 1990). The sizes range from a few pc in single small clouds to > 100 pc in the complexes. The bulk of the Galactic molecular mass ($\sim 90\%$) is in 5,000 GMCs with masses $> 10^5 M_{\odot}$ and sizes greater than 20 pc. A subset of those clouds (~ 1000) contain 50% of the molecular mass and have masses $> 10^6 M_{\odot}$ and sizes > 50 pc. With a few exceptions, most of the molecular clouds have an average temperature of 10 – 15 K, which is a result of a balance between heating by cosmic rays and radiative cooling from molecules. This type of cooling by molecules occurs as molecules become excited by collisions with H_2 ; these molecules then de-excite and emit radiation that escapes the cloud. The CO (1-0) and CO (2-1) lines are the principal coolants of molecular clouds. The cloud temperature can be determined from the brightness temperature of the CO emission. The lower rotational energy levels of CO are optically thick and are readily excited by collisions with H_2 . Under those conditions, the CO lines are thermalized and the kinetic temperature of the cloud is directly related to excitation temperature of the CO. A limiting factor with this kind of measurement is that the large optical depth of the CO lines will prevent measurement of cloud interiors. A molecule with optically thin transitions like NH_3 , can be used to measure the interior cloud temperatures because it is less abundant and not as easily excited as CO. The population distribution temperature of NH_3 can be acquired through comparison of column densities of different rotational transitions (Friberg and Hjalmarson 1990).

Molecular clouds are near virial equilibrium⁹ and are therefore bound through self-gravitation, not external pressure. Evidence for this conclusion presents itself in both the congruity of virial mass estimates and the empirical relationship discovered between the line widths (velocity dispersion, Δv) and the cloud diameter (D) as a result of the surveys. The relationship shows that $\Delta v \propto D^{1/2}$, which is consistent with the $M \propto D(\Delta v)^2$ condition for virial equilibrium (Friberg and Hjalmarson 1990).

The evolution of gravitationally bound clouds has yet to be understood. In the beginning, the assumption was that clouds evolved on free fall timescales (the amount of time it would take for a body to collapse under its own gravitational force), but that does not appear to be the case. This is because of the discrepancy between the actual rate of star formation, 3-100 M_{\odot}/yr and the rate that we should observe if the clouds were evolving on free fall time scales, 500 M_{\odot}/yr (Friberg and Hjalmarson 1990). Cloud rotation, stellar winds, supersonic turbulence and magnetic fields have all been suggested as mechanisms to support clouds and thus explain the disparity in the rates (Friberg and Hjalmarson 1990).

Not all molecular clouds in the Galaxy are GMCs. Small clouds (i.e., those entities with $M < 10^3 M_{\odot}$) can be divided into three categories based on extinction properties: diffuse, $A_v < 1$; translucent, $1 < A_v < 5$; and dark, $A_v \geq 5$ (Van Dishoeck et al. 1993). Diffuse clouds are optically transparent, primarily atomic (predominately HI with low molecular abundance) clouds with temperatures of roughly 100 K and densities of order 10 cm^{-3} . They are a few parsecs or less in size, have masses up to a few hundred M_{\odot} , and are distributed vertically to within 100 pc of the disk midplane (Elmegreen 1998).

⁹ Virial equilibrium is the condition for gravitationally bound systems where the total energy is equal to half of the time-averaged potential energy.

Translucent clouds are compositionally closer to the dark clouds but are not necessarily gravitationally bound like the latter. Translucent clouds have masses of hundreds of M_{\odot} , are a few pc in size and have been found primarily at high latitudes $|b| \geq 25^{\circ}$ (Magnani et al. 1985).

Dark clouds are compositionally complex and optically opaque, and most of their gas is in molecular form. They have masses of tens to hundreds of M_{\odot} , and individual clouds can be a few parsecs or less in size. Complexes of many small dark clouds can span tens of parsecs (i.e., the Taurus dark clouds). The smallest dark clouds, Bok globules, are dense spherical structures that have masses of about $10 M_{\odot}$ and sizes that are less than a parsec. These tiny clouds are active sites of star formation, although primarily of the low mass type (Elmegreen 1998). The search for dark clouds began in the early 20th century by Barnard (1919) and in 1927, he published a photographic study of dark nebulae identifying 182 objects. At that time, they were not known or suspected to contain molecular gas. Concurrently, Lundmark (1926) used photographic plates taken by the Franklin-Adams 1911 sky survey to identify 1550 dark nebulae (see figure 1-2). In 1962, Beverly T. Lynds conducted a complete survey of all of the dark clouds (1801 objects), in the northern hemisphere using the Palomar Observatory Sky Survey. Similar studies of the southern hemisphere were conducted by Feitzinger and Stuewe (1984), and Hartley et al. (1986), where the latter used European Southern observatory plates.

The astrochemistry of the various cloud types is a result of different processes. Diffuse cloud astrochemistry is regulated primarily by photoprocesses that result in relatively low molecular abundances. Dark cloud chemistry is predominately collisional in nature thus various molecular species have higher abundances. For example, in diffuse clouds, the CO/H₂ ratio is $< 10^{-6}$ while in dark clouds it is $< 10^{-4}$. Translucent cloud chemistry is a result of both photoprocesses and

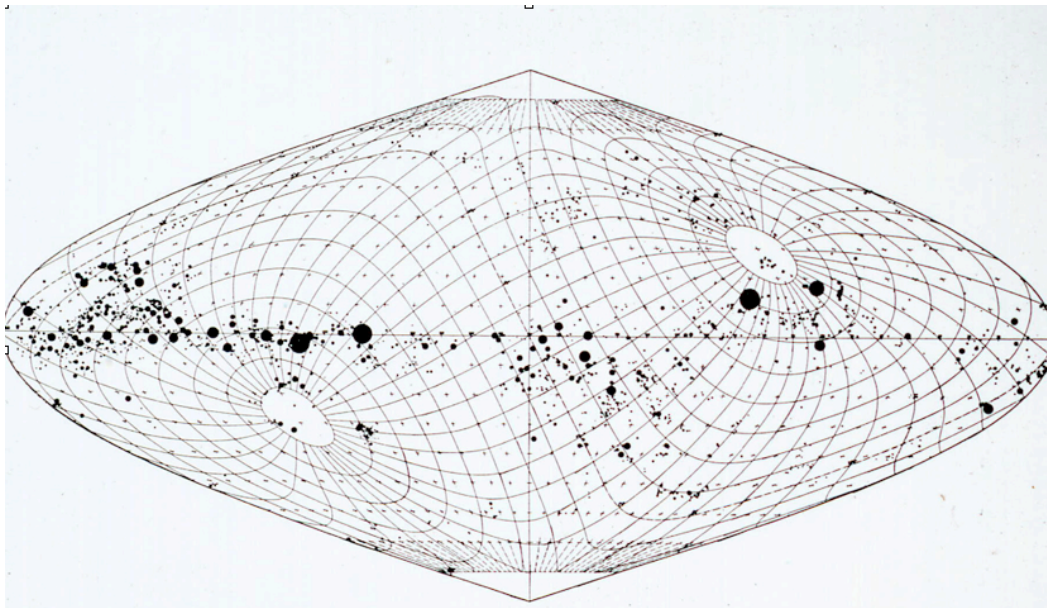


Figure 1-2 Distribution of dark clouds in the galaxy from a study of photographic plates by Lundmark (1926).

collisional reactions, hence they are considered transition objects between diffuse and dark clouds.

What kinds of molecules are present in molecular clouds? Dark clouds are rich in numerous organic and inorganic compounds. Some clouds like TMC-1, a dark cloud in the Taurus region, are enriched in unsaturated carbon chain compounds (C_2H , C_4H , and so on) compared with other molecular clouds with similar physical conditions, i.e. L134N. The reason for the compositional difference between TMC-1 and L134N is not well understood. GMCs and dark clouds are similar compositionally at least for the quiet areas of the GMC not actively forming stars. The regions in the GMC near stars however, are enriched in CH_3OH , H_2O and NH_3 , presumably because these species evaporate off of the grain surfaces readily in the warmer environment. Moreover, the chemistry becomes richer as the warmer environment allows previously forbidden endothermic reactions to proceed (Friberg and Hjalmanson 1990). The dense cores in GMCs have very large column densities along the line of sight and contain a cornucopia of molecular species¹⁰ including many organic species. Thus, molecular clouds contain many organic molecules, so they can “jump start” the formation of life by seeding the stellar systems forming within them with organic molecules.

The information on molecular clouds described above has been gathered over the last 4 decades. We know the distribution and abundances of molecular gas at the Galactic Center, The Inner Galaxy, the solar vicinity and out to the Perseus arm very well. However, there is one of the Galaxy that is still somewhat unexplored; the Outer Galaxy. Do molecular clouds out

¹⁰<http://www.cv.nrao.edu/~awootten/allmols.html>

there have sufficient abundances of molecules of biological significance to constitute a favorable region for the formation of life?

1.4 OUTLINE OF DISSERTATION

This dissertation presents the results of a study designed to explore the distribution and abundance of two important prebiotic precursor molecules, H_2CO and HCN , in the Far Outer Galaxy (i.e., those regions at a galactocentric distance $R_G > 16$ kpc). Chapter 2 will focus on the outer Galaxy, specifically the Far Outer Galaxy (FOG), and will compare properties of the molecular clouds in the FOG with those of the inner Galaxy including overall environment, metallicity, and basic GMC properties. The biological relevance of this study will be discussed in Chapter 3. The observational techniques used to gather the spectroscopic data for this study along with the data itself are presented in Chapter 4. Analysis of H_2CO abundance will be discussed in Chapter 5, and both a rough estimate and a more refined abundance determination using a Large Velocity Gradient statistical equilibrium code will be presented. The HCN analysis is also described in Chapter 5, along with an approximate determination of the abundance of this molecule. Finally, Chapter 6 will present conclusions and will discuss the direction of future work.

CHAPTER 2

THE OUTER GALAXY AND THE FAR OUTER GALAXY

2.1 THE MOLECULAR CLOUD DISTRIBUTION IN THE OUTER GALAXY

The outer Galaxy is a very different environment from the inner Galaxy. The outer Galaxy begins immediately beyond the Solar Circle, the imaginary circle with the distance of the Sun from the Galactic Center as radius, commonly denoted as R_0 . In 1985, the International Astronomical Union recommended that a value of 8.5 kpc be adopted for R_0 (Kerr and Lynden-Bell, 1986), although more recent work (Vallee 2005, and references therein) points to $R_0 \approx 7.9$ kpc as a more accurate value. In this thesis, we will retain $R_0 = 8.5$ kpc as the value for the distance of the Solar Circle from the Galactic Center. For this thesis, the “far outer Galaxy” is defined as the region beyond 16 kpc. At least two spiral arms are located beyond the Solar Circle, the Perseus spiral arm at ~ 9 -10 kpc from the Galactic Center in the first and second quadrant and the Outer or Cygnus arm at and beyond 12 kpc. Figure 2-1 presents a recent depiction of the Galactic spiral arms. Various surveys of the molecular material in the outer Galaxy have been carried out (Kutner and Mead 1981, Mead and Kutner 1988, Wouterloot and Brand 1989, Sodroski 1991, Digel et al. 1994, Heyer et al. 1998), from which it has been established that the molecular disk of the Galaxy extends to more than 20 kpc from the Galactic Center though, unlike the inner Galaxy, the outer Galaxy ISM is dominated by atomic gas.

Kutner and Mead (1981) reported the first detection of molecular clouds outside of the Solar Circle in the first quadrant. They mapped three strips at $b=1^\circ.3$, $1^\circ.5$, and $1^\circ.7$ and at $l = 55^\circ$ to

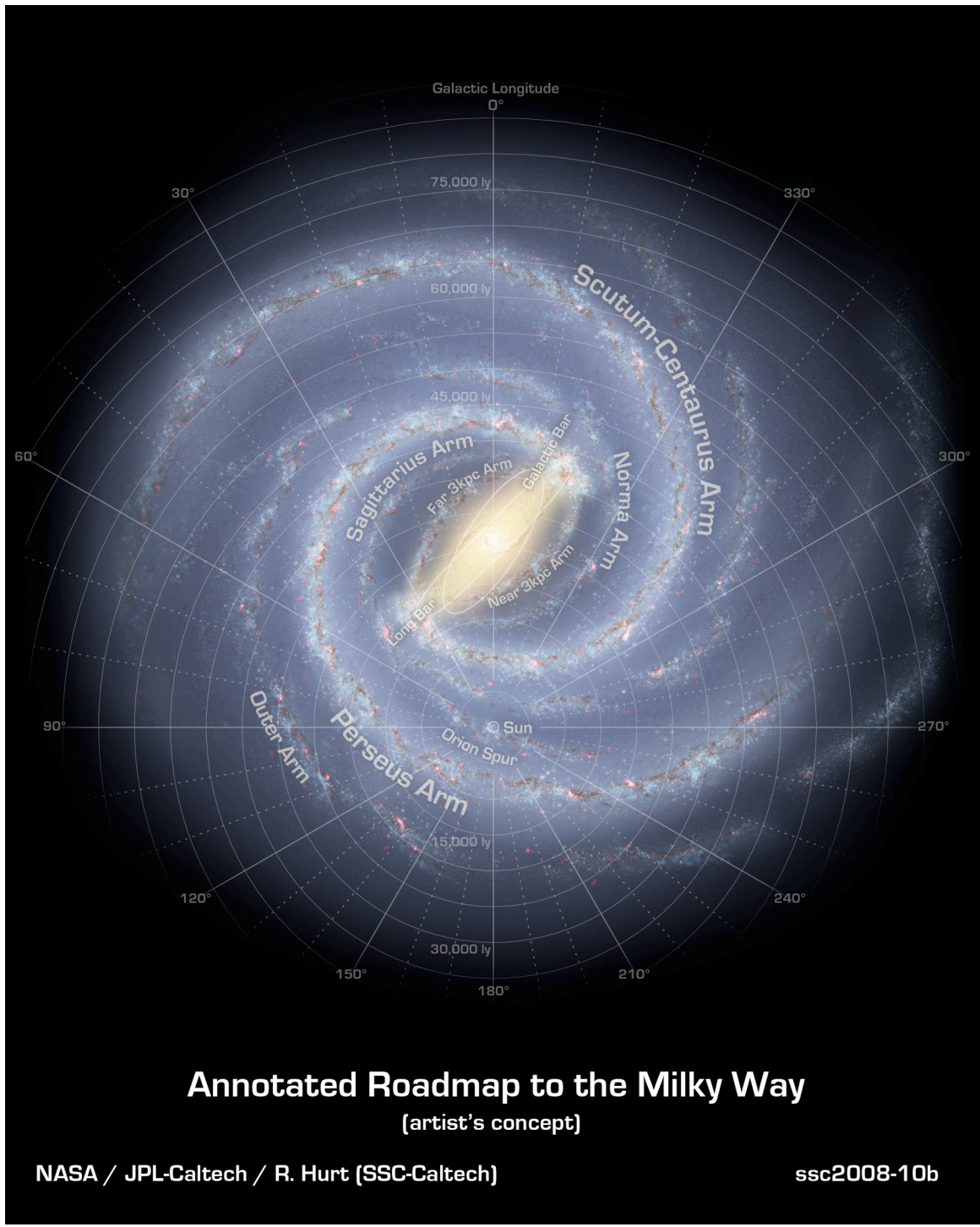


Figure 2-1 Spiral Arms of the Milky Way Galaxy. From http://ipac.jpl.nasa.gov/media_images/ssc2008-10b_mac.tif.

95° in the CO (1-0) transition at intervals of 0.1° in l , which was 5 times the beamwidth of the 70" beam of the old NRAO 36-ft telescope. The beamsize was such that clouds with an angular extent of a few tenths of a degree at 10-20 kpc should have been detected readily. The latitude values were chosen to match the 21cm HI warp¹¹ present in the Outer Galaxy. They observed T_R^* values of 1-2 K, had rms values of 0.3 K in general, and they produced higher resolution maps of 5 clouds randomly chosen from the areas showing strong CO emission. The maps demonstrated that the clouds were 60-80 pc in size and thus were GMCs.

Between 1982 and 1987, other mapping efforts contributed to the overall knowledge of the distribution of molecular gas in the outer Galaxy. The Blitz, Fich, and Stark (1982) survey looked at 242 HII regions in the Northern Galaxy in CO and included outer Galaxy HII regions in the second and third quadrants, and one in the first quadrant. Other outer Galaxy clouds searches were expanded to include the regions $l = 45^\circ$ to 160° and $l = 200^\circ$ to 255° , and 36 clouds were mapped in CO, 10 clouds in both ^{13}CO (1-0) and ^{12}CO (2-1) (Kutner 1983, Kutner and Mead 1985).

Mead and Kutner (1988) presented the results of a study of 31 individual molecular clouds in the outer Galaxy, 5 of which were reported in Kutner and Mead (1981). Figure 2-2 shows the location of the 31 clouds in the Galaxy. The 26 previously unreported clouds were chosen from an undersampled CO survey of part of the outer Galaxy conducted by Kutner and Mead (1981). All of the clouds were mapped in the CO (1-0) transition, 10 clouds were also mapped in ^{13}CO (1-0), and an overlapping subset of 11 clouds was mapped in the CO (2-1) transition. The clouds they chose to map had the most intense CO line strengths and were located between 10-14

¹¹The HI warp refers to distribution of HI above the Galactic plane ($b = 0^\circ$) in northern HI surveys, and below the Galactic plane in the southern surveys at $R_G > 11$ kpc (e.g., Wouterloot et al., 1990)

kpc¹², in a region thought to be the Outer spiral arm. The clouds they observed followed the HI warp, and beyond 14 kpc, only weak lines were detected. They reasoned that either 14 kpc was the edge of the molecular Galaxy, or that the CO was much colder in the outer Galaxy. They found the outer Galaxy peak line strengths to be less than those of the inner Galaxy, but suggested it was most likely a function of beam dilution. By comparing the excitation temperatures of the CO (1-0) transition with the CO (2-1) transition, and using modeling results to account for radiative transfer effects, the authors determined the cloud kinetic temperatures to be roughly 7 K, colder than the canonical value of 10 K for clouds near the Sun. For the models, they employed the typical density and abundance values for inner Galaxy GMCs. They claimed that the lines were thermalized and optically thick, based on line ratios of CO (1-0) and ¹³CO (1-0) of 3 to 6. The authors determined that the average outer Galaxy GMC had a radius of 11.5 pc and that the clouds had masses between 10⁴ and 10⁵ M_⊙.

A different approach to studying the molecular gas in the outer Galaxy was taken by Wouterloot and Brand. They observed the CO (1-0) line towards 1302 IRAS sources suspected of being star forming regions within molecular clouds at distances of $R_G > R_o$ (Wouterloot and Brand 1989). The resultant CO survey of the outer Galaxy is the most extensive one conducted thus far in terms of distance coverage in R_G . The survey region was located between $85^\circ < l < 280^\circ$ and within 10° of the Galactic plane. Wouterloot and Brand detected CO in 1077 out of 1302 lines of sight; for the detected clouds they derived kinematic distances from the Sun, the Galactic Center, and the Galactic midplane, as well as the bolometric luminosity of the IRAS sources. Figure 2-2 shows the locations of all of the IRAS sources towards which the CO (1-0) line was

¹²Corrected by using a value of 8.5 kpc for the distance of the Sun from the Galactic Center.

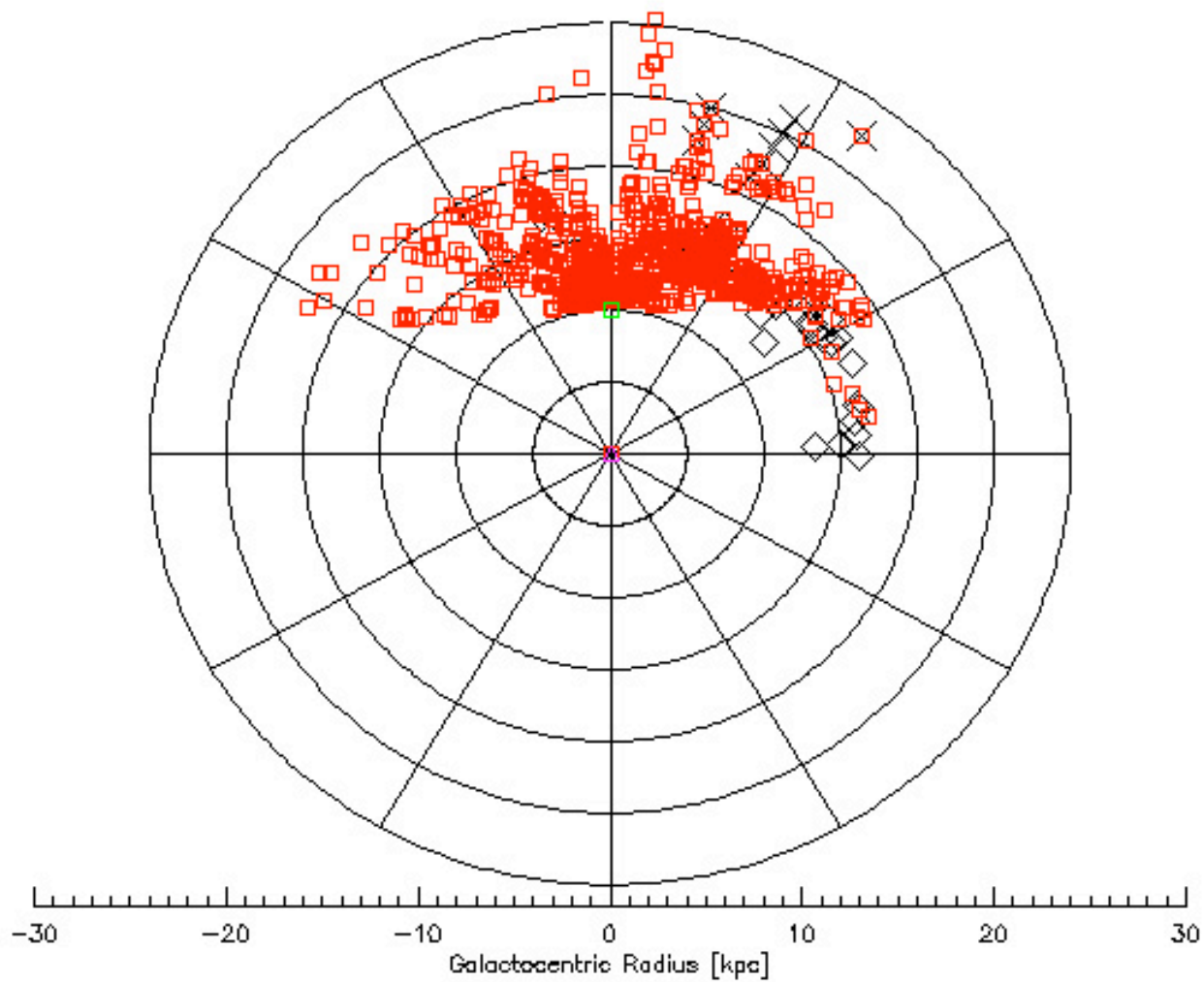


Figure 2-2 Distribution of molecular clouds from three CO (1-0) surveys. Red squares are from Wouterloot and Brand (1989), black X's are from Digel et al. (1994), and black diamonds are from Mead and Kutner (1988). The Sun is indicated by a green square and the Galactic Center by a purple triangle.

detected. However, a measure of caution must be taken when assigning kinematic distances to objects in the outer Galaxy in the longitude range $165^\circ < l < 195^\circ$, as the distance calculations for objects in this longitude range may produce unreliable results. This is the result of several factors, one being that the LSR velocity is not sensitive to distance in this longitude range. Other factors that influence kinematic distance determinations in general are cloud random motions, streaming or noncircular motions, and uncertainty in the rotation curve of the outer Galaxy (Digel et al. 1994).

The kinematic distance is given by

$$R_G = \Theta R_o \left[\left\{ v_{\text{LSR}} / (\sin l \cos b) \right\} + \Theta_o \right]^{-1} \text{ kpc},$$

where l and b are the galactic longitude and latitude of the source; R_o is taken to be 8.5 kpc; Θ_o (the circular rotation velocity at the position of the Sun) is 220 km s^{-1} ; and Θ is the circular rotation velocity of the object on question derived from the Galactic rotation curve. The calculation of $\Theta(R)$ can be obtained from the following expression:

$$\Theta(R) = \Theta_o [1.00777 \{R/R_o\}^{0.0394} + 0.00712] \text{ km s}^{-1},$$

(Brand and Blitz, 1993). An example of this uncertainty in kinematic distance determination can be seen when calculating the distance to one of the sources from the Wouterloot and Brand (1989) CO survey, WB89-730. Using the formulas above, the kinematic distance was calculated to be 23.5 kpc, but if the LSR velocity is changed by $\pm 5 \text{ km s}^{-1}$, which is the cloud to cloud velocity dispersion for GMCs in the Outer Galaxy (Brand and Blitz 1993), the kinematic distance changes to 12.5 kpc to 170 kpc for the 2 new velocities.

After their initial survey, Wouterloot and Brand wrote a series of papers that investigated various properties of outer Galaxy molecular clouds identified from IRAS sources beyond the solar circle. As discussed earlier, Paper I (Wouterloot and Brand, 1989) was the original CO

survey of 1302 of the IRAS sources beyond the solar circle discussed previously. The second paper (Wouterloot et al., 1990) compared the cloud distribution revealed in Paper I to that of the HI warp.

Paper III (Wouterloot and Brand, 1993) presented the results of an investigation into other observational phenomena that may be associated with star forming regions, such as maser emission of H₂O and OH. They searched for maser emission towards 1143 IRAS sources, not all of which had been detected in CO. The authors used 25 of the sources not observed in CO (1-0) to calculate kinematic distances using observations of the CO (2-1) and CO (3-2) lines. They also searched for OH towards 303 IRAS sources and for CH₃OH towards 19 sources (Wouterloot and Brand, 1993).

The fourth paper in the series by Brand and Wouterloot (1994) constructed maps in CO (1-0) of several far-outer Galaxy molecular clouds and presented estimations of radius, mass, and CO luminosity of the sources. Paper V (Brand and Wouterloot, 1995) analyzed properties of the far-outer Galaxy clouds and compared them to those of inner Galaxy clouds. In this study, Wouterloot and Brand augmented their data set with data from other outer Galaxy studies conducted by Mead and Kutner (1988), Digel et al. (1991), and Sodroski (1991). In addition, two inner Galaxy surveys conducted by Dame et al (1986) and Solomon et al. (1987) were included for comparison. The results of this particular study will be discussed later in this chapter because it helped to distinguish the differences between molecular clouds in the two very different Galactic environments.

Wouterloot et al. (1995), Paper VI, compared the presence and properties of H₂O maser and CO (1-0) emission in 1357 IRAS sources with FIR colors characteristic of star forming regions.

They found that H₂O maser emission increases with FIR luminosity and CO linewidth. The final paper in the series, Wouterloot and Brand (1996), estimated the ¹²C/¹³C abundance ratio in the far outer Galaxy, and determined that the gradient found for the inner Galaxy ratio extended out beyond the Solar Circle.

In addition to the fundamental work carried out by Brand and Wouterloot, two separate surveys of the outer Galaxy used the Goddard-Columbia/Harvard CfA 1.2 m millimeter-wave radio telescope. Sodroski (1991) used the Goddard-Columbia ¹²CO surveys of the Galactic plane conducted by Dame et al. (1987), Cohen et al. (1980), May et al. (1988) and Grabelsky et al. (1987) to ascertain the physical properties of 35 GMC complexes¹³ in the outer Galaxy between longitudes of 60° and 300°. Sodroski estimated the outer Galaxy cloud complex boundaries by creating longitude-latitude maps of the entire spatial and velocity coverage of the surveys, and identifying the spatial boundary of each emission maximum with a maximum contour intensity of at least 9 K km s⁻¹. He then derived the emission maximum in velocity space using the intensity-velocity distributions along the line of sight within the previously determined boundaries. After calculating the peak velocity and rms velocity dispersion for each emission maximum, the final complexes were delineated by grouping all of the emission maxima within contours of 3 K km s⁻¹ that had peak velocities within 1 standard deviation of adjacent maxima. Sodroski then separated the ¹²CO emission data into 69 distinct complexes, 35 of which he selected for further study based on the accuracy of their derived kinematic distances (uncertainties between 10% and 40%). He determined that the radii of the complexes ranged from 20 pc to 180 pc and the masses were > 10⁵ M_⊙ based on CO luminosity calculations. He

¹³The beam of the Harvard-Smithsonian CfA 1.2 m telescope is 8', significantly larger than that used by other surveys. Thus, the detections may not be individual molecular clouds but groups of related clouds known as molecular complexes.

also estimated that the ratio of H₂ column density to ¹²CO intensity, the so-called X factor, to be 2-3 times greater than that of the inner Galaxy.

The second survey using the 1.2 m CfA telescope and the 12 m NRAO telescope was conducted by Digel, de Geus, and Thaddeus (1994) towards 21 cm HI emission peaks in the outer Galaxy. Digel and coauthors found 11 molecular clouds with kinematic Galactocentric distances of 18-28 kpc in CO. However, the distance estimates in this region of the Galaxy are not necessarily reliable, as was discussed previously, and this survey is routinely quoted when distant molecular clouds or clouds at the edge of the Galaxy are discussed. For instance, while Digel et al. (1994) claimed that Cloud 2 is at R_G of 28 kpc, Smartt et al. (1996) revised the distance to 15-19 kpc by identifying the star exciting the HII region and obtaining its spectroscopic parallax. The clouds found by Digel et al. (1994) were at longitudes $131^{\circ}.05 < l < 150^{\circ}.15$ and latitudes ranging from $1^{\circ}.45$ to $-0^{\circ}.25$, and were found based on their association with large HI regions (see Figure 2-2). The authors found the CO luminosities of the clouds to be less than those of local massive star forming clouds, the most luminous of them being cloud 2 at $4.6 \text{ K km s}^{-1} \text{ pc}^2$, a value that is comparable to the luminosity of the diffuse Taurus cloud complex ($6.1 \text{ K km s}^{-1} \text{ pc}^2$). The diameters of the clouds were determined to be between 20-40 pc, and the kinetic temperatures to be 10-25 K.

At much higher resolution (45'' versus 8' for the 1.2 m telescope), Heyer et al. (1998) conducted the FCRAO CO survey of the Outer Galaxy using the 14 m FCRAO telescope. The FCRAO CO survey has the highest spatial dynamic range imaging of the molecular ISM thus far. The survey was conducted to examine the emission morphology of the molecular ISM in the outer Galaxy and to ascertain the origin of the CO emission. Heyer et al. (1998) gathered 1,696,800 CO (1-0) spectra between Galactic longitudes $102^{\circ}.49$ and $141^{\circ}.54$ and latitudes $-3^{\circ}.03$

and $5^\circ.41$. The observations revealed that the molecular gas in the outer Galaxy ISM assumes a complex morphology, and the integrated intensity images exhibited large voids in the CO emission. The authors postulated that the voids may have been caused by stellar winds from massive stars and the interaction of the ISM with associated HII regions. Heyer et al. (1998) speculated that a significant fraction of the observed ^{12}CO intensity emanated from regions with low excitation conditions, i.e., regions with gas densities ranging from $30\text{-}500\text{ cm}^{-3}$.

From the Southern hemisphere, there have been fewer molecular surveys. One relevant to the distribution of molecular gas in the outer Galaxy used the CS molecule rather than CO. The lower CS rotational transitions are more sensitive to higher density gas than the equivalent CO transitions, but work well in this context because of the high-density cores present in GMCs. Bronfman, Nyman, and May (1996) conducted a complete survey of the Galactic disk in the CS (2-1) line using the SEST 15 m telescope in Chile and the Onsala Space Observatory 20 m telescope in Sweden. They observed the CS (2-1) line towards IRAS point sources with colors characteristic of ultra-compact HII regions. They chose the CS (2-1) rotational transition line because it is a known tracer of dense molecular gas and the IRAS sources were chosen based on their potential to be OB star formation sites. The sources covered inner Galaxy longitudes of $360^\circ < l < 300^\circ$ and latitudes $-2^\circ < b < 2^\circ$. In the rest of the Galactic plane the latitude range was $-4^\circ < b < 4^\circ$. The authors observed 1427 sources and detected 843 of them in CS (2-1) with typical rms values of 0.1 K.

More recently, Nakagawa et al. (2005) searched for molecular clouds in the southern Galactic Warp using the NANTEN 4 m telescope in Chile. The survey was located primarily in the Galactic third quadrant, $l = 252^\circ\text{-}266^\circ$ and $-5^\circ < b < -1^\circ$, and they chose regions from the Parkes 21 cm HI (Kerr et al. 1986) survey that had strong HI emission at $R_G > 14.5\text{ kpc}$. The authors

observed 13,000 positions at a 4' grid spacing and 7,500 positions at a 2' grid spacing, and detected CO emission towards 702 positions. They identified 70 individual molecular clouds and estimated that the cloud masses ranged from $7.8 \times 10^2 M_{\odot}$ to $8.4 \times 10^4 M_{\odot}$. They also derived the X factor¹⁴ for the Warp to be $X = 5.6 \times 10^{20} \text{ cm}^{-2} [\text{K km s}^{-1}]^{-1}$ compared to the value for Galactic disk clouds of $2 \times 10^{20} \text{ cm}^{-2} [\text{K km s}^{-1}]^{-1}$. The value for the X factor derived by Nakagawa et al. was in agreement with work done by Mead and Kutner (1988), Sodroski (1991), and Digel et al. (1996) but was not consistent with Wouterloot and Brand (1995) and Snell, Carpenter, and Heyer (2002). The latter authors found that the X factor for the far-outer Galaxy did not differ appreciably from that of the inner disk ($2 \times 10^{20} \text{ cm}^{-2} [\text{K km s}^{-1}]^{-1}$, Digel et al. 1994). Snell et al. (2002) used an LTE model with previously calculated inner Galaxy $\text{H}_2/\text{}^{13}\text{CO}$ ratios, and Brand and Wouterloot (1995) estimated the outer Galaxy $\text{H}_2/\text{}^{13}\text{CO}$ ratio from the $\text{}^{12}\text{CO}$ integrated intensity.

In terms of cloud masses and sizes, Brand and Wouterloot (1995) compiled data from several studies of outer and inner Galaxy molecular clouds and recalculated d , R , M , L_{CO} , and T to make values from the surveys consistent. They determined that most of the outer Galaxy clouds had masses of $10^3 - 10^5 M_{\odot}$, and the most massive clouds in the surveys, those with masses on the order of $10^6 M_{\odot}$, reside inside of the solar circle. The authors showed that the outer Galaxy clouds had a peak in mass distribution around $10^4 M_{\odot}$, while in the inner Galaxy, the peak in mass distribution was roughly $10^6 M_{\odot}$. By placing all of the clouds in the combined data set on a plot of M_{wco} (the mass based on the $W_{\text{CO}} - \text{CO}$ luminosity relationship) versus R , they clearly

¹⁴The X factor is used to convert CO luminosity to molecular mass and can be calculated from $X = N(\text{H}_2)/\int T(\text{}^{12}\text{CO})d\nu \text{ cm}^{-2} [\text{K km s}^{-1}]^{-1}$ where $N(\text{H}_2)$ is the molecular hydrogen column density and $\int T(\text{}^{12}\text{CO})d\nu$ is the integrated CO antenna temperature.

demonstrated that the outer Galaxy cloud population is less massive than the inner Galaxy population. One reason the authors suggested for the lack of smaller clouds in the inner Galaxy studies may be that blending of clouds along the line of sight required removing the background emission, which also removed the smaller clouds.

In the far-outer Galaxy ($R_G \geq 16$ kpc), the nature of the Galactic molecular environment is significantly different from that in the Galaxy inside of the Solar Circle. Specifically, the HI and H₂ gas surface and volume densities are much smaller than in the inner Galaxy. It has already been noted in Chapter 1 that the mass surface density drops off rapidly beyond 12 kpc from the Galactic Center (Scoville 1987). Heyer et al. (1998) calculated the mass surface density out to 24 kpc and determined that the trend continued, which they described as “limited flaring of the molecular disk with increasing R_G ”. Using the Wouterloot and Brand (1989) catalog of IRAS sources and a mean cloud mass of $1.0 \times 10^5 M_\odot$ for all clouds located beyond 16 kpc, we estimated the mass surface density of the outer Galaxy at $R_G > 16.0$ kpc to be $0.095 M_\odot \text{pc}^{-2}$, significantly smaller than the mass surface density of the Solar Circle ($\sim 0.5 M_\odot/\text{pc}^2$; Blitz et al, 1984).

In the outer Galaxy, the scale heights are larger; the stellar density is much smaller; there is less star formation per pc^3 ; the interstellar radiation field is much weaker; there are fewer supernova remnants, so there are fewer and/or weaker triggers for star formation; abundances of helium and heavier elements are lower; the far-infrared emissivity of the dust in the interstellar medium is smaller; and the pressure of the intercloud medium is much smaller (Brand and Wouterloot 1996, and references therein). Although these factors might be expected to negatively influence the cloud- and star formation activity in the far-outer Galaxy, hundreds of molecular clouds are found there (Brand and Wouterloot 1995, Snell 2002, Brunt et al. 2003), as

well as substantial star formation given the lower density of GMC's (Wouterloot et al. 1988, Kobayashi and Tokunaga 2000, Santos et al. 2000, Brand and Wouterloot 2007). Thus, it is likely that hundreds - if not thousands - of planetary systems should be present even at these large distances from the Galactic Center.

2.2 METALLICITY IN THE OUTER GALAXY

Studies of metallicity¹⁵ in our galaxy spawned from the discovery of the first abundance gradients in external galaxies (Searle 1971). Searle (1971) found distinct differences in integrated HII spectra from inner and outer regions of Sc galaxies, which the author indicated was a result of differing abundances of metals in the inner and outer galaxy spiral arms. In the Milky Way, abundance gradients have been determined using tracers like HII regions, O/B stars, planetary nebulae, open clusters and Cepheid variables (Costa et al. 2004, Lemasle et al. 2008 and references therein).

The values determined for the abundance gradients in the Milky Way have varied depending on the class of tracer and between measurements within the same type of tracer. Several studies were undertaken using a combination of optical/IR spectroscopy and radio continuum maps of HII regions to measure electron temperature and derive abundances. Shaver et al. (1983) discovered gradients of O/H¹⁶, N/H, S/H and others at distances of 3.5 to 13.7 kpc from the Galactic center using optical recombination and forbidden lines of HII regions. Two further optical studies of HII regions, Fich and Silkey (1991) and Vilchez and Esteban (1996), investigated the outer Galaxy from R_0 to 18 kpc, and recognized a flattening of the N/H gradient

¹⁵Metallicity refers to the abundance of metals, elements with atomic masses greater than that of He, in a given region of the Galaxy

¹⁶Metallicity is generally expressed as a ratio of two elements and is frequently measured with respect to the H abundance, [X/H], where X is the metal.

at large R_G . Caplan (2000) observed several HII regions optically from 6.6 kpc to 17.7 kpc, and those observations, analyzed by Deharveng et al. (2000), yielded an estimate of the O/H gradient similar to that obtained by Vilchez and Esteban (1996). Afflerbach et al. (1997) observed IR fine-structure lines of [O III], [N III] and [S III] towards 34 compact and ultracompact HII regions out to 12 kpc R_G and estimated oxygen, nitrogen and sulfur abundance gradients. The abundances calculated for each of the HII region studies can be seen in Table 2-1.

Several groups have used young B-type stars to estimate abundance gradients because these stars have high luminosity, uncontaminated photospheres, and exhibit distinct metal line spectra (Rolleston et al. 2000). Smartt and Rolleston (1997) used observations of B-type objects in 18 O/B associations between 6 and 18 kpc from the Galactic Center, and calculated an oxygen abundance gradient for the Galaxy. Gummersbach et al. (1998) confirmed the value of the oxygen gradient calculated by the Smartt and Rolleston (1997) by estimating abundance gradients for He, C, N O, Mg, Al and Si from 16 young B-type stars at $5 \text{ kpc} < R_G < 14 \text{ kpc}$. Further confirmation for previously calculated abundances was given by Rolleston et al. (2000) from combined data from 80 B-type stars in 19 open clusters between 6 kpc and 18 kpc. The authors indicated that the distribution followed a linear, radial gradient (Rolleston et al. 2000). Daflon and Cunha (2004), using 69 objects from 25 open clusters, OB associations, and HII regions between 4.7 and 13.2 kpc from the Galactic Center, calculated slightly different abundances for oxygen and nitrogen than earlier studies. The authors suggested that their metallicity gradient calculations were flatter than previous calculations, and indicated a flattening of the radial gradient with time (Daflon and Cunha 2004).

Planetary nebulae have been employed to determine metallicity gradients in the Galaxy (Maciel and Quirereza 1999, and references therein). These objects are formed from intermediate

Table 2-1 Abundance gradient calculations from various studies.

<i>Tracer</i>	<i>Element</i>	<i>Gradient</i> dex* kpc ⁻¹	<i>Range</i> kpc	<i>Study</i>
HII regions	Oxygen	-0.070±0.015	3.5-13.7	Shaver et al. 1983
		-0.036±0.020	12-18	Vichez & Esteban 1996
		-0.064±0.009	0-12	Afflerbach et al. 1997
	Nitrogen	-0.039±0.005	5-15	Deharveng et al. 2000
		-0.09±0.015	3.5-13.7	Shaver et al. 1983
		-0.009±0.020	12-18	Vichez & Esteban 1996
	Sulfur	-0.072±0.006	0-12	Afflerbach et al. 1997
		-0.01±0.020	3.5-13.7	Shaver et al. 1983
		-0.041±0.020	12-18	Vichez & Esteban 1996
B type stars	Oxygen	-0.063±0.006	0-12	Afflerbach et al. 1997
		-0.070±0.010	6-18	Smartt & Rolleston 1997
		-0.067±0.024	5-14	Gummersbach et al. 1998
	Nitrogen	-0.067±0.008	6-18	Rolleston et al. 2000
		-0.031±0.012	4.7-13.2	Daflon & Cunha 2004
		-0.078±0.023	5-14	Gummersbach et al. 1998
	Sulfur	-0.09±0.01	6-18	Rolleston et al. 2000
		-0.06±0.011	4.7-13.2	Daflon & Cunha 2004
		-0.030±0.011	4.7-13.2	Daflon & Cunha 2004
Planetary nebulae	Oxygen	-0.069±0.006	3-14	Maciel and Koppen 1994
		-0.05	8-14	Costa et al. 2004
	Sulfur	-0.077±0.011	3-14	Maciel and Koppen 1994
Open clusters	Iron	-0.09±0.02	7-16	Friel and Janes 1993
		-0.067±0.008	6-16	Twarog et al 1997
		-0.09	7-16	Carraro et al 1998
		-0.06±0.01	7-16	Friel et al. 2002
		-0.018±0.02	12-21	Carraro 2007
Cepheids	Iron	-0.07	5-13.6	Harris & Pilachowski 1984
		-0.13±0.03	4-6	Andrievsky et al. 2002
		-0.02±0.01	6-10	Andrievsky et al. 2002
		-0.06±0.01	10-12.5	Andrievsky et al. 2002
		-0.068±0.003	5-12	Luck et al. 2006
		-0.052±0.003	10-12	Lemasle et al. 2008

*dex stands for decimal exponent where dex (x) = 10^x.

mass stars in their evolutionary phase between red giant and white dwarf, so are thought to adequately represent the ISM at the time of their formation (Allen et al. 1998 and references therein). Intermediate mass stars do not form or destroy elements like O, S, Ne, and Ar, therefore their planetary nebulae are relatively uncontaminated and are good tracers of abundances of metals in the local ISM (Allen et al. 1998). Maciel and Koppen (1994) sampled 200 planetary nebulae in the galactic disk and determined an O gradient that matched well with previous estimates, and an S gradient that was steeper than previously calculated. Maciel and Quireza (1999) determined abundance gradients for O, S, Ne and Ar from a sample of 130 planetary nebulae classified as Type II¹⁷ at $R_G > R_o$. The authors described a flattening of the gradient at large R_G , similar to that predicted by studies of HII regions. Further evidence for flattening ($R_G > 10$ kpc) was given in a study by Costa et al. (2004) of 30 planetary nebulae towards the galactic anticenter at distances greater than R_o . A comparison of gradient data for the two aforementioned studies is presented in Table 2-1. More recently, at least two studies have confirmed that the metallicity gradient flattens out at large R_G and over time using measurement of electron temperatures of HII regions from 0 to 17 kpc (Quireza et al. 2006), and by investigating the electron temperature gradient of combination of HII regions and planetary nebulae out to 12 kpc from the Galactic Center (Maciel et al. 2007).

Both open clusters and Cepheid variables have been used as tracers to establish the Fe metallicity gradient in the Galaxy. Old open clusters (lifetime of 3-4 Gyr) are good indicators of metallicity gradients because their distances are well-known, and their compositions can be used to investigate past and present metallicity gradients. The results for the prominent open cluster studies are presented in Table 2-1, and the spread in Fe abundance gradient estimates is apparent.

¹⁷See Peimbert (1978) for explanation of PN classification scheme.

Friel and Janes (1993) calculated an Fe abundance by looking at spectral indices of Fe peak and Fe-peak element blends in 31 open clusters with ages greater than 1 Gyr at distances of $7.9 < R_G < 15.4$ kpc. Twarog et al. (1997) calculated a shallower Fe gradient and announced a discontinuity at $R_G = 10$ kpc by conducting open cluster photometry on 76 open clusters at distances of 6 kpc to 16 kpc from the Galactic Center. Carraro et al. (1998) used age-metallicity of F and G stars and open clusters to derive a Fe abundance at distances between 7 kpc and 16 kpc. Friel et al. (2002) revised the Fe abundance gradient calculation made by Friel and Janes (1993) by using a larger sample of open clusters, 39 versus 31 in the previous study within the same distance range, and found the slope to be shallower than previously calculated. Carraro et al. (2007) used 5 old open clusters in conjunction with the sample from Friel et al. (2002) and calculated much shallower Fe abundance gradient for $R_G > 12$ kpc.

The Fe abundance gradient calculations that have used Cepheid variables as tracers have yielded more consistent values within the tracer type than have open clusters. Like B-type stars, Cepheid variables are luminous enough to be seen at great distances and give well-defined spectral lines, but unlike B-type stars, the distances to Cepheid variables are readily and accurately determined (Lemasle 2008). Harris and Pilachowski (1984) used spectroscopy of 8 Cepheids to determine the Fe abundance gradient for $6 \text{ kpc} < R_G < 14 \text{ kpc}$. The authors calculated an abundance gradient comparable to one calculated previously by Harris (1981) (see table 2-1 for the values). The work of Andrievsky et al. (2002a, 2002b, and 2002c) using Cepheid variables supported the discontinuity in the gradient discovered by Twarog et al. (1997). Additionally, Andrievsky and coauthors calculated Fe abundance gradients based on Galactic regions and found that the inner region ($4.0 \text{ kpc} < R_G < 6.5$) had a steep gradient, the middle region ($6.5 \text{ kpc} < R_G < 10 \text{ kpc}$) was essentially flat, and the outer region ($R_G > 10 \text{ kpc}$) had a

shallow gradient, verifying the flattening with R_G illustrated in other studies. Luck et al. (2006) confirmed the Fe gradient estimates previously calculated by examining the Fe content in 54 Cepheid variables at distances of 5 kpc to 12 kpc from the Galactic Center. Most recently, Lemasle et al. (2008) made Fe abundance measurements for 33 Cepheid variables at $R_G > 10$ kpc using near-infrared photometry. The authors found a Fe abundance gradient similar to others previously reported using Cepheid variables, but they concluded that the gradient across the disk fit a linear regime inside the solar circle, and flattened at larger R_G . Lemasle et al. (2008) found no evidence to support the discontinuity of the gradient at $R_G = 10$ kpc claimed by previously mentioned authors.

Evaluating all of the studies conducted on metallicity in the Galaxy points to the fact that the metallicity gradient in the outer Galaxy is shallower than that of the inner Galaxy, based on comparison of slopes of least squares fits for the various data. For oxygen, the slope of the O/H gradient ranges from -0.064 (Shaver et al. 1983, Afflerbach et al. 1997, Gummersbach et al. 1998, Maciel and Koppen 1994) in the inner Galaxy from $R_G = 03-14$ kpc to -0.036 (Vichez and Esteban 1996, Rolleston et al. 2000) at distances of 12- 18 kpc from the Galactic Center. For nitrogen, the N/H slope ranges from -0.084 (Shaver et al. 1983, Afflerbach et al 1997, Gummersbach et al. 1998) from 3-14 kpc, to -0.009 (Vichez and Esteban 1996) and -0.09 (Rolleston et al 2000) from 12-18 kpc. The sulfur gradient S/H has a slope of -0.05 (Shaver et al. 1983, Daflon and Cunha 2004, Maciel and Koppen 1994) in the inner Galaxy (3-14 kpc) and -0.04 (Vichez and Esteban 1996) in the outer Galaxy beyond $R_G = 12$ kpc. Finally, for iron the Fe/H gradient ranges from -0.13 (Andrievsky et al. 2002) at R_G of 4-6 kpc, -0.02 (Andrievsky et al. 2002) from 6-10 kpc, -0.056 (Andrievsky et al. 2002, Lemasle et al. 2008) from 10-12 kpc, and -0.018 (Carraro 2007) from 12-21 kpc.

In terms of overall abundances, Smartt et al. (2001) combined B-Type star results with those of Rolleston et al. (2000) and compared the abundances of several elements (C, O, and N to name a few) to abundances in the solar neighborhood. The combined studies combine data from the Galactic Center all the way out to a Galactocentric radius of roughly 15 kpc. The results can be seen in Table 2-2, where the abundance values were calculated by $A_x = \log(N_x/N_H) + \log(N_H)$. The results of this study and the previously discussed studies show an overall decreasing trend in metal abundance with increasing R_G . The next section, Chapter 3, will discuss the biological relevance of this study.

Table 2-2 Comparison of chemical abundances of C, O, and N in at different distances from the Galactic Center. Values are in dex where $[X] = 12 + \log[N_X/N_H]$, and the abundance of H is 12 dex (Smartt et al. 2006).

<i>Element</i>	<i>Inner Galaxy^a</i>	<i>Solar Circle^b</i>	<i>Outer Galaxy^a</i>
	$R_G = 0-6 \text{ kpc}$	$R_G = 6-10 \text{ kpc}$	$R_G = 10-15 \text{ kpc}$
CII	8.70	8.55	7.50
OII	9.00	8.87	8.00
NII	8.50	7.97	7.50

^aValues are approximated from Rolleston et al. 2000.

^bValues from Anders and Grevesse 1989.

CHAPTER 3
BASIC BIOLOGY

3.1 THE BASIC BUILDING BLOCKS OF LIFE

Living organisms are composed of complex assemblages of organic molecules. A supply of these molecules or their precursors must be present in the local environment for life to form in any region of the Galaxy. The basic building blocks of life are carbohydrates, DNA and RNA, amino acids, proteins, and lipids. Carbohydrates, like sugars, are molecules with the basic empirical formula $(\text{CH}_2\text{O})_n$ and they provide fuel for cells. They also serve as components of larger molecules like DNA and RNA. DNA is the molecule that contains the codes for all of the proteins in the cell. DNA is composed of nucleotides that contain a nitrogenous base (purine or pyrimidine), a pentose sugar (deoxyribose), and a phosphate group. The nucleotides are adenine, guanine, cytosine, thymine (only in DNA) and uracil (only in RNA). Each sequence of three nucleotides in the DNA molecule encodes one amino acid. RNA is the intermediate molecule between the DNA and the protein and is composed of nucleotides as well, but the sugar unit is ribose. RNA is transcribed from DNA and then translated into proteins, which are composed of amino acids subunits.

Proteins are the workhorses of the cell and perform numerous functions to include synthesis of molecules like carbohydrates. Proteins are composed of chains of amino acids called polypeptides and are usually folded into a three-dimensional structure. There are 20 amino acids

and they are composed of an amino (NH_2) group, a carboxyl (COOH) group, a hydrogen atom and a functional group or side chain (see Figure 3-1). The side chain component gives each amino acid its specific identity in terms of size, shape, charge, reactivity, and hydrophobicity. The smallest amino acid, glycine, has a side chain of a single H atom. The rest of the amino acids have side chains that are more complex and some contain cyclic ring structures. Lipids include the fats, steroids, waxes, oils and others. They are used for energy storage and are primary components of biomembranes (Lodish et al. 1986).

Studies of how organic molecules may have formed in a primitive Earth atmosphere began in the early 20th century and focused primarily on amino acids. Walther Loeb (1913) synthesized glycine from a mixture of CO , NH_4 and H_2O using electrical discharge. While it was debated whether or not the amino acid formed in the gas phase or in solution, this experiment was the first in establishing the study of the chemical origin of life (Miller 1955). The Russian biochemist Aleksander Oparin qualitatively suggested in 1924 that in a reducing atmosphere containing predominantly CH_4 , the basic molecules necessary for life could form (Oparin 1938, Bibring 2005). Using a thermodynamic approach, Urey (1952) proposed that the early atmosphere contained CH_4 , NH_3 , H_2O and H_2 based on the fact that CH_4 and NH_3 are stable in the presence of H_2 , furthering the argument for an early Earth with a reducing atmosphere. These qualitative ideas were explored quantitatively by Miller (1953; 1955) who demonstrated that reactions in a mixture of CH_4 , NH_3 , H_2O , and H_2 gases subjected to electrical discharge simulating lightning produced aspartic acid, glycine, α - and β -alanine and other organic compounds. Using a different mixture of precursor molecules, the amino acid glycine can be

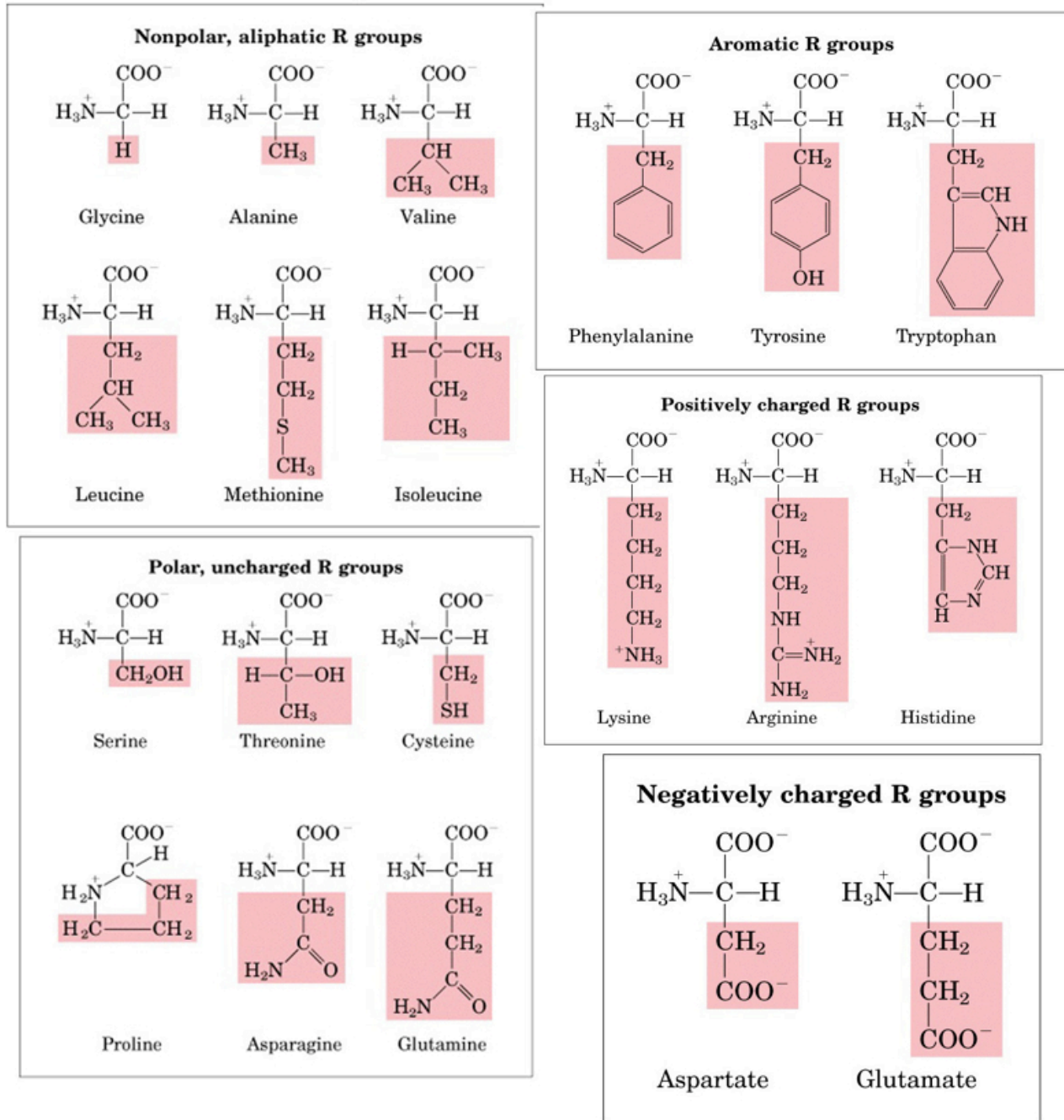


Figure 3-1: The twenty standard amino acids.

<http://trc.ucdavis.edu/biosci10v/bis10v/week2/2webimages/ch5-amino-acids.jpg>

formed from a reaction of H_2CO with NH_3 and HCN (Oro 1959, Miller 1992). To date, 17 amino acids have been created in this fashion using small precursor molecules like H_2CO and HCN (Bibring 2005).

Interestingly, Brooks and colleagues (2002) conducted a study to investigate the change in amino acid composition of proteins over vast evolutionary time. Using probabilistic methods, they inferred that the proteins of the Last Universal Ancestor¹⁸ (LUA) contained more of the amino acids thought to have been present in the early Earth environment, and fewer of those that are less likely to have been formed early on. Nine amino acids were thought to occur more frequently in the proteins of the LUA: alanine, asparagine, aspartic acid, glycine, histidine, isoleucine, serine, threonine, and valine. In Miller's first experiment alone, he synthesized 3 of these 9 amino acids (Miller 1953). These results lend some credibility to the idea of prebiotic synthesis for some amino acids on early Earth.

Several other investigations into the formation of amino acids under early Earth conditions have been conducted since the early experiments. Oro et al. (1959) reported that in highly acidic aqueous solutions, amino acids could be formed from paraformaldehyde and hydroxylamine with an enhancement in the presence of molybdate. Hatanaka and Egami (1977a) reported the production of amino acids from formaldehyde and hydroxylamine in modified sea mediums presumably representative of the primeval sea. In a paper in that same year, using the same precursors but enriching the media with molybdate, the authors demonstrated selective enhancement of the production of certain amino acids (i.e. proline and β -alanine), and decreased

¹⁸The LUA is the progenitor of all extant species and was the single cell that branched off into the eubacteria, the archaea, and the eukaryotes.

production of others (Hatanaka and Egami 1977b). They also found a striking similarity in the amino acid composition they created and that of the Murchison meteorite (Hatanaka and Egami 1977a).

Chandha and Choughuley (1984) formed aminoacetonitrile (AAN) and methyleneaminoacetonitrile (MAAN) using Strecker synthesis, a pathway commonly believed to have formed amino acids on primitive Earth. In this reaction, aminoalkylnitriles are formed from mixtures of an aldehyde, HCN and NH_3 . The aminoalkylnitriles can then be hydrolyzed to amino acids. The investigators demonstrated both the formation of AAN and MAAN utilizing the Strecker synthesis reaction, and subsequent formation of amino acids by hydrolysis of the two products. The authors showed the formation of other important biological molecules like the nucleotide thymine from a reaction of H_2CO with uracil. Using the previously established pyrrole-aldehyde reaction (Szutka 1964), they also demonstrated that upon heating serine, porphyrins, constituents of molecules like chlorophyll and heme, were formed. The authors speculated that on the early Earth in warmer volcanic regions, pyrrole could have been formed and then reacted with aldehydes to form porphyrins (Chadha and Choughuley 1984).

Of the 20 amino acids found in living systems, all were produced in prebiotic type reactions with the exception of histidine, lysine, and arginine. Histidine has an imidazole side chain therefore the prebiotic formation of imidazoles on early Earth would be necessary for the presence of this amino acid. Oro et al. in 1984 demonstrated the production of imidazoles from an aldehyde, glyoxal, and NH_3 under prebiotic conditions (Oro et al. 1984). Later, Shen et. al (1987) reported the prebiotic formation of several imidazole compounds from mixtures of both

erythrose and formamidine and erythrose, formaldehyde and ammonia. The authors speculated that via Strecker synthesis, one of the products, imidazole-4-acetaldehyde, could have been transformed into histidine on the early Earth.

3.2 SUGARS

Another class of biological molecules that is important for life to develop is sugars. Previously, the importance of pentose sugars to the molecules DNA and RNA was discussed. Sugar is also the basis of modern metabolic processes like photosynthesis, which fixes CO₂ into sugar, and cellular respiration, which breaks sugar down for energy. Therefore, the ability to form sugars in the early Earth environment is an important issue to explore.

It is known that H₂CO molecules can polymerize via the formose reaction to form sugars including ribose (Butlerow 1861). The stability, or resistance of sugars to degradation by UV radiation, formed from the formose reaction in an early Earth environment has been a subject of controversy. Early studies showed the formation of sugar from highly concentrated formaldehyde under very alkaline conditions, but neither high concentrations of formaldehyde nor alkaline conditions were thought to exist on early Earth (Gabel and Ponnampereuma 1967). These early experiments also showed a high rate of degradation in the sugars produced after a short period of time (Reid and Orgel 1967). Abelson (1966) believed that the pH of the oceans has not changed much over time, therefore, would not have been a highly alkaline environment for the formation of sugars on early Earth.

Later studies began to look at the synthesis of sugars from aldehydes in closer to neutral pH conditions. Weber (1992) demonstrated the production of hexose sugars from glyceraldehyde in the presence of the catalyst iron (III) hydroxide oxide [Fe(OH)O]. Weber (1992) suggests that

Fe(OH)O could have been produced by photooxidation of Fe(III). Weber (1998) demonstrated a “one-pot”¹⁹ reaction, wherein sugars were produced from formaldehyde and glycoaldehyde, and then transformed into alanine and homoserine in the presence of a thiol (a compound containing an -SH group) and ammonia. Weber (2000) claims that sugars may be an optimal biosynthetic substrate involved in the chemical origin of life. His reasons are twofold: 1) sugars contain high-energy electrons that can be used in both biological and prebiotic chemical reactions and, 2) sugars can be formed from formaldehyde, which could likely have been synthesized on the early Earth. Furthermore, Weber (2000) has postulated that the reactions that transform sugars into molecules like amino acids may have been possible and are perhaps favored in an early Earth environment devoid of molecular oxygen. While the stability of specifically ribose synthesis from H₂CO under prebiotic conditions has been questioned, a recent study by Ricardo et al. (2004) has demonstrated the stability of pentose sugar synthesis from H₂CO in the presence of borate minerals.

3.3 THE IMPORTANCE OF H₂CO AND HCN

We have seen that of the precursor organic molecules, H₂CO and HCN are important for the formation of amino acids and sugars. Thus, the early Earth must have had both of these molecules in sufficient abundance to jump-start these reactions. Where did the early Earth’s H₂CO come from? Their ability to form formaldehyde under early Earth conditions in environments ranging from highly reducing to slightly oxidizing has been firmly established (see Weber 2000). One method involves the discharge of electricity in the early atmosphere in various redox states. Miller and Schlesinger (1984) produced formaldehyde using electrical

¹⁹One-pot” refers to a contained system where products of the reaction can react with chemical intermediates to yield new products.

discharge in a slightly reducing mixture of CO₂, H₂, H₂O, NH₄ and N₂. Other experiments were carried out under highly and moderately reducing conditions and they also formed formaldehyde (Weber 2000).

A second method of producing formaldehyde on early Earth is from UV irradiation of the atmosphere in various redox states. In a highly reducing atmosphere of CH₄, H₂O and N₂, Ferris and Chen (1975) demonstrated the production of formaldehyde by UV photolysis. Bar-Nun and Hartman (1978) produced a mixture of aldehydes and other organic products from the photolysis of H₂O and CO. Pinto et. al. (1980) used a photochemical model which demonstrated the production of reduced organic compounds like formaldehyde in an early atmosphere dominated by CO₂, and subsequent dissolution into the primitive ocean. They reported the formation of H₂CO in the upper atmosphere, and while most of it was destroyed by photolysis, about 1% of it was delivered to the ocean via raindrops. Canuto et al. (1983) also used a modeling approach to look at formation of organics in the early atmosphere, but they included an estimated UV flux of a young Sun using existing data from T Tauri stars. From this they analyzed the production of organics in different concentrations of H₂ and CO₂, and were better able to estimate abundances of organics like formaldehyde. For instance for formaldehyde under the present solar UV flux, pre-industrial CO₂ levels (280 ppm), and an H₂ concentration of 17 ppm, they determined a surface concentration of 1.62 cm⁻³. Under the same UV flux and CO₂ level, but an H₂ concentration of 10⁻³ ppm, they estimated an H₂CO abundance of 4.14 cm⁻³. Canuto et. al. (1983) verified the resulting formaldehyde abundances predicted by Pinto et al (1980), and also determined that the production in H₂CO was highly dependent on H₂ concentration.

A third method of producing formaldehyde is the photoreduction of CO_2 in an early Earth environment in the presence of sensitizers like uranyl acetate and clay minerals like kaolinite (Ferris 2005 and references therein). The sensitizers are inorganic molecules that may serve as catalysts and/or adhesion sites for molecules. Bernal (1951) and Goldschmidt (1952) independently suggested the importance of clay minerals in the origin of biomolecules, and Ferris (2005) claimed that clay minerals from weathered volcanic ash may have played a central role in early prebiotic evolution. Harvey et al. (1971) reported the synthesis of carbohydrates and lipids on kaolinite. Franchi et. al. (2003) demonstrated the adhesion of single-stranded and double-stranded nucleic acids on montmorillonite and kaolinite, and suggested this as a means to avoid degradation and to form polynucleotides. Ferris (2005) has shown the binding and oligomerization of RNA molecules on montmorillonite, suggesting that RNA may have been the first nucleic acid formed.

The examples above demonstrate the synthesis of formaldehyde in highly reducing to slightly reducing atmospheres is viable, but what about that of HCN? Using a photochemical computer model, Zahnle (1986) showed that HCN could be formed photochemically in the ionosphere of the early Earth from CH_4 and N_2 in the presence of CO_2 . A complication with this pathway is that there is evidence that the early terrestrial atmosphere may have been more neutral than reducing (Kasting 1993). If the Earth's core formed slowly over time, the mantle would have had more free iron to sequester the oxygen and bind it into iron oxides, and the mantle would have been more reduced. Volcanic outgassing under those conditions may have contained plentiful CH_4 and NH_3 thus making the atmosphere more reducing (Chyba 2005). It is thought, however, that the Earth had a hot beginning, and that the core may have formed quickly, pulling the free iron out of the mantle as it settled towards the core, and leaving the mantle more

oxidized. In this scenario, outgassing would have been in the form of CO₂ and N₂, not reduced prebiotic compounds like CH₄ as the carbon would be bound to oxygen rather than hydrogen (Zahnle 1986). An alternative source of CH₄ may have been outgassing from mid-oceanic ridges where low temperature and high pressure would have created an optimal environment (Zahnle 1986). Fortunately, there are two other plausible means for obtaining HCN, H₂CO, and other prebiotic molecules: 1) production of prebiotic molecules in hydrothermal vents (Corliss and Baross 1981) and, 2) delivery onto a planetary surface via impacting comets and asteroids (Chyba et al. 1990).

The idea that hydrothermal vents may have supplied prebiotic molecules or reduced compounds has been studied, primarily theoretically (Corliss et al. 1981, Shock 1990). Shock (1990) investigated the geochemical constraints under which prebiotic compounds could be synthesized abiotically in hydrothermal systems. He concluded that it would be kinetically feasible to reduce CO₂ and H₂ in temperatures of 200 °C in a system containing mineral types found in ocean crust. Voglesonger et al. (2001) demonstrated the abiotic synthesis of methanol in hydrothermal system-like conditions. The authors used an experimental chamber that mimicked seafloor temperatures and pressures, and used a CO₂-H₂-H₂O gas mixture in the presence of clay minerals, and ultimately produced methanol. They claimed that during an event called magmatic diking²⁰, abundant CO₂ and H₂ could be released locally within a hydrothermal system and serve as substrates for subsequent reduction. For a review of more recent experiments see reference Holm and Andersson (2005).

The second method of supplying prebiotic molecules to the early Earth is delivery of organics by comets and asteroids (Chyba et al. 1990). The Murchison meteorite has been the primary extraterrestrial laboratory for the study of organic molecules that may have been delivered early

²⁰ Magmatic diking is an event where magma thrusts towards the surface laterally, releasing gas.

in Earth's history. Upon analyzing water extracted from the meteorite, Kvenvolden et al. (1970) reported the presence of several amino acids, and near equal amounts of D and L enantiomers (biological systems contain L-forms only), suggesting an extraterrestrial origin for the molecules. Chyba et al. (1990) also implicated cometary delivery as a means to supply the early Earth with organics. The authors ran a hydrodynamic simulation investigating the survival rate of organics during impact. They determined that if the early atmosphere had a higher CO₂ level, organics molecules may have survived impact if the comet made contact with water upon collision with the surface. Chyba et al. (1990) pointed out the fact that the conditions that make cometary delivery favorable as a source of organics on the early Earth are the conditions that are unfavorable for the Miller-Urey type reactions.

It is clear from the above exposition that under both reducing and neutral atmospheric conditions, both H₂CO and HCN could have formed on and/or been delivered to the early Earth. In recent years, dozens of planetary systems have been discovered (Butler et al. 2006). Unfortunately, the techniques used to identify these planetary systems favor the detection of Jupiter-sized objects. Thus, we do not yet know how typical Earth-like planets are in extra-solar systems. However, regardless of whether terrestrial planets in extrasolar systems are like early earth or not, H₂CO and HCN can always be delivered to these planets by cometary delivery. It is this particular scenario that would benefit most from a normal to high abundance of H₂CO in the parent molecular cloud, since the comets and asteroids that would form directly from the protoplanetary disk would, in turn, directly reflect the cloud's chemical composition. Thus, sufficient abundance of these molecules in the parent molecular clouds would be an important consideration for the formation of life in the planets that would subsequently form.

The above arguments have described at length the importance of H₂CO and HCN to prebiotic chemistry on early Earth. Thus, for the formation of life as we know it in the outer Galaxy, an optimal situation would include fairly abundant concentrations of H₂CO and HCN in the molecular clouds that give birth to the planetary systems out there. In the next section, we discuss the previous surveys for H₂CO and HCN and our own survey of these molecules in the outer Galaxy.

CHAPTER 4

OBSERVATIONS

4.1 REVIEW OF PREVIOUS H₂CO AND HCN OBSERVATIONS

Formaldehyde was the first polyatomic organic molecule detected in the ISM (Synder et al., 1969). It is detected more readily in the Galaxy than other species like NH₃ or HCN (Zuckerman, 1970) but not as easily as CO or OH, and it is thought to follow the general distribution of CO (Few, 1979). There are no extensive surveys of H₂CO in any region of the Galaxy. Few (1979) observed the 4.83 GHz transition of H₂CO for 38 lines of sight along the Galactic plane between longitudes 8° and 60°, and showed that the H₂CO distribution in the inner Galaxy follows that of CO. Zylka et al. (1992) observed the H₂CO 4.83 and 14.5 GHz transitions near the Galactic Center between the longitudes of 0.5° and 4°. Dieter (1973) detected the H₂CO 4.83 GHz line in 73 Lynds (1962) dark clouds with $90^\circ \leq l \leq 270^\circ$ predominately within the Galactic plane.

Formaldehyde was detected in a sample of higher Galactic latitude, small, local molecular clouds by Heithausen et al. (1987) and Turner (1993). Several groups (Liszt and Lucas 1995, and references therein), have observed H₂CO absorption against extra-galactic radio continuum sources, again, mostly at high latitude. Most recently, Rodriguez et al. (2006) conducted a blind survey of the 4.83 GHz line toward the Galactic anticenter in the range $-1^\circ \leq b \leq +1^\circ$. The authors had a 10% detection rate in 143 lines of site in molecular clouds thought to reside in the

nearby Perseus spiral arm. This survey and all the previous ones cover clouds with R_G no greater than 10-11 kpc. Prior to the results of this thesis, there was no systematic search for H_2CO in GMCs of the far outer Galaxy.

For HCN, the situation is even more severe: no systematic Galactic surveys have been made, so it is not clear whether or not HCN follows the CO distribution. Surprisingly, surveys of HCN in other galaxies are more common (e.g. Nguyen-Q-Rieu et al. 1992, Papadopoulos et al. 2008). In general, HCN observations of objects in the Milky Way tend to focus on individual star-forming regions rather than broad surveys to determine the overall distribution. For example, Burov et al. (1982) observed 19 dark clouds in the 1st and 2nd quadrants in the 3.4 mm HCN line and the continuum, and detected the HCN (1-0) line in 9 of the sources. Churchwell et al. (1984) observed HCN (1-0), HNC (1-0) and HC_3N (2-1 and 10-9) at 9 positions, 6 in the Taurus dark cloud complex, a Lynds dark cloud (L183), and 2 warm clouds associated with HII regions. These examples are not meant to be exhaustive but rather to indicate how HCN observations are typically used. Recently, HCN (1-0) observations have undergone somewhat of a renaissance as the transition may be best suited to identify the denser regions of a molecular cloud where star formation is almost sure to occur (e.g., Narayanan et al. 2008).

4.2 THE EXCITATION OF H_2CO

A rigid molecule with arbitrary shape can be viewed as rotating about an axis that is the superposition of the 3 free rotations about each of the 3 principal axes of the inertial ellipsoid of the molecule. If the moments of inertia about all 3 principal axes are equal, the molecule is considered to be a spherical top. If 2 of the principal axes are equal, it is a symmetric top, and if all are unequal it is an asymmetric top molecule. Formaldehyde is considered a planar

asymmetric top. The moments of inertia about the three axes are $A > B > C$ where the orientations of the axes are shown in Figure 4-1. Because moments of inertia B and C are almost the same in magnitude, the energy-level structure is typical of an almost prolate symmetric top molecule.

Each of the levels of H₂CO has to be characterized by 3 quantum numbers. The usual designation is $J_{K_a K_c}$, where J is the total angular momentum, K_a is the component of J along the A axis, and K_c is the component along the C axis. A prolate symmetric top has J and K_a as good quantum numbers, an oblate symmetric top has J and K_c , and intermediate states like formaldehyde have superpositions of the 2 descriptions.

Molecules that contain identical nuclei may undergo exchange processes by a mechanism like axis rotation, and if the interchange involves fermions, then certain selection rules must be followed. The symmetry of the spin wavefunction depends on the orientation of the spin and is *ortho*- if the wavefunction is symmetric and *para*- if antisymmetric. In the case of H₂CO, a rotation about the A axis will exchange two protons, but not change the molecule itself. If the proton spins are parallel, the molecule is in the *ortho*- configuration and if they are anti-parallel, the molecule is in the *para*- configuration. The ratio of *ortho*-H₂CO to *para*-H₂CO is 3 based on the number of orientations that can be assumed by the parallel case (3) or the antiparallel case (1). Energy can only be transferred between levels within either *ortho*- or *para*- forms. In H₂CO, the 4.83 GHz and the 140.8 GHz lines are emitted from *ortho*- species where $K_a = 1$ (Rohlfs and Wilson 2006). A schematic energy level diagram is shown in Figure 4-2, where the energy axis is not to the correct scale for H₂CO. A scaled energy level diagram can be found in Mangum and Wooten (1993).

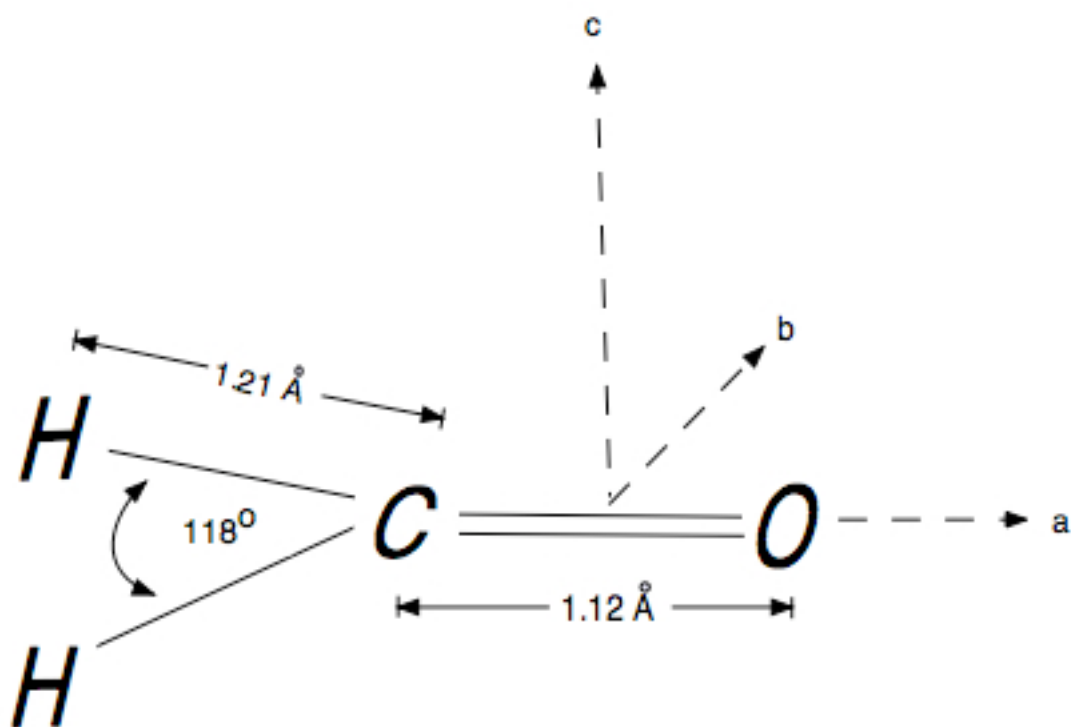


Figure 4-1 Structure of the H₂CO molecule adapted from Rohlf's and Wilson (2006). (Not to scale).

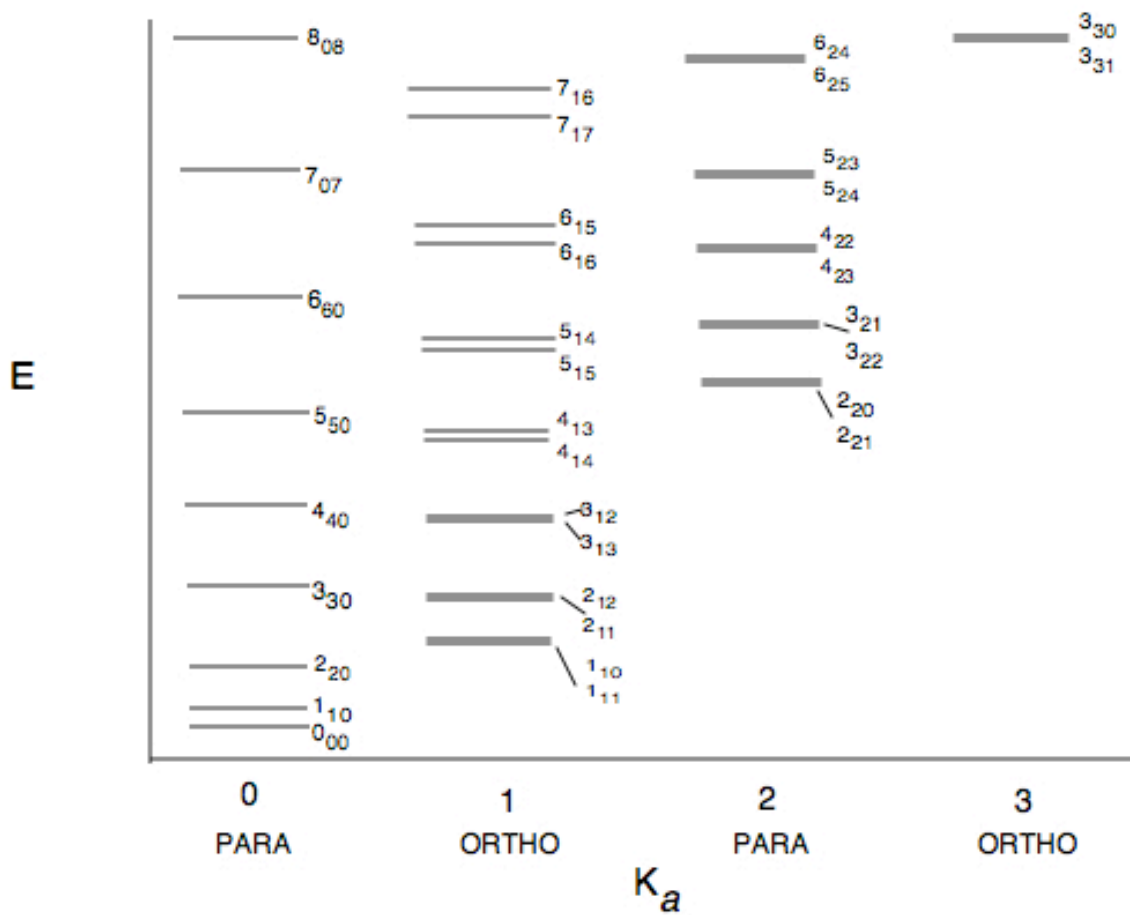


Figure 4-2 Diagram of energy levels in formaldehyde; adapted from Rohlfs and Wilson (2006).

The 6 cm ($1_{11}-1_{10}$) and the 2 cm ($2_{12}-2_{11}$) H_2CO transitions may exhibit anomalous excitation when observed towards molecular clouds with densities less than 10^6 cm^{-3} . In this scenario, the lines appear in absorption against the cosmic microwave background radiation (CMBR) rather than in emission. Townes and Cheung (1969) proposed a nonthermal mechanism to explain the excess population in the $J = 1,2$ states necessary to produce absorption lines. In this model, collisions between the H_2CO and H_2 molecules would populate the lower level of the 2 cm doublet (2_{12}) state and it would rapidly decay to the lower level of the 6 cm (1_{11}) doublet state, giving both lower levels of the doublets greater than equilibrium populations. This implies the excitation temperature for both of the transitions would be below the CMBR temperature, and the lines would be observed in absorption according to the radiative transfer equation in the Rayleigh –Jeans approximation:

$$T_B = (T_{\text{ex}} - T_{\text{BG}})(1 - e^{-\tau})$$

where T_B is the brightness temperature of the line, T_{ex} is the excitation temperature of the transition, T_{BG} in this case is the temperature of the CMBR, and τ is the optical depth of the transition. At densities $\geq 10^6 \text{ cm}^{-3}$ for the 6 cm line and somewhat less for the 2 cm line, collisions with H_2 molecules are frequent enough to thermalize the level populations and the lines will appear in emission. Thus, as the density increases from 10^3 cm^{-3} , these 2 transitions appear as weaker and weaker absorption lines, eventually become undetectable, and then appear in emission. Density is clearly an important factor in determining the excitation behavior of the 6 cm and 2 cm H_2CO transitions (Evans et al. 1975). In contrast, the 140.8 and 225.6 GHz transitions are rotational transitions and are populated in the usual manner by collisions so that the lines appear in emission.

4.3 THE H₂CO OBSERVATIONS

To study the extent of H₂CO in the outer Galaxy, 70 molecular clouds were selected from 3 distinct catalogs as follows:

(1) The Wouterloot and Brand (1989) catalog of IRAS²¹ sources beyond the Solar Circle. The IRAS sources are located primarily in the second and third quadrants of the Galaxy. The IRAS sources were subsequently surveyed for CO emission which, in most cases, was detected (1077 out 1302 sources).

(2) The Digel, de Geus, and Thaddeus (1994) compilation of 11 molecular clouds in the extreme outer Galaxy ($18 < R_G < 28$ kpc). As described in Chapter 2, these sources were selected on the basis of their association with large HI regions.

(3) The Bronfman, Nyman, and May (1996) catalog of CS (2-1) emission towards IRAS sources in the galactic plane. This latter survey differs from the Wouterloot and Brand (1989) survey in that the CS (2-1) line traces denser molecular gas than the CO (1-0) line and this catalog includes full coverage of the first quadrant.

From these 3 sources, candidates were selected on the basis of kinematic distance from the Galactic Center (the farther the object, the more preferable for our purposes), CO (1-0) line strength, and galactic longitude and sidereal time considerations. Of the 70 GMCs observed, 59 are from the Wouterloot and Brand (1989) catalogue, 5 are from Digel et al. (1994) survey, and 6 are from the Bronfman et al. (1996) survey. The 70 GMCs from the 3 sources described above cover a range in R_G between 8.5 and 23.5 kpc, and a total of 75 lines of sight were observed.

²¹Infrared Astronomical Satellite (Low et al. 1984).

Sixty-nine of the clouds are at $R_G \geq 12$ kpc, with only one cloud WB89-002 at $R_G \approx 8.6$ kpc being relatively close to the Sun. The position of all the observed lines of sight are listed in Table 4-1, and histograms of the galactocentric distribution of all clouds and detections are shown in Figure 4-3. The positions of all lines of sight are displayed in Figure 4-4 where the Galactic Center is the purple square in the center, the Sun is shown by a green asterisk, and the Perseus spiral arm and the Outer spiral arm are shown in purple. Figure 4-5 shows all of the sources with the Sun in the center (green circle). In Table 4-1, the first column gives the name of the cloud; columns 2, 3, and 4 list the galactic longitude and latitude of the object and its R_G ; columns 5, 6, and 7 list the radiation temperature T_R^* , line width (Full Width at Half Maximum, FWHM), and velocity with respect to the LSR of the line emission (for the lines of sight with detections). Finally, the last column gives the rms noise level for each observation. Some clouds were observed at another position besides the one from the Wouterloot and Brand (1989) catalogue (designated by an “a” at the end of the source name). The “a” positions were chosen by looking for the most intense dust emission from the cloud in question by way of Finkbeiner et al. (1999) dust maps. In Table 4-1, kinematic distances are listed even though, as has been discussed in Chapter 2, these distance determinations may be subject to large uncertainties. Toward each object, the $2_{12}-1_{11}$ transition of ortho- H_2CO was observed at 140.8 GHz with the Arizona Radio Observatory 12 m millimeter-wave telescope on Kitt Peak, Arizona, during May and November of 2005²².

The $2_{12}-1_{11}$ transition of H_2CO was chosen despite its fairly high critical density because at the 12 m telescope, the angular resolution at this frequency is 44". For a cloud at a distance of 10 kpc, this corresponds to a linear size of 2 pc. To maximize velocity coverage, all of the

²²The 12 meter millimeter wave radio telescope is operated by the Arizona Radio Observatory, Steward Observatory, University of Arizona.

Table 4-1 H₂CO (2₁₂-1₁₁) Observations at 140.8 GHz of Outer Galaxy Giant Molecular Clouds.

<i>Source</i>	<i>l</i>	<i>b</i>	<i>R_G</i>	<i>T_R[*]</i>	Δv	<i>v_{LSR}</i>	<i>rms</i>
	degrees	degrees	Kpc	K	km s ⁻¹	km s ⁻¹	K
WB002	85.41	3.74	8.6	0.114	1.54	-2.75	0.025
WB006	86.27	3.21	14.9	0.163	2.71	-91.38	0.019
WB013	88.21	3.27	15.3	-----	-----	-----	0.028
WB013I	87.61	3.49	15.3	-----	-----	-----	0.029
WB014	88.99	3.45	15.5	0.081	2.00	-96.03	0.013
WB031	88.06	-0.02	14.6	0.099	1.21	-89.40	0.011
WB035	89.94	1.45	13.4	0.175	2.16	-77.68	0.010
WB040	90.68	1.78	12.1	0.145	1.90	-62.65	0.020
WB040A	91.11	1.56	12.1	-----	-----	-----	0.020
WB059	92.90	1.93	14.3	-----	-----	-----	0.025
WB060	95.06	3.97	14.0	0.362	2.78	-84.29	0.025
WB066	95.59	3.90	13.9	-----	-----	-----	0.008
WB076	95.25	2.40	15.7	0.243	2.04	-97.17	0.026
WB080	95.45	2.18	13.1	0.191	2.50	-74.24	0.018
WB083	96.08	2.56	15.3	0.172	1.46	-93.77	0.015
WB098	98.51	3.31	14.8	-----	-----	-----	0.013
WB145	102.64	3.76	14.8	-----	-----	-----	0.009
WB152	104.01	4.20	14.8	0.087	2.05	-88.13	0.012
WB283	114.27	2.02	16.5	0.210	1.30	-94.49	0.026
WB288	114.34	0.79	17.5	0.113	1.31	-100.87	0.026
WB315	117.98	1.66	17.1	0.023	3.77	-95.09	0.012
WB361	122.60	1.64	18.2	-----	-----	-----	0.033
WB361I	122.79	2.53	18.2	-----	-----	-----	0.033
WB365	123.08	1.36	17.2	-----	-----	-----	0.033
WB379	124.56	2.53	17.3	0.204	2.21	-89.32	0.011
WB380	124.65	2.54	17.0	0.457	3.46	-86.67	0.018
WB391	125.81	3.05	16.9	0.277	2.32	-86.06	0.016
WB398	128.11	1.93	17.4	-----	-----	-----	0.018
WB399	128.78	2.01	16.8	0.354	1.68	-82.19	0.028
WB434	135.99	0.67	17.9	-----	-----	-----	0.012
WB437	135.28	2.80	16.2	0.456	2.81	-71.72	0.014
WB438	136.35	0.82	16.9	-----	-----	-----	0.012
WB440	135.63	2.76	16.4	0.055	2.21	-72.20	0.014
WB453	133.40	8.88	20.2	-----	-----	-----	0.028
WB501	145.20	2.99	16.4	0.246	2.55	-58.44	0.028
WB523	149.04	1.28	19.0	-----	-----	-----	0.013
WB529	149.59	0.90	17.8	0.107	1.73	-60.08	0.014
WB540	151.23	1.02	19.7	-----	-----	-----	0.017
WB572	156.90	0.21	20.4	0.252	0.60	-48.23	0.028
WB621	168.06	0.82	22.6	0.629	2.58	-25.38	0.023

<i>Source</i>	<i>l</i>	<i>b</i>	R_G	T_R^*	Δv	v_{LSR}	<i>rms</i>
WB625	168.68	1.09	17.8	0.116	1.82	-25.98	0.018
WB629	170.82	0.00	16.4	0.054	2.72	-16.83	0.014
WB636	166.26	3.55	19.0	0.173	1.38	-24.37	0.016
WB640	167.06	3.46	18.4	0.382	2.37	-25.42	0.012
WB656	171.26	2.54	21.9	0.108	1.64	-10.53	0.012
WB658	171.14	2.76	21.8	-----	-----	-----	0.011
WB670	173.02	2.38	23.5	0.317	1.71	-17.57	0.013
WB705	174.74	3.72	21.4	0.226	1.03	-12.10	0.012
WB730	184.00	1.83	23.1	0.109	5.87	10.10	0.018
WB745	182.03	4.39	21.0	-----	-----	-----	0.012
WB789	195.82	-0.57	20.3	0.174	1.82	34.33	0.028
WB793	195.82	-0.21	18.1	0.369	2.02	30.48	0.016
WB794	195.65	-0.11	17.8	0.133	3.59	30.06	0.020
WB847	209.08	-1.95	16.5	0.196	1.62	49.98	0.013
WB898	217.62	-2.62	16.4	0.244	2.77	63.41	0.013
WB904	211.04	1.18	17.0	0.091	2.15	55.16	0.013
WB910	212.19	1.31	15.9	0.237	1.98	51.07	0.014
WB1000	234.72	-0.92	15.1	-----	-----	-----	0.012
WB1012	239.34	-2.74	15.4	0.128	2.02	83.33	0.015
WB1023	238.77	-1.81	16.4	-----	-----	-----	0.023
WB1074	250.01	-3.34	16.5	-----	-----	-----	0.039
WB1103	255.55	-2.52	17.5	-----	-----	-----	0.031
DdGT01	131.38	1.79	22.0	-----	-----	-----	0.029
DdGT01a	131.14	1.39	22.0	-----	-----	-----	0.028
DdGT02	137.75	-0.98	17.0	-----	-----	-----	0.025
DdGT04a	145.05	-0.10	19.0	-----	-----	-----	0.011
DdGT04b	145.40	-0.10	20.0	-----	-----	-----	0.016
DdGT05	145.30	-0.25	18.0	-----	-----	-----	0.015
DdGT07	148.90	0.90	18.0	-----	-----	-----	0.028
20321+4112	80.351	0.72	12.2	0.062	6.87	-65.64	0.009
20243+3853	77.605	0.56	12.9	0.356	2.95	-73.06	0.013
19383+2711	62.575	2.39	13.2	0.215	5.69	-66.85	0.010
19423+2541	61.719	0.86	13.6	0.385	3.93	-72.62	0.014
19489+3030	66.609	2.06	13.0	0.132	2.10	-68.91	0.013
19571+3113	68.146	0.92	12.2	0.043	8.70	-62.48	0.011

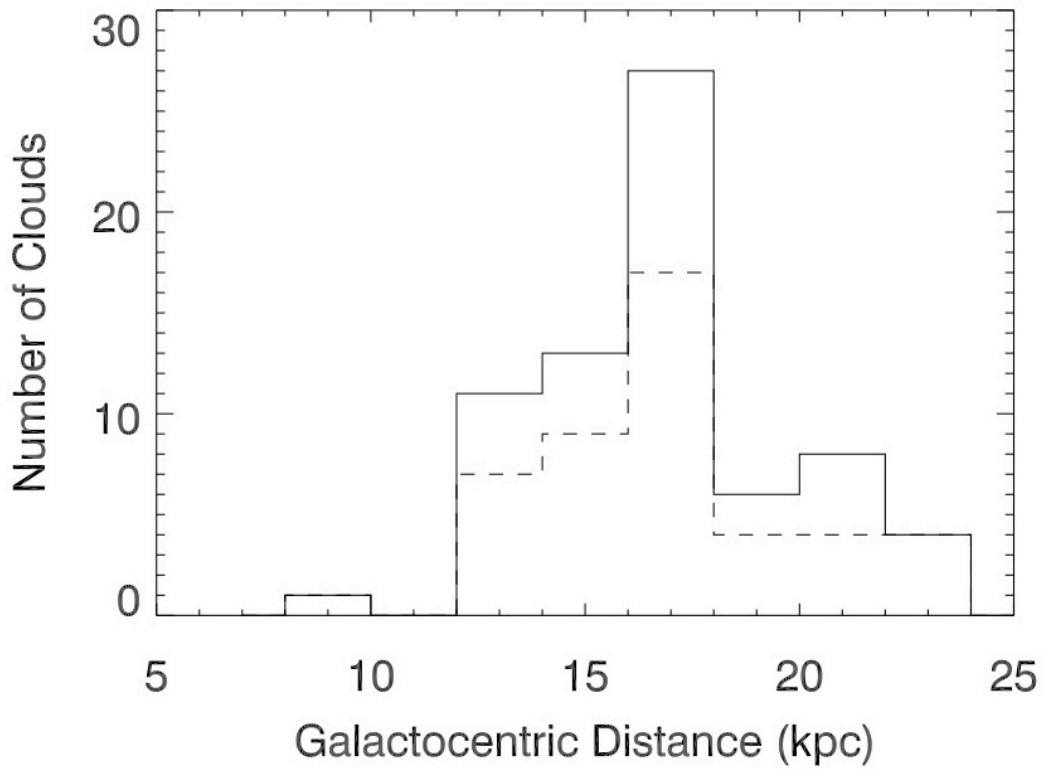


Figure 4-3 Histogram of the galactocentric distribution of the observed clouds. The distance is the kinematic distance and is in units of kpc. The total number of clouds (70) is represented by the dark line and detections (46) by the dashed lines.

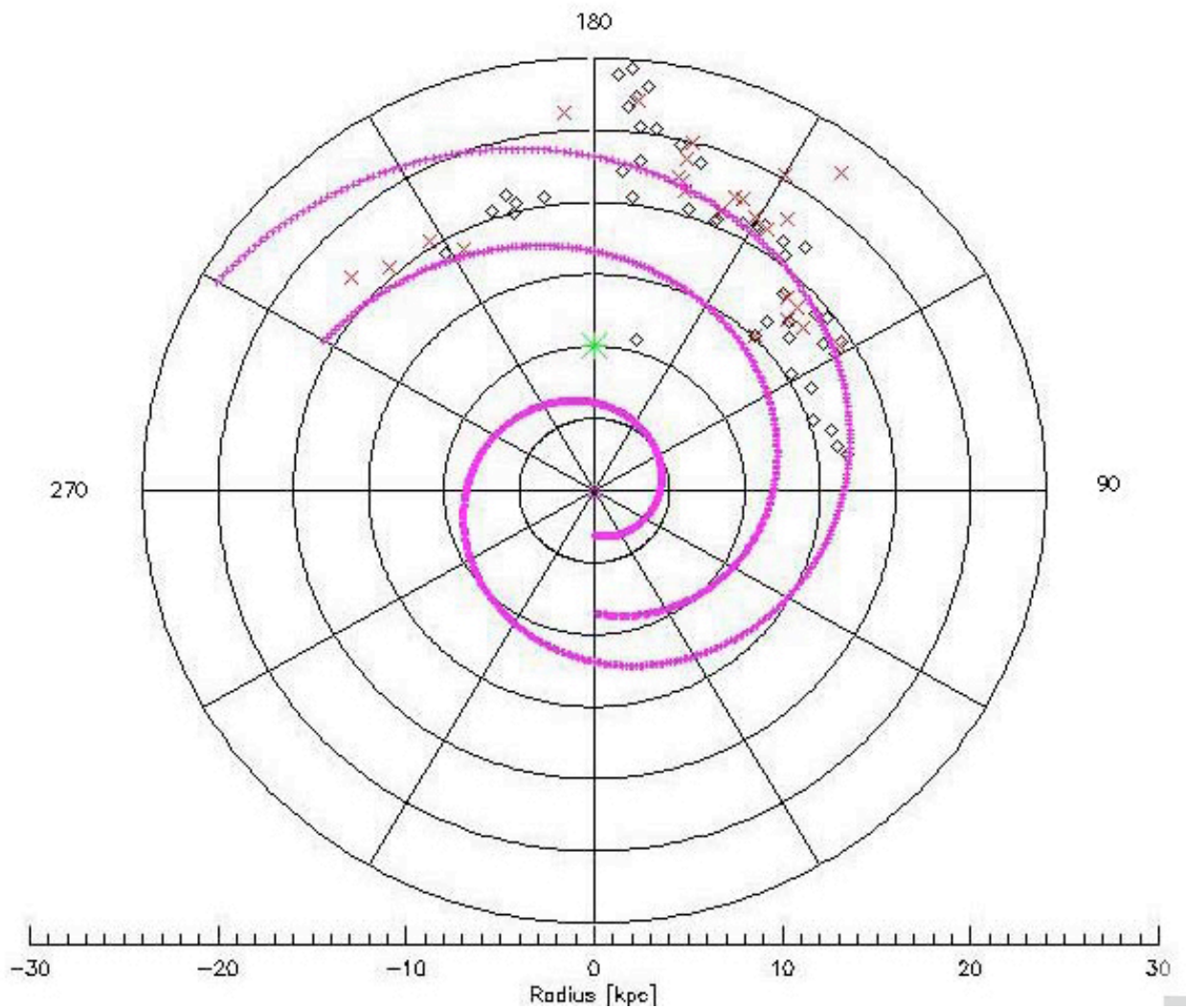


Figure 4-4 Diagram of all sources observed at 140.8 GHz. Black diamonds represent detections and red X's represent non-detections. The Galactic Center is in the center of the plot, and the Sun is shown as a green asterisk. The longitude is indicated along the respective axes. Each concentric circle is 4 kpc in radius from the next one. Spiral arms were calculated based on Vallee 2005.

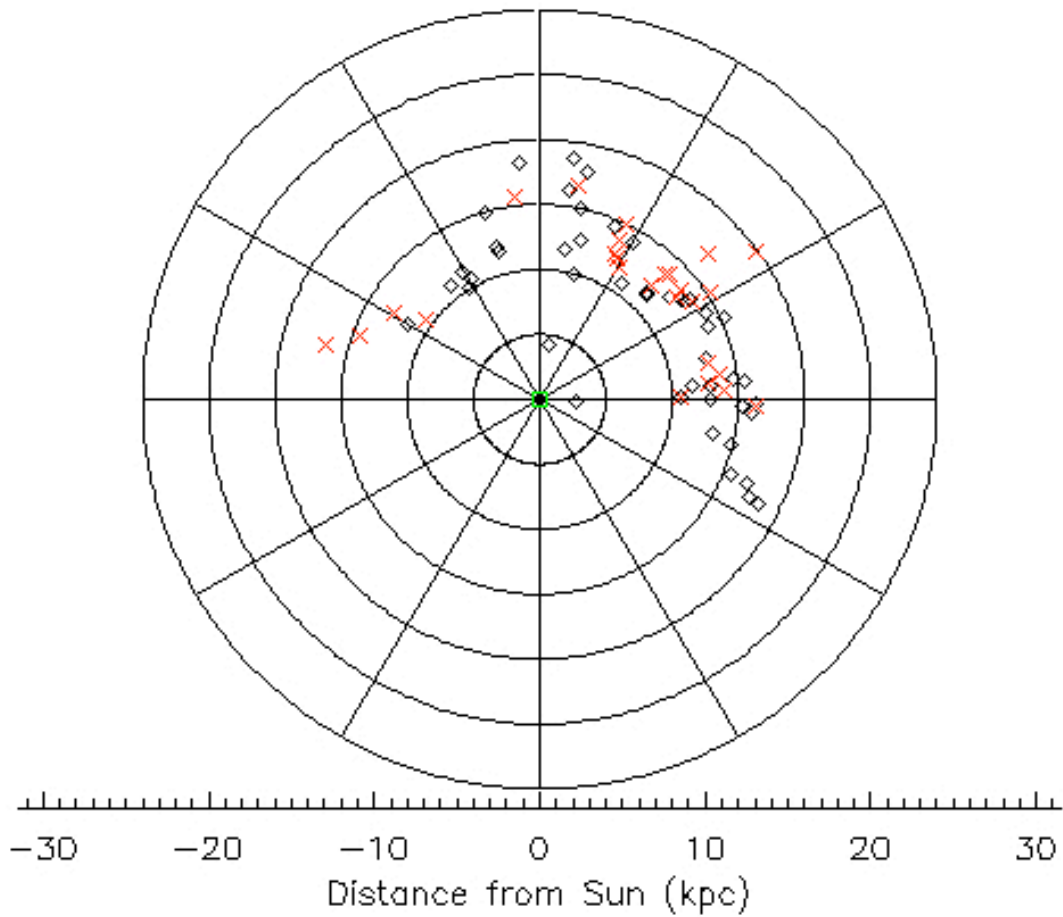


Figure 4-5 Diagram of all sources observed at 140.8 GHz. Black diamonds represent detections and red X's represent non-detections. The Sun is shown as a green circle in the center of the plot. Each concentric circle is 4 kpc in radius from the next one.

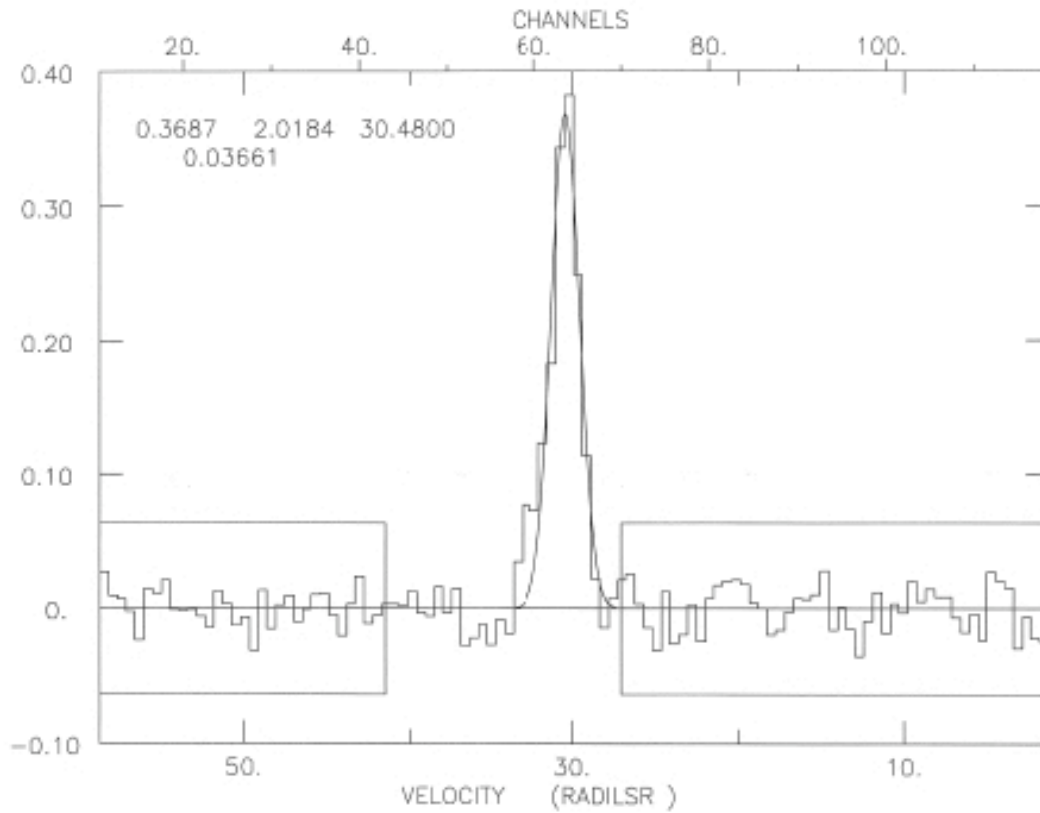
observations were made in position-switched mode with the off position chosen to be 1° east or west of the source in azimuth. The 100 kHz and 250 kHz filter banks were chosen to provide velocity coverages of 27 and 68 km s^{-1} respectively, and velocity resolutions of 0.21 and 0.53 km s^{-1} . Because many of the lines of sight had CO emission at 2 or even 3 different velocities (see Digel et al. 1994), the filter banks were centered at the Local Standard of Rest (LSR)²³ velocity of the molecular cloud with the greatest R_G .

At the 12 m telescope, the H_2CO line antenna temperature (T_A^* see Kutner and Ulrich, 1981) is corrected for spillover and scattering efficiency of the antenna, η_{fss} , so that the resulting quantity is T_R^* , the radiation temperature uncorrected for the antenna-source coupling efficiency, η_C . For the 12 m telescope at 140.8 GHz, η_C is approximately 0.7 (Apponi et al. 2006). Another correction is for the beam dilution which we assume to be equal to 1 (in other words, we assume the source fills the beam completely).

Typical rms noise values per channel in the 250 kHz filter banks ranged from 10 to 30 mK. The stronger H_2CO lines were integrated for shorter periods of time because the primary emphasis in the initial phase of the project was the detection and identification of those molecular clouds in the outer Galaxy that are good subjects for multi-transition H_2CO studies. The 140.8 GHz spectrum for cloud WB89-793 at $R_G \approx 18.1$ kpc is shown in Figure 4-6 (more spectra can be seen in Appendix A).

Of the 75 lines of sight observed in 70 outer Galaxy molecular clouds at 140.8 GHz, 46 clouds were detected, a detection rate of 66%. A detection rate of 65%, 45 out of 69 clouds, was achieved when excluding WB89-002, a cloud located at $R_G = 8.6$ kpc and the only cloud located

²³LSR is the Local Standard of Rest and refers to the frame of reference where the motion of stars in the local neighborhood averages out to zero. The solar LSR is a point at the distance of the Sun from the Galactic Center that has a circular orbit around the GC. The orbital velocity of the LSR about the Galactic Center is 220 km s^{-1} .



WB793 6 SCANS: 363.03- 365.04 INT= 01:00: 0 DATE: 15 NOV 2005
 1950RADC=06:15:50.0 15:06:09 (06:15:50.0 15:06:09) CAL= 422.7 TS= 289.
 FREQ=140839.52 SYN=1.98754418 VEL= 30.0 DV= -0.53 FR= 250 SB=2

Figure 4-6 Typical spectrum for the H₂CO (2₁₂-1₁₁) transition. The source is WB89-793. The boxes indicate the region where a polynomial was fit and removed from the raw data. The numbers in the upper left represent the parameters of the best-fit Gaussian (shown superimposed on the data). From left to right: T_R*, Δv (FWHM), and centroid velocity with respect to the LSR. The number on the second row is the rms of the fit.

close to the Sun. For objects at $R_G > 16$ kpc, 26 out of 44 clouds were detected, a detection rate of 59%. At $R_G > 20$ kpc, 6 of 11 clouds were detections which is a 55% detection rate, and comparable to the detection rate of the entire ensemble. Figure 4-7 shows a histogram of clouds detected versus those not detected in the 140.8 GHz transition based on galactic longitude.

To better estimate the abundance of H_2CO in the outer Galaxy, a multi-transition study was undertaken which required observations of more than one H_2CO transition. The $1_{11}-1_{10}$ transition at 4.83 GHz is sensitive to lower density gas because of its anomalous excitation (see Evans et al. 1975), but a comparable angular resolution to the 12 m is available only at the Arecibo 305 m telescope which has limited sky coverage. Most of the lines of sight traverse high-density gas regions so that the relatively high critical density of the 140.8 GHz transition should not present a significant handicap. However, it is plausible that some of the nondetections in our survey might be detectable via the 4.8 GHz observations.

The $1_{11}-1_{10}$ transition of ortho- H_2CO at 4.83 GHz was observed in nine sources with the Arecibo Observatory²⁴ 305 m telescope located in Arecibo, Puerto Rico, during September of 2006. Arecibo Observatory has a declination range of $-1^\circ 20'$ to $+38^\circ 02'$, so only a subset of the sources between declinations of $+36^\circ 05'$ and $+1^\circ 19'$ were chosen for observation. Table 4-2 shows the lines of sight observed at 4.83 GHz. The columns in the table represent the same quantities as Table 4-1 with the exception that the antenna temperature, T_A , is related to the brightness temperature T_B , by $T_B = T_A/\eta_B$, where η_B is the beam efficiency of the Arecibo telescope at 4.83 GHz (typically ~ 0.5). Figure 4-8 shows a typical spectrum towards WB89-793, the same cloud shown in Figure 4-6 (more spectra can be seen in Appendix A).

The C-band receiver was used in conjunction with the Interim Correlator with 4 digital filter

²⁴The Arecibo Observatory is part of the National Astronomy and Ionosphere Center, which is operated by Cornell University under cooperative agreement with the National Science Foundation.

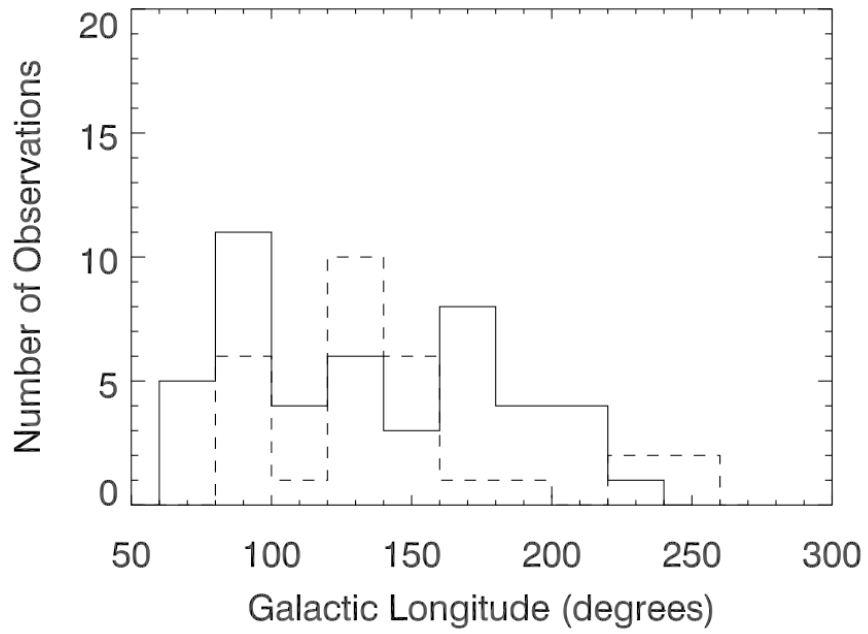


Figure 4-7 Histogram of observations at 140.8 GHz in terms of Galactic longitude. The solid lines represent detections and the dashed lines represent nondetections.

Table 4-2 H₂CO (1₁₁-1₁₀) Observations at 4.83 GHz of Outer Galaxy Giant Molecular Clouds.

<i>Source</i>	<i>L</i>	<i>b</i>	<i>R_G</i>	<i>T_A</i>	$\Delta\nu$	<i>v_{LSR}</i>	<i>rms</i>
	degrees	degrees	kpc	K	km s ⁻¹	km s ⁻¹	K
WB670	173.02	2.38	23.5	-0.348	0.833	-17.57	0.0207
WB705	174.74	3.72	21.4	-0.546	0.543	-12.10	0.0150
WB730	184.00	1.83	23.1	-0.021	0.778	10.10	0.0117
WB745	182.03	4.39	21.0	-0.065	0.295	4.537	0.0157
WB789	195.82	-0.57	20.3	-0.831	0.842	34.11	0.0125
WB793	195.82	-0.21	18.1	-0.299	1.265	31.91	0.0175
WB794	195.65	-0.11	17.8	-0.056	1.046	30.06	0.0128
WB904	211.04	1.18	17.0	-0.555	0.815	55.02	0.0150
WB910	212.19	1.31	15.9	-----	-----	-----	0.0391

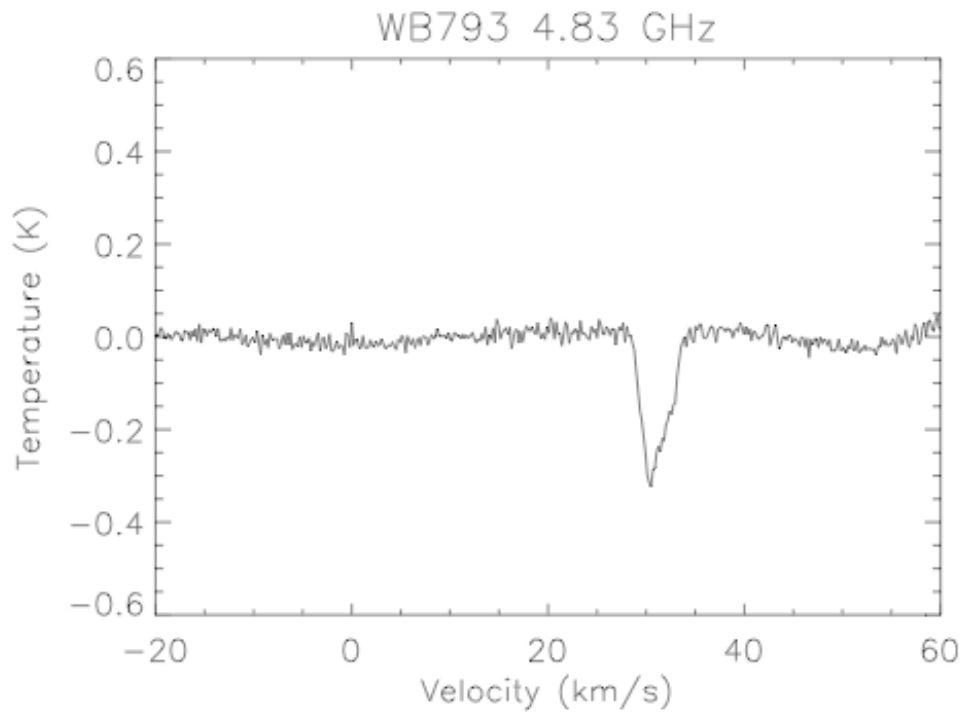


Figure 4-8 Typical spectrum of H_2CO ($1_{11}-1_{10}$) line. The source is WB89-793 (same as Fig. 4-5). No baseline has been removed from the data.

boards. The 9-level, 2 polarization configuration was assumed, and for each filter board, the 3.125 MHz bandwidth with 2048 channels was chosen to get a velocity coverage of 193 km s^{-1} and velocity resolution of 0.19 km s^{-1} . The sources were observed in position-switched mode with the off position chosen to be 1° east or west of the source in azimuth. Typical rms noise values per channel ranged from 10 to 20 mK. For each source, six 5 minute scans were taken for a total integration time of 30 minutes on source. The stability of the receiver was sufficient to permit only “ON” scans to be taken.

The final H_2CO transition observed was the ortho- H_2CO ($3_{12}-2_{11}$) 225.6 GHz line. The 225.6 GHz line was observed towards 15 Wouterloot and Brand (1989) IRAS sources in March and April of 2007 using the James Clerk Maxwell Telescope²⁵ (15 m) at Mauna Kea Observatory, Hawaii. Table 4-3 shows the lines of sight that were observed, and the columns represent the same quantities described in previous tables. The receiver employed was the RxA3 and the back end was the ASCIS digital auto correlation spectrometer. The sources were observed using position switching. The bandwidth was 250 MHz with 8192 channels corresponding to a velocity coverage of 332 km/s and a velocity resolution of 0.04 km/s. Typical rms values ranged from 96 mK to 483 mK. Five points of fifteen were detected.

Figure 4-9 shows the spectrum of the 225.6 GHz transition for cloud WB89-793 (more spectra can be seen in Appendix A). The angular resolution of the JCMT at 225.6 GHz is $22''$, which corresponds to a linear size of 1.06 pc at a distance of 10 kpc.

Eight of the nine positions observed in the 4.83 GHz transition were detected as were five of the fifteen positions observed in the 225.6 GHz transition. The eight 4.83 GHz detections are also detected in the 140.8 GHz line, as are the five of the 225.6 GHz detections.

²⁵The James Clerk Maxwell Telescope is operated by the Joint Astronomy Centre and is located on the summit of Mauna Kea in Hawaii. It is an establishment of the UK Science and Technologies Facilities Council in partnership with the Netherlands and Canada.

Table 4-3 H₂CO (3₁₂-2₁₁) Observations at 225.6 GHz of Outer Galaxy Giant Molecular Clouds.

<i>Source</i>	<i>l</i>	<i>b</i>	<i>R_G</i>	<i>T_R</i> [*]	Δv	<i>v_{LSR}</i>	<i>rms</i>
	degrees	degrees	kpc	K	km s ⁻¹	km s ⁻¹	K
WB060	95.06	3.97	14.0	0.584	0.22	-82.8	0.132
WB076	95.25	2.40	15.7	-----	-----	-----	0.128
WB283	114.27	2.02	16.5	-----	-----	-----	0.136
WB379	124.56	2.53	17.3	-----	-----	-----	0.144
WB380	124.65	2.54	17.0	0.574	0.67	-85.4	0.156
WB391	125.81	3.05	16.9	-----	-----	-----	0.483
WB501	145.20	2.99	16.4	-----	-----	-----	0.237
WB572	156.90	0.21	20.4	-----	-----	-----	0.122
WB621	168.06	0.82	22.6	0.631	0.31	-24.0	0.118
WB640	167.06	3.46	18.4	-----	-----	-----	0.199
WB670	173.02	2.38	23.5	-----	-----	-----	0.215
WB705	174.74	3.72	21.4	-----	-----	-----	0.236
WB793	195.82	-0.21	18.1	0.195	0.41	30.6	0.023
WB898	217.62	-2.62	16.4	0.317	0.59	64.2	0.095
WB910	211.04	1.18	17.0	-----	-----	-----	0.095

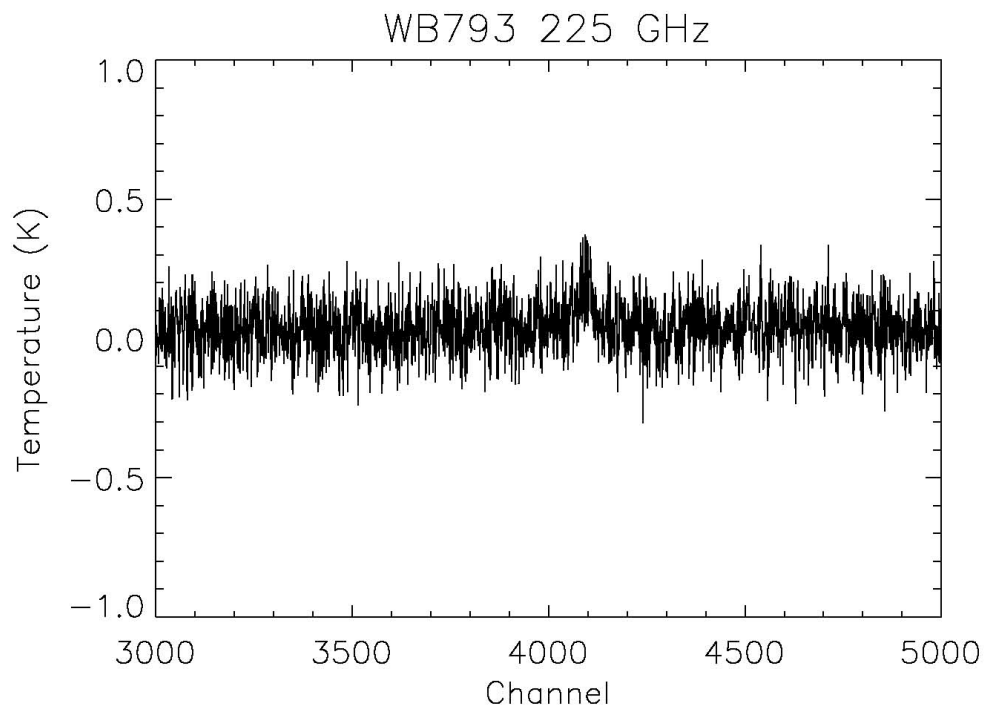


Figure 4-9 Typical spectrum for the H_2CO ($3_{12}-2_{11}$) 225.6 GHz line. The velocity of channel 4096 is 30.6 km s^{-1} . The source is WB89-793.

Table 4-4 Molecular clouds with more than one H₂CO transition observed.

<i>Cloud</i>	$\int T_{140.8} dv$ (K km s ⁻¹)	$\int T_{4.83} dv$ (K km s ⁻¹)	$\int T_{225} dv$ (K km s ⁻¹)
WB 060	1.078	*****	0.137
WB 380	1.694	*****	-0.413
WB 621	1.739	*****	0.213
WB 670	0.579	-0.622	-----
WB 705	0.247	-0.634	-----
WB 730	0.684	-0.017	*****
WB 745	-----	-0.035	*****
WB 789	0.338	-0.041	-----
WB 793	0.796	-1.497	0.002
WB 794	0.510	-0.810	-----
WB 847	0.339	-----	*****
WB 898	0.244	*****	-0.200
WB 904	0.208	-0.967	-----
WB 910	0.501	-----	-----

- Line not detected.

* Cloud not observed in specific transition.

However, only 1 object (WB 793) has detections in all three transitions. Table 4-4 shows the objects that have detections in two or more transitions. We will use these objects to determine the abundance of H₂CO via a Large Velocity Gradient code (See Ch. 5).

4.4 THE EXCITATION OF HCN

HCN is a linear molecule where a hydrogen atom is bonded to a complex ion CN⁻. A single bond exists between the hydrogen and the cyanide ion, which is a carbon triple bonded to a nitrogen atom (see Figure 4-10). The rotational transitions of HCN show hyperfine structure because of the interaction between the magnetic field of the electron and the spin-induced magnetic moment of the nucleus, which is known as the Stark effect. The HCN J=1-0 transition is thus resolved into 3 hyperfine components: F=2-1, F=1-1, and F=0-1, where F refers to the total angular momentum $F = J + I$ which accounts for the nuclear spin I. Figure 4-11 depicts the hyperfine structure of HCN. Rotational excitation of the HCN J=1-0 state will result in a spectrum with three peaks corresponding to the hyperfine splitting. The peaks for the HCN J=1-0 transition are located at 88.630 GHz for F=1-1, 88.631 GHz for F=2-1, and 88.633 GHz for F=0-1. The molecule is excited in the normal way; i.e., by collisions with H₂, and appears in emission from dense gas ($n \geq 10^5 \text{ cm}^{-3}$).

4.5 THE HCN OBSERVATIONS

The HCN (1-0) 88.631 GHz transition was observed towards 46 of the original 70 sources observed in H₂CO with the Arizona Radio Observatory 12 m millimeter-wave telescope on Kitt Peak, Arizona, during March 2008. Table 4-5 lists all of the positions of the observed lines of

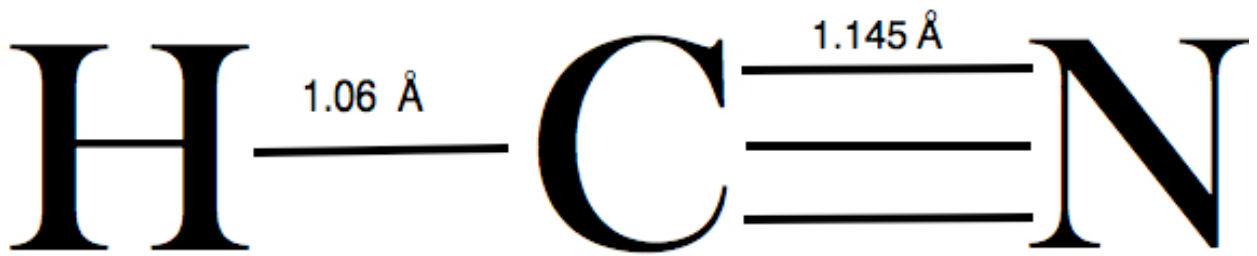


Figure 4-10 The structure of HCN. Bond lengths were calculated from Rao et al. 1996.

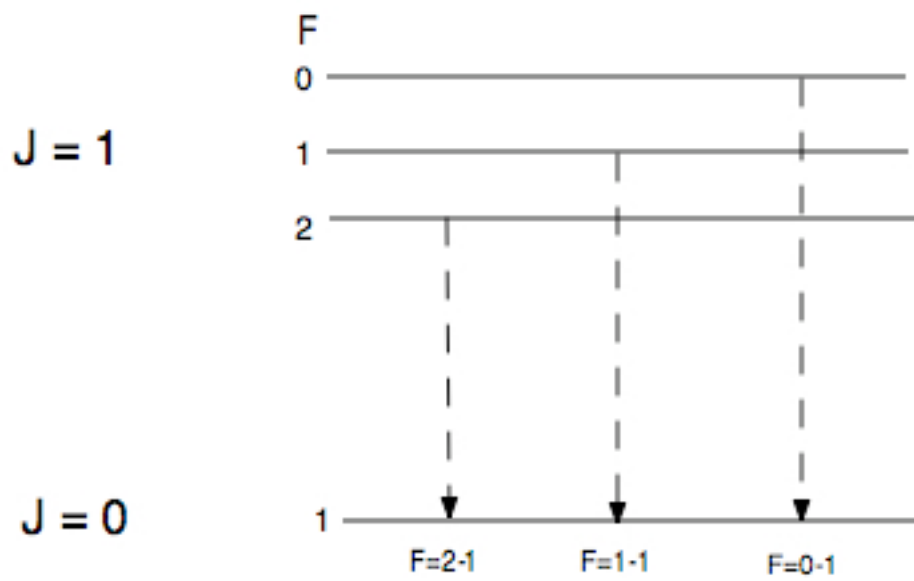


Figure 4-11 Energy level diagram showing the hyperfine splitting of the HCN $J=1-0$ transition.

Table 4-5 HCN (1-0) Observations of Outer Galaxy Giant Molecular Clouds

<i>Source</i>	<i>l</i>	<i>b</i>	R_G	T_R^*	Δv	v_{LSR}	<i>rms</i>
	degrees	degrees	kpc	K	km s ⁻¹	km s ⁻¹	K
WB006	86.27	3.21	14.9	0.129	3.35	-91.48	0.015
WB013	88.21	3.27	15.3	-----	-----	-----	0.017
WB035	89.94	1.45	13.4	0.175	1.87	-77.72	0.010
WB040A	91.11	1.56	12.1	-----	-----	-----	0.019
WB059	92.90	1.93	14.3	-----	-----	-----	0.025
WB060	95.06	3.97	14.0	0.302	3.92	-84.35	0.018
WB066	95.59	3.90	13.9	0.126	3.67	-83.35	0.008
WB076	95.25	2.40	15.7	0.155	3.86	-97.94	0.018
WB080	95.45	2.18	13.1	0.149	2.71	-74.21	0.020
WB098	98.51	3.31	14.8	-----	-----	-----	0.015
WB145	102.64	3.76	14.8	-----	-----	-----	0.019
WB152	104.01	4.20	14.8	0.092	1.64	-88.36	0.012
WB283	114.27	2.02	16.5	0.090	1.71	-94.42	0.020
WB288	114.34	0.79	17.5	-----	-----	-----	0.022
WB315	117.98	1.66	17.1	-----	-----	-----	0.021
WB361	122.60	1.64	18.2	0.112	2.28	-96.21	0.021
WB365	123.08	1.36	17.2	-----	-----	-----	0.044
WB379	124.56	2.53	17.3	0.149	1.99	-89.48	0.017
WB380	124.65	2.54	17.0	0.322	4.25	-86.65	0.015
WB391	125.81	3.05	16.9	0.163	2.21	-85.99	0.024
WB398	128.11	1.93	17.4	-----	-----	-----	0.018
WB399	128.78	2.01	16.8	0.367	2.31	-82.13	0.028
WB434	135.99	0.67	17.9	-----	-----	-----	0.019
WB437	135.28	2.80	16.2	0.445	4.08	-71.21	0.016
WB438	136.35	0.82	16.9	0.145	2.13	-59.46	0.016
WB440	135.63	2.76	16.4	0.084	2.85	-72.04	0.015
WB501	145.20	2.99	16.4	0.218	2.42	-58.29	0.014
WB523	149.04	1.28	19.0	-----	-----	-----	0.014
WB529	149.59	0.90	17.8	-----	-----	-----	0.016
WB540	151.23	1.02	19.7	-----	-----	-----	0.016
WB572	156.90	0.21	20.4	0.069	2.42	-47.76	0.018
WB621	168.06	0.82	22.6	0.421	3.37	-25.51	0.016
WB625	168.68	1.09	17.8	0.300	1.81	-25.83	0.016

<i>Source</i>	<i>l</i>	<i>b</i>	R_G	T_R^*	Δv	v_{LSR}	<i>rms</i>
WB629	170.82	0.00	16.4	0.226	1.75	-17.54	0.016
WB636	166.26	3.55	19.0	0.157	1.54	-24.43	0.016
WB640	167.06	3.46	18.4	0.291	2.26	-24.43	0.016
WB670	173.02	2.38	23.5	0.330	1.89	-17.56	0.018
WB705	174.74	3.72	21.4	0.148	1.73	-17.14	0.016
WB730	184.00	1.83	23.1	0.095	2.11	8.55	0.017
WB745	182.03	4.39	21.0	-----	-----	-----	0.014
WB789	195.82	-0.57	20.3	0.257	2.28	34.32	0.018
WB793	195.82	-0.21	18.1	-----	-----	-----	0.023
WB794	195.65	-0.11	17.8	0.424	3.32	30.43	0.015
WB847	209.08	-1.95	16.5	0.127	1.62	49.86	0.017
WB898	217.62	-2.62	16.4	0.217	2.68	63.35	0.016
WB904	211.04	1.18	17.0	0.164	2.11	55.13	0.023

sight and Figure 4-12 shows the positions of all of the lines of sight observed in the HCN (1-0) transition. Figure 4-13 shows a typical spectrum, WB89-793 (more spectra can be seen in Appendix B). The HCN (1-0) line was chosen because it has a high critical density, $n_{\text{CRIT}} \sim 10^5 \text{ cm}^{-3}$, which is comparable to that of the H_2CO ($2_{12} - 1_{11}$) line at $n_{\text{CRIT}} \sim 10^5 \text{ cm}^{-3}$ (Mangum and Wooten 1993, Narayanan et al. 2008). The angular resolution of the 12 m telescope at this frequency is $70''$, which for an object at 10 kpc, corresponds to a linear size of roughly 3 pc.

In the same manner as the H_2CO observations, all of the observations were made in position-switched mode with the off position chosen to be 1° east or west of the source in azimuth. The 100 kHz and 250 kHz filter banks were chosen to provide velocity coverages of 43 km s^{-1} and 108 km s^{-1} , and velocity resolutions of 0.33 km s^{-1} and 0.84 km s^{-1} . Once again, the filter banks were centered on the LSR velocity of the molecular cloud with the greatest R_G . Each source was integrated for a total of 15 minutes resulting in typical rms noise values per channel in the 250 kHz filter banks ranging from 15 to 50 mK. Of the 46 lines of sight observed in the HCN (1-0) line, 31 were detected – a slightly higher percentage than for the 140.8 GHz line of H_2CO . Of the 31 HCN detections, 28 were also detected in H_2CO .

4.6 CORRELATION BETWEEN H_2CO AND HCN IN THE OUTER GALAXY

The 46 HCN detections can be plotted versus the H_2CO detections for the same line of sight. The integrated line intensities were used and the results is shown in Figure 4-14. A clear correlation exists between the two molecules. A linear fit yields a relationship with a correlation coefficient of 0.80. This means that, for the 28 points, there is less than 1/10th of 1% chance that the correlation arises from an uncorrelated population.

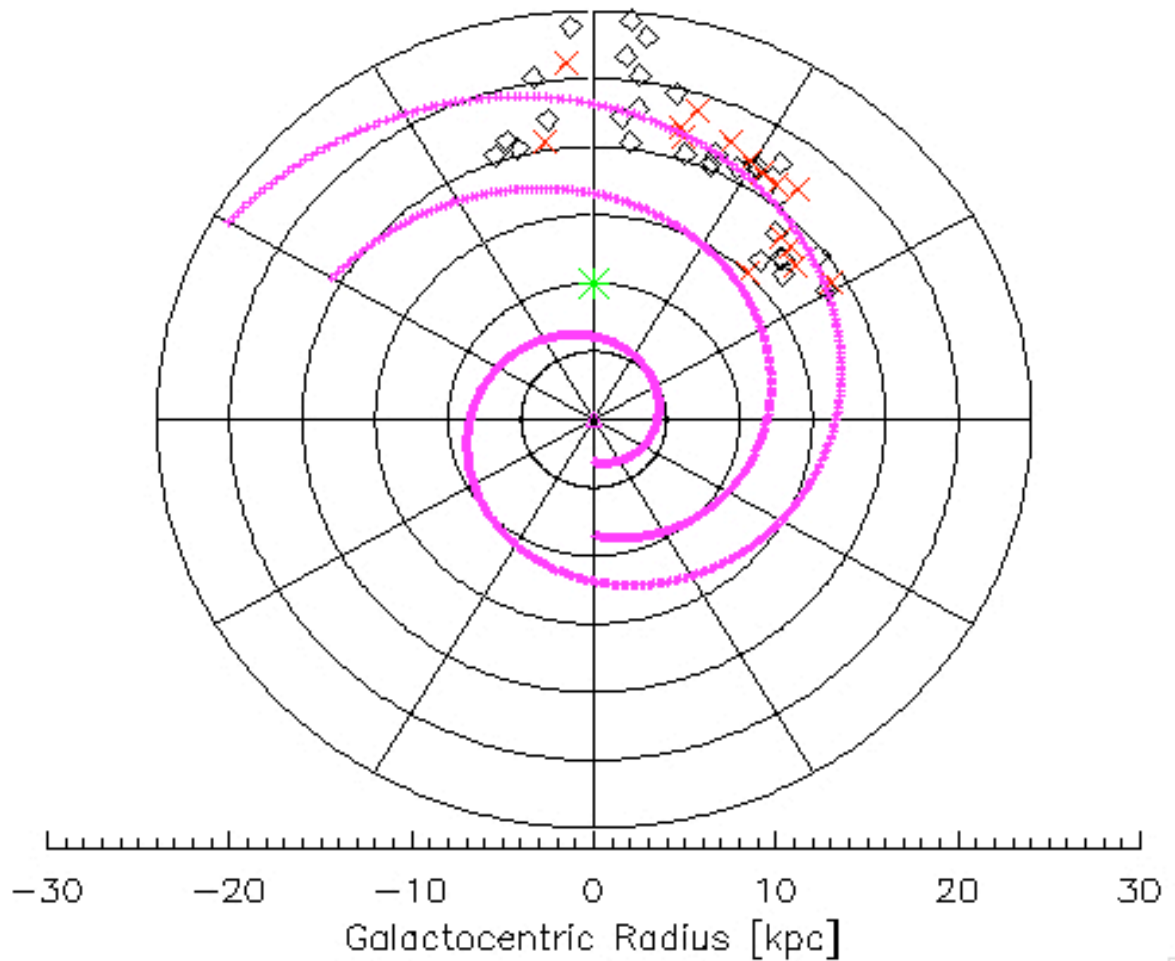


Figure 4-12: Diagram of all sources observed in the HCN (1-0) transition at 88.6 GHz. Black diamonds represent detections and red X's represent non-detections. The Galactic Center is in the center of the plot and the Sun is shown as a green asterisk. Spiral arms were calculated based on Vallee 2005.

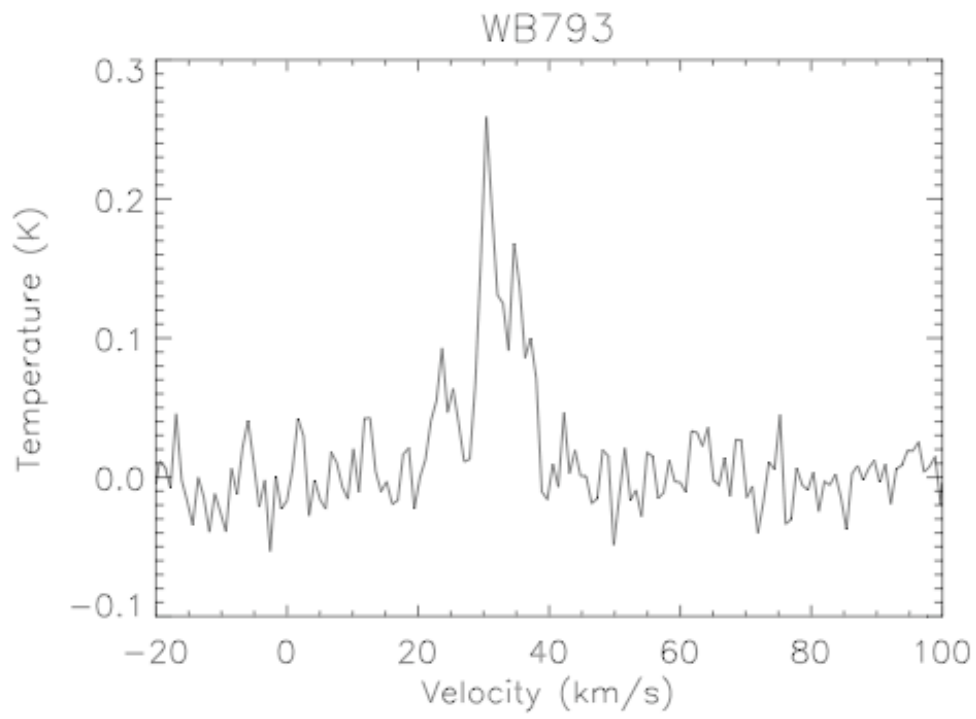


Figure 4-13 Typical HCN (1-0) spectra. The source shown is WB89-793.

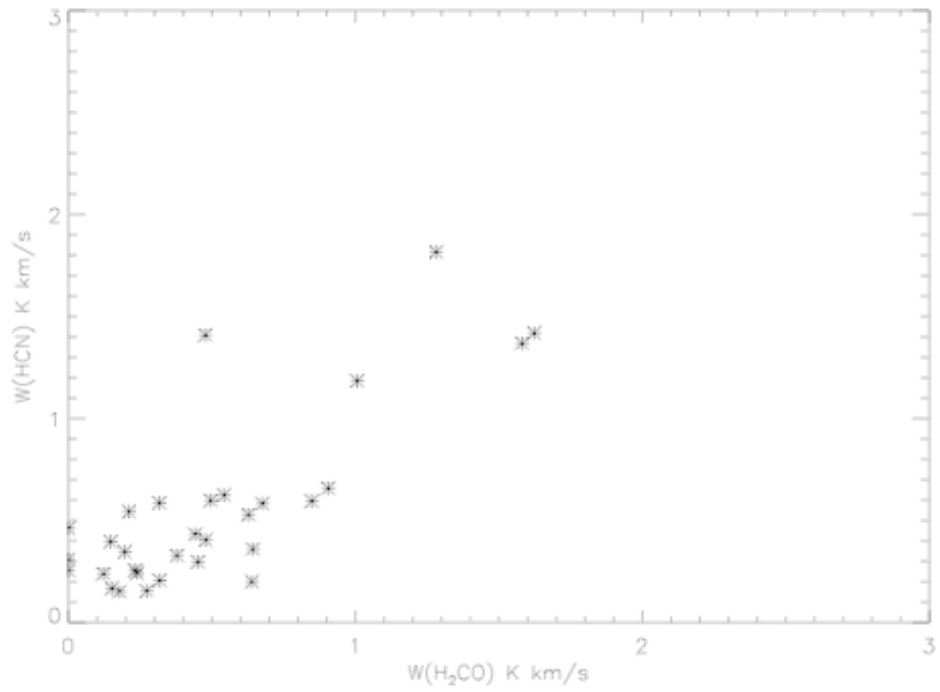


Figure 4-14 The correlation between $W(\text{HCN})$ and $W(\text{H}_2\text{CO})$. Linear fit yielded $W(\text{HCN}) = 0.87W(\text{H}_2\text{CO}) + 0.09$. The correlation coefficient was 0.80 for 28 data points.

The similarity between the two molecules reflects that the two transitions involved (the 140.8 GHz line for H₂CO and the 88.6 GHz line for HCN) both are good tracers of high density molecular gas ($n \geq 10^3 \text{ cm}^{-3}$). The lines of sight selected by Wouterloot and Brand (1989) sample primarily the densest regions of the clouds in question so that the likelihood of finding line emission is good. Of perhaps more importance, the likelihood of HCN having the same decrease in abundance as H₂CO is also good. This aspect of the correlation will be discussed in the next chapter.

CHAPTER 5

THE H₂CO AND HCN ANALYSES

5.1 DERIVATION AND CALCULATION OF THE COLUMN DENSITY OF THE H₂CO TRANSITIONS

To get an estimate of the abundance of H₂CO in outer Galaxy GMCs, column densities²⁶ must first be calculated. In order to derive a relationship between the column density (N_u) and observed line parameters like antenna temperature (T_R^*) and line width ($\Delta\nu$), one must start with the relation between the quantum mechanical absorption coefficient, κ_ν , and the spectral intensity distribution over the line (cf. Lang 1999):

$$\kappa_\nu = [c^2 g_u n_l A_{ul} / (8\pi \nu^2 g_l)] [1 - (g_l g_u^{-1})(n_u n_l^{-1})] \varphi(\nu)$$

where the u and l stand for upper and lower quantum states of the particular transition, g is the statistical weight of the state, n_l is the population in the lower state, n_u is the population in the upper state, A_{ul} is the Einstein A coefficient, c is the speed of light, ν is the transition frequency, and $\varphi(\nu)$ is the line shape.

The optical depth τ_ν is related to κ_ν by

$$\tau_\nu = \kappa_\nu L$$

where L is the path length through the cloud.

Thus

$$\tau_\nu = g_u n_l L \lambda^2 A_{ul} / (g_l) [1 - e^{-h\nu/kT_{\text{ex}}}] \varphi(\nu) / 8\pi$$

²⁶The column density of a species refers to the number of atoms or molecules of a species that would be contained in a hollow tube with a cross-section of 1 cm² stretched from the observer through the object.

where we have used the Boltzmann factor for $(g_l/g_u)(n_u/n_l)$. Note that the column density N is just nL so

$$\tau_\nu = (\varphi(\nu)/8\pi)(g_u N_u \lambda^2 A_{ul}/g_l) [1 - e^{-h\nu/kT_{ex}}].$$

For a Gaussian line shape of full width at half maximum of $\Delta\nu_L$, the line profile can be described in terms of the full width at half maximum, $\Delta\nu_L$ (see Lang 1999):

$$\varphi(\nu) = ((2\ln 2)/\pi)^{1/2} \Delta\nu_L^{-1}.$$

Thus, the optical depth becomes

$$\tau_\nu = (2\ln 2/\pi)^{1/2} \Delta\nu_L^{-1} [g_u N_u \lambda^2 A_{ul}/(g_l 8\pi)] [1 - e^{-h\nu/kT_{ex}}].$$

We assume the transition in question is optically thin so the solution to the radiative transfer equation in this case can be employed:

$$\Delta T_B = (T_{ex} - T_{BG})\tau_\nu.$$

By making a substitution for τ_ν in the above equation we get

$$\Delta T_B \Delta\nu_L / (T_{ex} - T_{BG}) = (2\ln 2/\pi)^{1/2} [g_u N_u \lambda^2 A_{ul}/(g_l 8\pi)] [1 - e^{-h\nu/kT_{ex}}]$$

and we can solve for N_u

$$N_u = (g_l/g_u)(1/A_{ul})(1/\lambda^2)(8\pi^{1/2}/(2\ln 2)^{1/2})[1 - e^{-h\nu/kT_{ex}}]^{-1}(\Delta T_B \Delta\nu_L / (T_{ex} - T_{BG})).$$

Now, $\Delta\nu = (\nu_0/c)\Delta v$ so $\Delta\nu_L = \Delta v/\lambda$, and N_u becomes

$$N_u = (g_l/g_u)(1/A_{ul})(1/\lambda^3)(8\pi^{1/2}/2(\ln 2)^{1/2})[1 - e^{-h\nu/kT_{ex}}]^{-1}(T_{ex} - T_{BG})^{-1} \Delta T_B \Delta v.$$

With this expression, the column density of each of the transitions can be calculated.

The statistical weights are determined by $g = 2J+1$, where J is the angular momentum quantum number for the upper or lower level. The Einstein A coefficient, A_{ul} , represents the transition probability per unit time for spontaneous emission and can be calculated by using the following:

$$A_{ul} = (64\pi^4 \nu_L^3 / 3hc^3) |\mu_J|^2$$

where μ_J is the permanent electric dipole moment of the molecule in units of Debyes. The wavelength, λ , is the wavelength of the photon absorbed or emitted during the rotational transition. The excitation temperature, T_{ex} , is a measure of the population in a level and must be estimated, guessed, or obtained from another source. The brightness temperature, ΔT_B , is the intensity of the source in units of K, and is related to the antenna temperature by $\Delta T_B = T_R^* / \eta_C$, where η_C is a telescope dependent parameter. Finally, the line width or $\Delta\nu$ is the FWHM of the observed spectral line.

For the 4.83 GHz line of H₂CO, after calculating the constants, N_u becomes

$$N_{4.83} = (3.12 \times 10^{12} \text{ s cm}^{-3}) [1 - e^{-h\nu/kT_{ex}}]^{-1} (T_{ex} - T_{BG})^{-1} \Delta T_B \Delta\nu.$$

Because of the peculiar excitation characteristics of the 4.83 GHz transition discussed in Chapter 4, Cohen et al. (1983) suggest using $T_{ex} = 1.7$ K. Other authors use excitation temperatures more similar to the kinetic temperatures of the cloud (10-20K). Results for calculation of $N_{4.83}$ using the above equation for $T_{ex} = 1.7$ K, 10 K, and 20 K are shown in Table 5-1.

For the 140.8 GHz and the 225.6 GHz transitions of H₂CO, the column density equations become

$$N_{140.8} = (3.10 \times 10^{12} \text{ s cm}^{-3}) [1 - e^{-h\nu/kT_{ex}}]^{-1} (T_{ex} - T_{BG})^{-1} \Delta T_B \Delta\nu$$

and

$$N_{225.6} = (2.96 \times 10^{12} \text{ s cm}^{-3}) [1 - e^{-h\nu/kT_{ex}}]^{-1} (T_{ex} - T_{BG})^{-1} \Delta T_B \Delta\nu,$$

respectively. Since these transitions are not expected to experience peculiar excitation, the column density will be calculated at excitation temperatures of 10 K and 20 K. Table 5-2 shows the column density values for the 140.8 GHz transition, and Table 5-3 shows the values for the 225.6 GHz transition.

Table 5-1 Calculation of column density of the 4.83 GHz line of H₂CO in units of cm⁻².

<i>Source</i>	$\Delta T_B \Delta \nu^*$	$N_{4.83}$	$N_{4.83}$	$N_{4.83}$
		$T_{ex} = 1.7 K$	$T_{ex} = 10 K$	$T_{ex} = 20 K$
WB 670	-0.581	1.41×10^{13}	1.08×10^{13}	9.06×10^{12}
WB 705	-0.593	1.44×10^{13}	1.10×10^{13}	9.26×10^{12}
WB 730	-0.033	8.07×10^{11}	6.15×10^{11}	5.16×10^{11}
WB 745	-0.033	9.41×10^{11}	7.17×10^{11}	6.01×10^{11}
WB 789	-0.038	3.41×10^{13}	2.60×10^{13}	2.18×10^{13}
WB 793	-1.398	1.84×10^{13}	1.40×10^{13}	1.18×10^{13}
WB 794	-0.757	2.87×10^{13}	2.19×10^{13}	1.83×10^{13}
WB 904	-0.904	2.21×10^{13}	1.68×10^{13}	1.41×10^{13}

*Units are K km s⁻¹

Table 5-2 Column density values for the 140.8 GHz transition of H₂CO.

<i>Source</i>	$\Delta T_B \Delta \nu^*$	$N_{140.8}^+$	$N_{140.8}^+$
		$T_{ex} = 10 K$	$T_{ex} = 20 K$
WB002	0.251	2.16	1.56
WB006	0.629	5.43	3.92
WB014	0.231	2.00	1.44
WB031	0.171	1.48	1.07
WB035	0.540	4.67	3.37
WB040	0.394	3.40	2.46
WB060	1.439	12.4	8.98
WB076	0.708	6.11	4.42
WB080	0.680	5.88	4.25
WB083	0.357	3.08	2.23
WB152	0.254	2.19	1.59

<i>Source</i>	$\Delta T_B \Delta v^*$	$N_{140.8}^+$	$N_{140.8}^+$
		$T_{ex} = 10 K$	$T_{ex} = 20 K$
WB283	0.389	3.36	2.42
WB288	0.210	1.82	1.31
WB315	0.123	1.06	7.69
WB379	0.642	5.55	4.01
WB380	2.262	19.5	14.1
WB391	0.919	7.94	5.74
WB399	0.850	7.34	5.30
WB437	1.826	15.8	11.4
WB440	0.174	1.51	1.09
WB501	0.893	7.72	5.58
WB529	0.264	2.28	1.64
WB572	0.216	1.87	1.35
WB621	2.322	20.0	14.9
WB625	0.302	2.61	1.88
WB629	0.208	1.79	1.30
WB636	0.341	2.95	2.13
WB640	1.296	11.2	8.09
WB656	0.252	2.17	1.57
WB670	0.773	6.68	4.82
WB705	0.331	2.86	2.06
WB730	0.910	7.87	5.68
WB789	0.451	3.90	2.81
WB793	1.063	9.18	6.63
WB794	0.681	5.89	4.25
WB847	0.453	3.92	2.83
WB898	0.963	8.32	6.01
WB904	0.278	2.41	1.74
WB910	0.669	5.78	4.18
WB1012	0.367	3.17	2.29
20321+4112	0.607	5.25	3.79
20243+3853	1.503	12.9	9.37
19383+2711	1.743	15.0	10.9
19423+2541	2.165	18.7	13.5
19489+3030	0.396	3.43	2.47
19571+3113	0.533	4.61	3.33

* Units are $K \text{ km s}^{-1}$.

+ Column density values are in units of 10^{11} cm^{-2} .

Table 5-3 Calculation of column density of the 225.6 GHz line of H₂CO in units of cm⁻².

<i>Source</i>	$\Delta T_B \Delta \nu^*$	$N_{225.6}$ $T_{ex} = 10 K$	$N_{225.6}$ $T_{ex} = 20 K$
WB 60	0.203	1.25×10^{11}	8.31×10^{10}
WB 380	-0.613	3.76×10^{11}	2.50×10^{11}
WB 621	-0.316	1.94×10^{11}	1.29×10^{11}
WB 793	-0.003	1.87×10^{09}	1.24×10^{09}
WB 898	-0.297	1.82×10^{11}	1.21×10^{10}

*Units are K km s⁻¹.

So far, we have just determined the column density values of each individual transition, not the total column density of the species. In order to estimate the total column density of H₂CO in outer Galaxy GMCs, the partition function must be estimated and included in the calculation

5.2 THE TOTAL COLUMN DENSITY OF H₂CO USING SIMPLISTIC ASSUMPTIONS

The total column density of H₂CO over all of the transitions is given by

$$N_{\text{H}_2\text{CO}} = N(J_{KaKc})Q/(g_u e^{-h\nu/kT_{\text{ex}}}),$$

where $N(J_{KaKc})$ is the column density of a specific transition (Lang 1999). In our analysis, we will use the 2₁₂ - 1₁₁ transition because we have the most data for that line. The statistical weight of the upper level is given by $g_u = (2J+1)$. The rotational partition function, Q , is given by

$$Q = \sum_{J=1}^5 (2J+1) \exp[-E_J/kT_{\text{ex}}],$$

where E_J is the energy of the upper level of the transition above the ground state. For this calculation, we will assume that only the 5 lowest levels of the $K=0$ para-ladder and $K=1$ ortho-ladder are populated. We used the upper level energies for the 72.8 GHz, 140.8 GHz, 211.2 GHz, 281.5 GHz, and 352.8 GHz transitions [see Green (1991) for a tabulation of upper level energies of H₂CO levels] as representative transitions for the 5 lowest populated levels. Using $Q = 2.98$ for $T_{\text{ex}} = 10$ K, and $Q = 6.69$ for $T_{\text{ex}} = 20$ K, and the column density values for the 140.8 GHz transition, the total column density was calculated for each cloud at the two excitation temperatures. To account for the ortho-H₂CO to para-H₂CO ratio, we multiplied the column density by 1.33 (Liszt and Lucas 2006). Total column density values of H₂CO for each cloud detected in the 140.8 GHz line are given in Table 5-4. The column density of H₂ has been included for comparison and was calculated by assuming the X-factor is the same in the

outer Galaxy as in the inner Galaxy [$X = 1.8 \times 10^{20} \text{ cm}^{-2} [\text{K km/s}]^{-1}$] from Dame et al. (2000)], and by using the W_{CO} values calculated for each source by Wouterloot and Brand (1989).

To estimate the fractional abundance of H_2CO to H_2 in outer Galaxy molecular clouds, the total column density of H_2CO was compared to that of H_2 . Table 5-5 contains the estimated abundances for the first 40 of the 46 sources detected in the H_2CO 140.8 GHz transition. The last six sources were not observed in the CO (1-0) transition, so a column density for H_2 could not be determined. The abundances range from 4.32×10^{-11} to 7.06×10^{-10} , and have averages of 1.90×10^{-10} and 2.32×10^{-10} for $T_{\text{ex}} = 10 \text{ K}$ and 20 K , respectively. The H_2CO abundances in GMCs at the Solar Circle is in the range of $5\text{-}8 \times 10^{-9}$ for moderate density clouds (Mundy et al. 1987). Turner (1994) focused primarily on dark clouds in the Galactic plane and determined H_2CO abundances of $0.2\text{--}4.0 \times 10^{-8}$.

The above estimations of the fractional abundance of H_2CO in outer Galaxy clouds suggest that, while H_2CO is present in amounts that are readily detectable, there is at least an order of magnitude decrease in abundance compared to GMCs inside the Solar Circle (Turner 1993). In order to determine more reliable abundances of H_2CO , a multi-transition study was conducted, and a Large Velocity Gradient code was employed and will be discussed in section 5-4.

5.3 THE TOTAL COLUMN DENSITY OF HCN USING SIMPLISTIC ASSUMPTIONS

To calculate the column density of the HCN (1-0) transition, we start with the same formulation we used for H_2CO in section 5.1:

$$N_u = (g_l/g_u)(1/A_{ul})(1/\lambda^3)(8\pi^{1/2}/2(\ln 2)^{1/2})[1 - e^{-h\nu/kT_{\text{ex}}}]^{-1}(T_{\text{ex}} - T_{\text{BG}})^{-1} \Delta T_{\text{B}} \Delta v .$$

For the HCN 88.6 GHz transition, $g_l/g_u = 1/3$ and $A_{ul} = 2.4 \times 10^{-5} \text{ cm}^{-1}$, so the equation becomes

Table 5-4 Total H₂CO column density values using the 140.8 GHz transition.

<i>Source</i>	$N_{H_2CO^+}$	$N_{H_2CO^+}$	$N(H_2)^*$
	$T_{ex} = 10 K$	$T_{ex} = 20 K$	
WB002	3.37	3.90	7.8
WB006	8.47	9.80	6.3
WB014	3.12	3.60	4.6
WB031	2.31	2.67	1.2
WB035	7.29	8.42	5.2
WB040	5.31	6.15	4.1
WB060	19.35	22.44	9.3
WB076	9.53	11.05	5
WB080	9.18	10.62	8.5
WB083	4.81	5.57	2.8
WB152	3.42	3.97	2.8
WB283	5.24	6.05	5.8
WB288	2.84	3.27	3.4
WB315	1.65	19.22	3.7
WB379	8.66	10.02	6.5
WB380	30.43	35.24	11.4
WB391	12.39	14.35	5.2
WB399	11.45	13.25	6.3
WB437	24.65	28.49	14.2
WB440	2.36	2.72	4.1
WB501	12.05	13.95	11.2
WB529	3.56	4.10	4.7
WB572	2.92	3.37	3.8
WB621	31.21	37.24	13
WB625	4.07	4.70	4.8
WB629	2.79	3.25	4.9
WB636	4.60	5.32	3.8
WB640	17.48	20.22	3.2
WB656	3.39	3.92	3.7
WB670	10.42	12.05	7.3
WB705	4.46	5.15	1.7
WB730	12.28	14.20	2.8
WB789	6.09	7.02	5.8
WB793	14.32	16.57	5.9
WB794	9.19	10.62	3.9
WB847	6.12	7.07	1.2
WB898	12.98	15.02	2.5
WB904	3.76	4.35	4.1
WB910	9.02	10.45	3.3
WB1012	4.95	5.72	0.81
20321+4112	8.19	9.47	-----
20243+3853	20.13	23.42	-----
19383+2711	23.41	27.24	-----

<i>Source</i>	$N_{H_2CO^+}$	$N_{H_2CO^+}$	$N(H_2)^*$
	$T_{ex} = 10 K$	$T_{ex} = 20 K$	
19423+2541	29.18	33.74	-----
19489+3030	5.35	6.17	-----
19571+3113	7.19	8.32	-----

+ Column density values are in units of 10^{11} cm^{-2} .

* Units are 10^{21} cm^{-2} .

Table 5-5: Fractional abundance of H₂CO to H₂ in outer Galaxy GMCs.

<i>Source</i>	<i>Abundance</i> $\times 10^{-11}$ $T_{ex} = 10 K$	<i>Abundance</i> $\times 10^{-11}$ $T_{ex} = 20 K$
WB002	4.32	5.00
WB006	13.45	15.55
WB014	6.78	7.82
WB031	19.24	22.29
WB035	14.01	16.20
WB040	12.94	15.00
WB060	20.81	24.13
WB076	19.07	22.09
WB080	10.79	12.50
WB083	17.16	19.91
WB152	12.20	14.19
WB283	9.04	10.43
WB288	8.35	9.63
WB315	4.47	51.95
WB379	13.32	15.42
WB380	26.69	30.91
WB391	23.83	27.59
WB399	18.18	21.03
WB437	17.36	20.07
WB440	5.75	6.64
WB501	10.76	12.45
WB529	7.57	8.72
WB572	7.68	8.88
WB621	24.01	28.65
WB625	8.48	9.79
WB629	5.70	6.63
WB636	12.11	14.01
WB640	54.61	63.19
WB656	9.15	10.61
WB670	14.28	16.50
WB705	26.25	30.29
WB730	43.86	50.70
WB789	10.49	12.11
WB793	24.28	28.09
WB794	23.57	27.24
WB847	50.97	58.94
WB898	51.93	60.08
WB904	9.17	10.61
WB910	27.33	31.66
WB1012	61.07	70.66

$$N_{(J=1-0)} = (9.67 \times 10^{11} \text{ s cm}^{-3}) [1 - e^{-h\nu/kT_{\text{ex}}}]^{-1} (T_{\text{ex}} - T_{\text{BG}})^{-1} \Delta T_{\text{B}} \Delta \nu .$$

Table 5-6 shows the column density values for sources detected in the HCN (1-0) transition for 10 and 20 K.

When comparing the column density values of the 88.6 GHz line of HCN to the 140.8 GHz line of H₂CO, only WB625, WB629, and WB794 have higher column density values for the 88.6 GHz line of HCN. The remaining sources detected in both lines show higher column densities for the 140.8 GHz H₂CO line consistently. The column density of the HCN (1-0) line was calculated in three sources not detected in H₂CO 140.8 GHz line: WB066, WB361, and WB438. The column densities for these sources in the HCN (1-0) line are comparable to the other HCN lines of sight, so why they were not detected in H₂CO is somewhat of a mystery. Without more data on the chemistry of these objects, we cannot speculate further.

Using the method employed to calculate the total column density for H₂CO, we can estimate the total HCN column density by using the following equations:

$$N_{\text{HCN}} = N(J=1-0)Q/(g_u e^{-h\nu/kT_{\text{ex}}}) ,$$

and

$$Q = \sum (2J+1) \exp[-E_J/kT_{\text{ex}}] .$$

Once again, for the partition function, the 5 lowest levels are assumed to be populated, and the energies for those levels above ground state can be calculated using $E_J = B_0 J(J+1)$ for $J = 1-5$. The rotational constant, B_0 , for HCN is 1.48 cm⁻¹ (Green and Thaddeus 1974). The total column densities of HCN in outer Galaxy molecular clouds based the HCN (1-0) transition are given in Table 5-7.

Table 5-6: Column density values for the 88.6 GHz transition of HCN.

<i>Source</i>	$\Delta T_B \Delta \nu^*$	$N_{(J=1-0)}^+$ $T_{ex} = 10 K$	$N_{(J=1-0)}^+$ $T_{ex} = 20 K$
WB006	0.604	2.31	1.76
WB035	0.462	1.76	1.34
WB060	1.693	6.47	4.93
WB066	0.665	2.54	1.93
WB076	0.854	3.26	2.49
WB080	0.578	2.21	1.68
WB152	0.262	0.89	0.68
WB283	0.221	0.84	0.64
WB361	0.369	1.41	1.07
WB379	0.425	1.62	1.24
WB380	1.955	7.47	5.69
WB391	0.513	1.96	1.49
WB399	1.213	4.63	3.53
WB437	2.598	9.93	7.56
WB438	0.441	1.69	1.28
WB440	0.345	1.32	1.00
WB501	0.755	2.88	2.20
WB572	0.242	0.92	0.70
WB621	2.028	7.75	5.90
WB625	0.777	2.97	2.26
WB629	0.567	2.17	1.65
WB636	0.347	1.32	1.01
WB640	0.941	3.59	2.74
WB670	0.891	3.41	2.59
WB705	0.369	1.41	1.07
WB730	0.287	1.10	0.86
WB789	0.837	3.21	2.43
WB794	2.016	7.70	5.87
WB847	0.296	1.13	0.86
WB898	0.836	3.19	2.43
WB904	0.494	1.89	1.44

* Units are $K \text{ km s}^{-1}$.

+ Column density values are in units of 10^{11} cm^{-2} .

Table 5-7 Total HCN column density values using the 88.6 GHz transition.

<i>Source</i>	N_{HCN^+} $T_{ex} = 10 K$	N_{HCN^+} $T_{ex} = 20 K$	$N(H_2)**$
WB006	4.81	6.16	6.3
WB035	3.67	4.71	5.2
WB060	13.46	17.27	9.3
WB066	5.29	6.78	9.0
WB076	6.79	8.71	5.0
WB080	4.59	5.89	8.5
WB152	1.85	2.37	2.8
WB283	1.76	2.25	5.8
WB361	2.93	3.76	3.9
WB379	3.38	4.33	6.5
WB380	15.54	19.94	11.4
WB391	4.08	5.24	5.2
WB399	9.65	12.37	6.3
WB437	20.66	26.50	14.2
WB438	3.51	4.50	0.35
WB440	2.74	3.52	4.1
WB501	6.00	7.70	11.2
WB572	1.92	2.46	3.8
WB621	16.13	20.69	13.0
WB625	6.18	7.92	4.8
WB629	4.51	5.79	4.9
WB636	2.76	3.54	3.8
WB640	7.48	9.59	3.2
WB670	7.09	9.09	7.3
WB705	2.93	3.76	1.7
WB730	2.28	2.92	2.8
WB789	6.65	8.53	5.8
WB794	16.03	20.56	3.9
WB847	2.36	3.02	1.2
WB898	6.65	8.53	2.5
WB904	3.92	5.03	4.1

+ Column density values are in units of 10^{11} cm^{-2} .

** Units are 10^{21} cm^{-2}

Churchwell et al. (1984) observed the HCN (1-0) line towards several locations in the Taurus Dark Cloud complex, which is located roughly 140 pc from the Sun. They estimated total column densities of HCN (1-0) line of $3.31 \times 10^{12} \text{ cm}^{-2}$ to $1.00 \times 10^{15} \text{ cm}^{-2}$ using a T_{ex} of either 5 K or 7 K. We calculated column density values of HCN ranging from 1.76×10^{11} to $2.06 \times 10^{12} \text{ cm}^{-2}$ for $T_{\text{ex}}=10$ K, and from 2.25×10^{11} to $2.65 \times 10^{12} \text{ cm}^{-2}$ for $T_{\text{ex}} = 20$ K. The values we calculated for outer Galaxy GMCs are up to 4 orders of magnitude less than the values for inner Galaxy dark clouds.

The fractional abundance of HCN in the outer Galaxy molecular clouds can be calculated using the same H_2 abundance values employed previously for the H_2CO calculations. Table 5-8 shows the fractional abundance of HCN to H_2 using the total column density values calculated from the HCN (1-0) transition. The data indicate that in some outer Galaxy clouds, there is over an order of magnitude difference between the abundance of H_2CO and that of HCN. For example, in WB060 the abundance of H_2CO at 10 K is 2.08×10^{-10} , while that of HCN for the same cloud is 1.45×10^{-11} . For an outer Galaxy cloud that was included in this survey, DdGT02, Ruffle et al. (2007) also estimated a lower abundance for HCN (1-0) line [$\text{N}(\text{HCN})/\text{N}(\text{H}_2) = 1.7 \times 10^{-11}$], relative to that of the H_2CO ($1_{01} - 1_{11}$) [$\text{N}(\text{H}_2\text{CO})/\text{N}(\text{H}_2) = 7.6 \times 10^{-11}$].

The decrease in column density of the HCN (1-0) line compared to the H_2CO ($2_{12}-1_{11}$) line implies a similar drop in abundance (though a reliable determination would have to include a multitransition study and LVG analysis for the HCN). This result is somewhat surprising given astrochemistry models (e.g., Viala 1986) that predict, for dense molecular regions, HCN abundances in the range of $2.4 \times 10^{-9} - 9.7 \times 10^{-10}$ for model densities from $1 \times 10^3 \text{ cm}^{-3} - 1 \times 10^5 \text{ cm}^{-3}$ compared to H_2CO abundances $6.0 \times 10^{-11} - 2.0 \times 10^{-10}$ for the same density range. Thus equilibrium chemical models predict that the HCN abundance decreases in

Table 5-8: Fractional abundance of HCN to H₂ in outer Galaxy GMCs.

<i>Source</i>	<i>Abundance</i> $\times 10^{-11}$	<i>Abundance</i> $\times 10^{-11}$
	$T_{ex} = 10 K$	$T_{ex} = 20 K$
WB006	0.76	0.98
WB035	0.71	0.91
WB060	1.45	1.86
WB066	0.59	0.75
WB076	1.36	1.74
WB080	0.54	0.69
WB152	0.66	0.85
WB283	0.30	0.39
WB361	0.75	0.96
WB379	0.52	0.67
WB380	1.36	1.75
WB391	0.78	1.01
WB399	1.53	1.96
WB437	1.45	1.87
WB438	10.03	12.86
WB440	0.67	0.86
WB501	0.54	0.69
WB572	0.51	0.65
WB621	1.24	1.59
WB625	1.29	1.65
WB629	0.92	1.18
WB636	0.73	0.93
WB640	2.34	3.00
WB670	0.97	1.25
WB705	1.72	2.21
WB730	0.81	1.04
WB789	1.15	1.47
WB794	4.11	5.27
WB847	1.97	2.52
WB898	2.66	3.41
WB904	0.96	1.23

dense molecular gas as the cloud density increases, while the H₂CO abundance increases. However, given the increase in H₂CO with or even at the maximum density of Viala's (1986) model, the H₂CO abundance is lower than that of HCN. This is in contrast to our data where our simplistic derivation for the HCN abundance implies that H₂CO has a higher abundance than HCN in outer Galaxy clouds.

While this is an interesting result, at this stage it is at best, preliminary. As stated above, a more reliable determination of the HCN abundance would involve a multitransition study and an LVG analysis. Moreover, chemistry models are very nonlinear. They depend strongly on initial conditions such as metallicity and radiation field, which are lower in the outer Galaxy. Astrochemistry models to date have not dealt with the specific initial conditions in the outer Galaxy. Other conditions such as non-equilibrium chemistry models could also reverse the trends discussed above.

What if the simplistic HCN abundance determined above is correct, and the equilibrium chemistry models like the one by Viala (1986) discussed above are also correct? In other words, in "normal" inner Galaxy clouds the HCN abundance is greater than that of H₂CO, while the situation in the outer Galaxy is reversed. If this were indeed the case, this would be a significant result which would have to be understood and explained. An interesting speculation might involve a significant drop in the abundance of nitrogen which would be reflected in the drop in abundance of N-bearing molecules (such as HCN). This would have significant consequences for the question of how suitable the outer Galaxy is for the formation of life. However, before this interesting avenue of inquiry can be pursued, the HCN abundance needs to be determined more reliably and astrochemistry models need to be run for conditions more suitable to the outer Galaxy.

5.4 LARGE VELOCITY GRADIENT CODE ABUNDANCE CALCULATIONS FOR H₂CO

A large velocity gradient (LVG) model can be used to better estimate abundances of H₂CO when more than one rotational transition of the molecule has been observed. In the LVG approximation (Goldreich and Kwan 1974), two assumptions are made: the cloud possesses a systematic velocity gradient where the velocity is a function of distance from the cloud core [$v = v_0(r/r_0)$], and the width of the line in velocity is much smaller than the systematic velocity (Rohlfs and Wilson 2006). The LVG approximation effectively accounts for photon transport when lines are optically thick by allowing photons emitted at a specific position to interact only with neighboring molecules. While the LVG approximation is helpful in determining physical conditions in clouds, the simplistic assumptions like spherical cloud shape and uniform cloud density can introduce significant error and lead to unphysical or misleading results (Wootten et al. 1980). However, it is generally accepted by the astronomical community that LVG abundance estimates are more reliable than those from single transition studies where one has to assume a τ_{ex} .

The LVG statistical equilibrium model we used for our multi-transitional study calculates population levels based on collisional excitation rates and the excitation temperature using Boltzmann's law. It was originally written by Malcolm Walmsley of Arcetri Observatory in Italy and kindly provided to us by Dr. Walmsley. In the program, line strengths are then calculated using the radiative transfer equation and can be compared to measured values. The model requires the input of the energies for the first 40 ortho-H₂CO and para-H₂CO rotational levels and collisional excitation rates for H₂CO-He (Green 1978). For this study, the parameters that we varied were the velocity gradient, the excitation temperature, the density of molecular hydrogen, and the abundance of formaldehyde. The velocity gradient was varied from 2-5 km/s,

the excitation temperature was varied from 10-30 K, the density of molecular hydrogen was varied from $8 \times 10^3 - 1.28 \times 10^5 \text{ cm}^{-3}$, and the abundance was varied from 1×10^{-11} to 1×10^{-9} .

The results from the model for an excitation temperature of 10 K and a velocity gradient of 5 km/s/pc are presented in Figure 5-1. The ratio of the line strengths of the 140.8 GHz line to the 4.83 GHz line (y-axis) is plotted against the line strength of the 140.8 GHz transition (x-axis). Each line represents a different abundance, ranging from 5.0×10^{-11} (line with asterisks) to 1.0×10^{-9} (line with squares). Along each abundance line, data points correspond to different densities of molecular hydrogen ranging from $8 \times 10^3 \text{ cm}^{-3}$ where the line for a particular abundance begins, to $1.28 \times 10^5 \text{ cm}^{-3}$ at its end. The 7 sources detected in both transitions are indicated by larger triangles, and include WB670, WB705, WB730, WB789, WB793, WB794, and WB904.

The plot shows that WB730 lies near the abundance of $\sim 5.0 \times 10^{-11}$, WB794 is positioned between 7.5×10^{-11} and 2.5×10^{-10} , and WB670, WB705, WB789, WB793 and WB904 all lie along or just below the line for an abundance of 1×10^{-9} . The values calculated for abundance using simplistic assumptions were all on the order of 10^{-10} , so the range of abundances predicted by the model is fully consistent with our simplistic assumptions and single transition results. Each abundance line is comprised of points of different densities of molecular gas, so for each data point, the predicted abundance value would be based on the density of molecular gas in the cloud. All of the data points lie below a molecular gas density of $6.4 \times 10^4 \text{ cm}^{-3}$, which may suggest that the averaged molecular gas densities in the cores of outer Galaxy GMCs may be close to this value for cloud temperatures of 10 K. This is a reasonable result and does not differ significantly from what is expected in cores in GMCs at the Solar Circle (e.g., $10^5 - 10^6 \text{ cm}^{-3}$, Goldsmith 1987).

The plot for the model run at a temperature of 20 K and a velocity gradient of 5 km/s/pc is shown in Figure 5-2. The axes are the same as those in Figure 5-1. The abundances range from 1.0×10^{-11} to 5.0×10^{-11} and the molecular gas densities range from 8×10^3 to $1.28 \times 10^4 \text{ cm}^{-3}$ in the manner described previously. The abundances of the 7 positions suggested in this plot do not differ greatly from those calculated using simplistic assumptions. These data also indicate that clouds with a temperature of 20 K have lower abundances of H₂CO than that of clouds at 10 K for the same range of molecular gas densities.

The model was also run at T= 10 K and 20 K for a velocity gradient of 2 km/s/pc, Figures 5-3 and 5-4 respectively. The molecular gas density for these plots ranges from 1.0×10^3 to roughly $1.28 \times 10^5 \text{ cm}^{-3}$. At molecular gas densities above $2.0 \times 10^5 \text{ cm}^{-3}$, the 4.83 GHz line strength became positive, indicating emission. The abundances suggested in Figure 5-3 do not differ greatly from those predicted by the model run with a velocity gradient of 5 km/s/pc. Figure 5-4 does suggest that the column density of the sources may be lower, as WB730 lies near the 5.0×10^{-12} line shown in red, but on the other three plots is an order of magnitude higher.

The information extracted from the LVG code plots in this study support our previous calculations using only the 140.8 GHz transition (and CO data) in determining the abundance of H₂CO in outer Galaxy molecular clouds. The limited number of observations of the sources in the 4.83 GHz line and the 225.6 GHz line prevent us from doing a thorough analysis of the abundance of H₂CO in the 69 clouds using the LVG model. Ideally, all the clouds should be observed in the 4.83 GHz transition. However, given that the only telescope that has a beam size at 4.83 GHz even vaguely comparable to the one used for the 140.8 GHz transitions is the Arecibo radio telescope, the latter's inability to observe sources with declinations below -2° and above $+38^\circ$, effectively precludes further study. For this analysis we chose to use the 140.8 GHz

line because it had the highest number of detections, and we compared it to the 4.83 GHz line which had a greater number of detections than the 225.6 GHz line. By looking at only 7 data points, all of which were detected in both the 4.83 GHz line and the 140.8 GHz line from a total of 46 detections, we cannot establish the actual abundance of H₂CO in the outer Galaxy. More observations at 225.6 GHz would be the only option at this point, but given how difficult it is to get observing time on the JCMT, this would also be a difficult endeavor. However, LVG results do support our earlier estimate of the H₂CO abundance and thus we have more confidence in our conclusions.

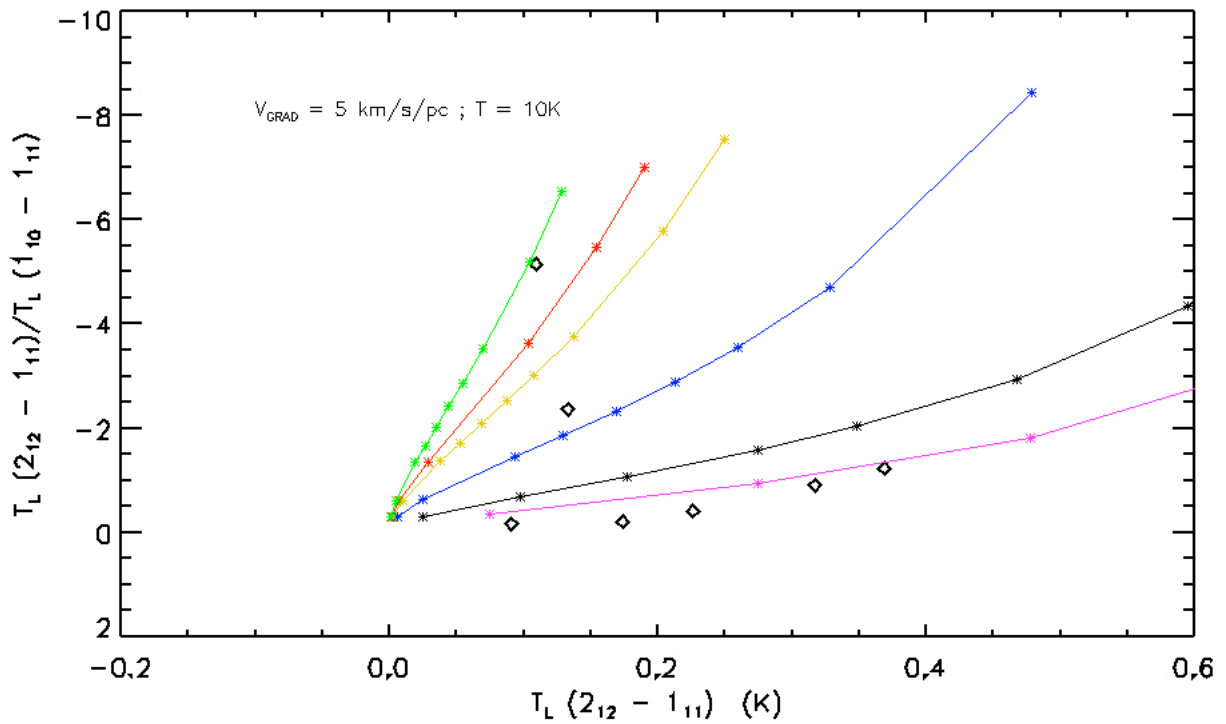


Figure 5-1 LVG model calculations of line strength ratios at different molecular gas densities compared to measured values for sources detected in both the 4.83 GHz and the 140.8 GHz line at a temperature of 10 K and velocity gradient of 5 km/s/pc. Data points are represented by \diamond . The abundances are as follows: green = 5.0×10^{-11} , red = 7.5×10^{-11} , yellow = 1.0×10^{-10} , blue = 2.5×10^{-10} , black = 1.0×10^{-9} , and purple = 3.0×10^{-9} . The density of molecular gas ranges from $8 \times 10^3 \text{ cm}^{-3}$ near (0,0) to 1.28×10^5 at the endpoints of the lines.

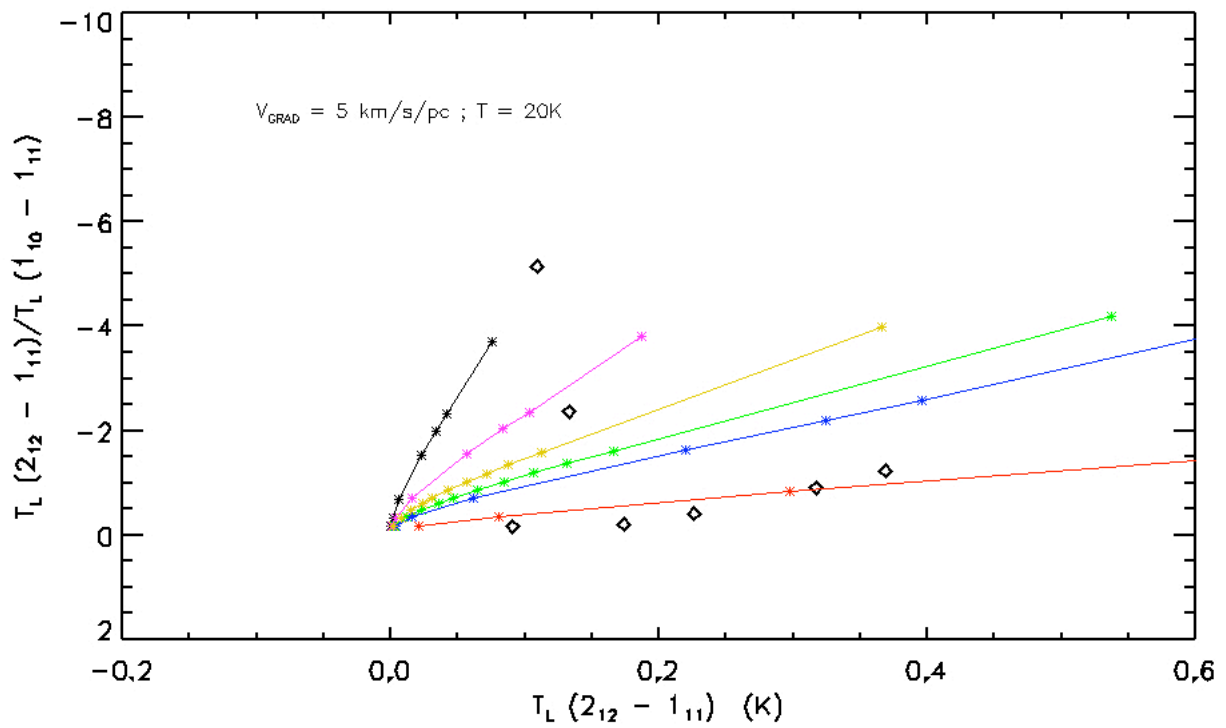


Figure 5-2 LVG model calculations of line strength ratios at different molecular gas densities compared to measured values for sources detected in both the 4.83 GHz and the 140.8 GHz line at a temperature of 20 K and a velocity gradient of 5 km/s/pc. Data points are represented by \diamond . The abundances are as follows: black = 1.0×10^{-11} , purple = 2.5×10^{-11} , yellow = 5.0×10^{-11} , green = 7.5×10^{-11} , blue = 1.0×10^{-10} , and red = 5.0×10^{-10} . The density of molecular gas ranges from $8 \times 10^3 \text{ cm}^{-3}$ near (0,0) to 1.28×10^5 at the endpoints of the lines.

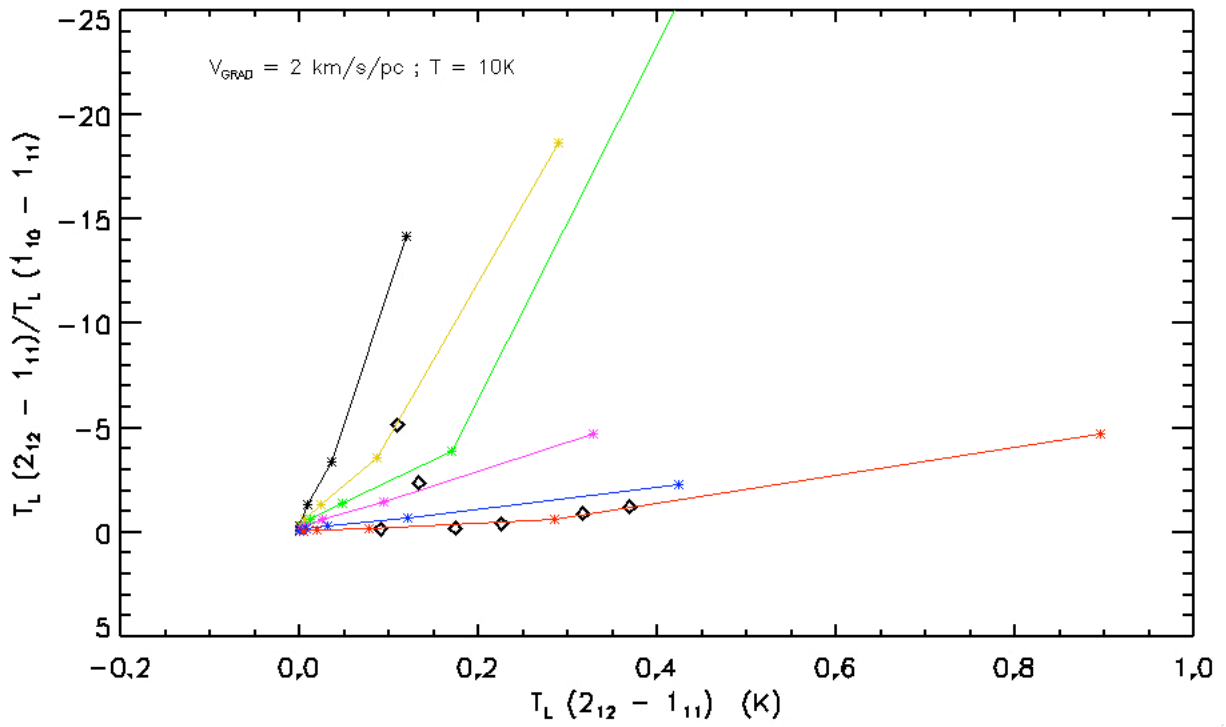


Figure 5-3 LVG model calculations of line strength ratios at different molecular gas densities compared to measured values for sources detected in both the 4.83 GHz and the 140.8 GHz line at a temperature of 10 K and a velocity gradient of 2 km/s/pc. Data points are represented by \diamond . The abundances are as follows: black = 1.0×10^{-11} , yellow = 2.5×10^{-11} , green = 5.0×10^{-11} , purple = 7.5×10^{-11} , blue = 5.0×10^{-10} , and red = 5.0×10^{-9} . The density of molecular gas ranges from $1 \times 10^3 \text{ cm}^{-3}$ near (0,0) to 1.28×10^5 at the endpoints of the lines.

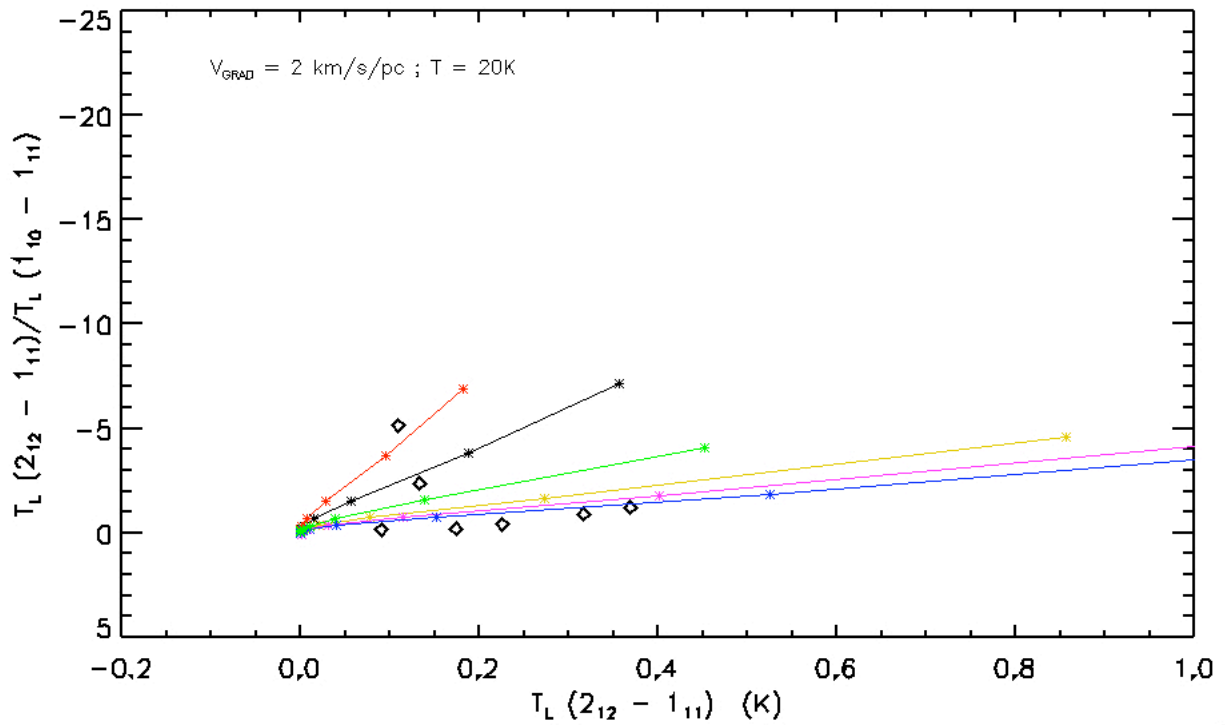


Figure 5-4 LVG model calculations of line strength ratios at different molecular gas densities compared to measured values for sources detected in both the 4.83 GHz and the 140.8 GHz line at a temperature of 20 K and a velocity gradient of 2 km/s/pc. Data points are represented by \diamond . The abundances are as follows: red = 5.0×10^{-12} , black = 1.0×10^{-11} , green = 2.5×10^{-11} , yellow = 5.0×10^{-11} , purple = 7.5×10^{-11} , and blue = 5.0×10^{-10} . The density of molecular gas ranges from $1 \times 10^3 \text{ cm}^{-3}$ near (0,0) up to 2.00×10^5 at the endpoints of the lines.

CHAPTER 6

CONCLUSIONS AND FUTURE WORK

This study was conducted to estimate the distribution and abundance of biologically important molecules H_2CO and HCN in outer Galaxy molecular clouds. A secondary goal was to take a first step in determining the suitability of this region of the Galaxy beyond the presently defined Galactic Habitable Zone for the formation of life. After looking at the results of this study, both goals were met, but at different levels.

After studying a sample of 69 molecular clouds in three different transitions of H_2CO , the $(1_{01}-1_{11})$, the $(2_{12}-1_{11})$ and the $(3_{12}-2_{11})$ transition, the prevalence of H_2CO in outer Galaxy molecular clouds has been firmly established. The clouds (with one exception) range in distance from 12 – 23.5 kpc in galactocentric radius and are located from galactic longitude 85° to 255° . Detections in the 140.8 GHz line were made out to 23.5 kpc with a detection rate of 26/69 of the clouds at $R_G > 16$ kpc and 6/69 clouds at $R_G > 20$ kpc. Solely from a detection standpoint, this is a significant achievement. No survey of the Galaxy in H_2CO had ever been done in this region and the drop in abundance of atomic species like C, N, and O made it difficult to predict how the molecular abundances would behave. It was not at all clear before undertaking this study that both H_2CO and /or HCN could be readily detected in reasonable integration times. The fact that detections were made over such a wide range in longitude clearly demonstrates the widespread

distribution of H₂CO in the outer Galaxy. The 88.6 GHz line of HCN was detected out to $R_G = 23.5$ kpc and to a galactic longitude of 211° (the greatest longitude to which it was observed). Thus, HCN also shares the widespread distribution exhibited by H₂CO, and like H₂CO, it is readily detected to the edge of the molecular disk.

The column densities of each molecule were calculated for each source using simplistic assumptions and a fractional abundance compared to H₂ was estimated. Column density values were calculated for all of the H₂CO transitions, and the column density for the 140.8 GHz transition was used to determine the total column density of H₂CO in the clouds. Column densities of H₂CO were on the order of 10^{11} - 10^{12} cm⁻² and fractional abundances ranged from 10^{-11} - 10^{-10} . For HCN, the column density of the 88.6 GHz transition was calculated and used to estimate a total column density of the molecule in the clouds. Column densities for HCN were of order 10^{11} cm⁻² and the abundances ranged from 10^{-12} - 10^{-10} , in some clouds an order of magnitude lower than that of H₂CO. This is an interesting result per se, given that astrochemistry models of clouds in the inner Galaxy and the Solar Circle usually predict that HCN should be more abundant than H₂CO – at least in the denser regions of GMCs. Whether our results indicate a difference in the chemistry of outer Galaxy GMCs, or whether this difference reflects the changes in external parameters like radiation field is an avenue for future work.

A multi-transition study of H₂CO was made using an LVG code and the (2₁₂-1₁₁) and (1₀₁-1₁₁) transition data. The code was run for a variety of conditions, and the 7 sources having overlapping detections in the 140.8 GHz and the 4.83 GHz line were compared to the model results. The abundance ranges calculated by the model were comparable to those we calculated using simplistic assumptions, but more observations are needed to model the ensemble with

more certainty. One might naively expect the abundance of H₂CO and HCN to be down by 2 orders of magnitude from abundances in the inner Galaxy, but our results show that it is only down by 1 order of magnitude. A future project would involve either gathering more data in the transitions already observed or switching to another frequency like the 14.5 GHz line, a transition that can be readily observed at the Green Bank telescope in Green Bank, West Virginia. Of the observed transitions, the 4.83 GHz is likely to not be employed because of the lack of sky coverage provided by Arecibo, the only telescope large enough to permit comparisons between similar beams sizes.

In terms of whether or not the outer Galaxy warrants further study as a candidate region for the formation of life, the answer is clear from the results of the study. The raw materials in the form of H₂CO and HCN are present and widespread, and things are in general calmer out there in terms of supernovae frequency and radiation flux. This, of course, is counterbalanced by the decrease in metallicity, and the significant drop in the number of star forming regions, both of which would limit habitable planet formation. We do not claim that the outer Galaxy is a better habitable zone than the region surrounding the Solar Circle. However, we do claim that the outer Galaxy is worth a closer look in regards to this issue. A next step would be to look for other molecules of biological interest that include elements like P, K, and Mg, all elements that essential for Earth-like life to exist and flourish.

REFERENCES

- Abelson, P. 1966. Proc. Natl. Acad. Sci., USA, 55, 1365-1372.
- Afflerbach, A., Churchwell, E., Werner, M. W. 1997. *Astrophys. J.*, 478, 190.
- Allen, C., Carigi, L., Peimbert, M. 1998. *Astrophys. J.*, 494, 247.
- Anders, E., Grevesse, N. 1989. *Geochim. Cosmochim. Acta.*, 53, 197-214.
- Andrievsky, S. M., Kovtyukh, V. V., Luck, R. E., Lépine, J. R. D., Bersier, D., Maciel, W. J., Barbuy, B., Klochkova, V. G., Panchuk, V. E., Karpishech, R. U. 2002a. *Astron. Astrophys.*, 381, 32-50.
- Andrievsky, S. M., Bersier, D., Kovtyukh, V. V., Luck, R. E., Maciel, W. J., Lépine, J. R. D., Beletsky, Yu. V. 2002b. *Astron. Astrophys.*, 384, 140-144.
- Andrievsky, S. M., Kovtyukh, V. V., Luck, R. E., Lépine, J. R. D., Maciel, W. J., Beletsky, Yu. V. 2002c. *Astron. Astrophys.*, 392, 491-499.
- Apponi, A.J., Hoy, J.J., Halfen, D.T., and Ziurys, L.M. 2006. *Astrophys. J.*, 652, 1787–1795.
- Balázs, B.A. 1986. *Acta Astronaut.*, 13, 123–126.
- Balázs, B.A. 1988. In *Bioastronomy: The Next Steps*, edited by G. Marx, Kluwer, London, pp. 61–66.
- Bar-Nun, A. and Hartman, H. 1978. *Orig. Life*, 9, 93–101.
- Bernal, J.D. 1951. *The Physical Basis of Life*, (London, Routledge and Kegan Paul).
- Bibring, Jean-Pierre. 2005. in *Lectures in Astrobiology*, Vol. 1, edited by M. Gargaud, B. Barbier, H. Martin and J. Reisse, Springer, pp 353-375.
- Blitz, L., Magnani, L.A., and Mundy, L. 1984. *Astrophys. J.*, 282, L9-L12.
- Blitz, L. 1990. In *Molecular Astrophysics*, edited by T.W. Harquist, Cambridge University Press, 35-55.
- Blitz, L. 1991. In *The Physics of Star Formation and Early Stellar Evolution*, edited by C.J. Iada and N.D. Kylafis, Kluwer Academic Publishers, 3-29.
- Blitz, L., Fich, M., Stark, A. A. 1992. *Astrophys. J. Suppl. Ser.*, 49, 183-206.

- Blitz, L. 1993. In *Protostars and Planets III*, edited by E.H Levy and J.I. Lunine, The University of Arizona Press, 125-163.
- Brand, J. and Blitz, L. 1993. *Astron. Astrophys.*, 275, 67.
- Brand, J., and Wouterloot, J.G.A. 1994. *Astron. Astrophys. Suppl. Ser.*, 103, 503-540.
- Brand, J. and Wouterloot, J.G.A. 1995. *Astron. Astroph.*, 303, 851–871.
- Brand, J. and Wouterloot, J.G.A. 1996. In *Proceedings of the 169th Symposium of the International Astronomical Union*, edited by L. Blitz and P. Teuben, Kluwer, Dordrecht, pp. 561–566.
- Brand, J. and Wouterloot, J.G.A. 2007. *Astron. Astrophys.* 464, 909–920.
- Bronfman, L., Nyman L.-A., and May, J. 1996. *Astron. Astrophys. Suppl. Ser.*, 115, 81–95.
- Brooks, D.J., Fresco, J.R., and Singh, M. 2002. *Bioinformatics*, 20(14), 2251-2257.
- Brunt, C.M., Kerton, C.R., and Pomerleau, C. 2003. *Astrophys. J. Suppl. Ser.*, 144, 47–70.
- Burov, A. B., Voronov, V. N., Zinchenko, I. I., Krasilnikov, A. A., Kukina, E. P. 1982. *Sov. Astron.*, 26, 163.
- Butler, R.P., Wright, J.T., Marcy, G.W., Fischer, D.A., Vogt, S.S., Tinney, C.G., Jones, H.R.A., Carter, B.D., Johnson, J.A., McCarthy, C. & Penny, A.J. 2006. *Astrophys. J.*, 646, 505-522.
- Butlerow, A. 1861. *C.R. Acad. Sci.* 53, 145–147.
- Canuto, V.M., Levine, J.S., Augustsson, T.R., Imhoff, C.L., and Giampapa, M.S. 1983. *Nature*, 305, 281–286.
- Caplan, J., Deharveng, L., Peña, M., Costero, R., Blondel, C. 2000. *Mon. Notic. Roy. Astron. Soc.*, 311, 317-328.
- Carraro, G., Ng, Y. K., Portinari, L. 1998. *Mon. Notic. Roy. Astron. Soc.*, 296(4), 1045-1056.
- Carraro, G., Geisler, D., Villanova, S., Frinchaboy, P. M., Majewski, S. R. *Astron Astrophys.*, 476(1), 217-227.
- Chadha, M.S. and Choughuley, A.S.U. 1984. *Orig. Life Evol. Biosph.* 14, 469–476.
- Chittenden, G.J.F. and Schwartz, A.W. 1981. *Biosystems*, 14, 15–32.
- Churchwell, E., Nash, A. G., Walmsley, C. M. 1984. *Astrophys. J.*, 287, 681-693.

- Chyba, C.F., Thomas, P.J., Brookshaw, L., and Sagan, C. 1990. *Science*, 249, 366–373.
- Chyba, C.F. 2005. *Science*, 308, 962-963.
- Cohen, R. S.; Cong, H.; Dame, T. M.; Thaddeus, P. 1980. *Astrophys. J.*, 239, L53-L56.
- Corliss, J.B., and Baross, J.A., and Hoffman, S.E. 1981. *Ocean Acta*, 4, 59.
- Costa, R.D.D., Uchida, M.M.M, and Maciel W.J. 2004. *Astron. and Astrophys.* 423, 199.
- Cox, D. P. 2005. *ARA&A*, 43(1), 337-385.
- Daflon, S., Cunha, K. 2004. *Astrophys. J.*, 617, 1115-1126.
- Dame, T. M., Ungerechts, H., Cohen, R. S., de Geus, E. J., Grenier, I. A., May, J., Murphy, D. C., Nyman, L.-A., Thaddeus, P. 1987. *Astrophys. J.*, 322, 706-720.
- Dame, T.M., Hartmann, D., and Thaddeus, P. 2001. *Astrophys. J.*, 547, 792-813.
- Deharveng, L., Peña, M., Caplan, J., Costero, R. 2000. *Mon. Notic. Roy. Astron. Soc.*, 311, 329-345.
- Dieter, N.H. 1973. *Astrophys. J.*, 183, 449–468.
- Digel, S., de Geus, E., and Thaddeus, P. 1994. *Astrophys. J.*, 422, 92–101.
- Digel, S.W., Lyder, D. A., Philbrick, A. J., Puche, D., Thaddeus, P. 1996. *Astrophys. J.*, 458, 561.
- Elmegreen, D.E. 1998, *Galaxies and Galactic Structure*, (New Jersey, Prentice Hall)
- Evans, N.J., II 1975. *Astrophys. J.*, 201, 112–117. Few, R.W. 1979. *Mon. Not. R. Astron. Soc.*, 187, 161–178.
- Feitzinger, J.V., and Stuewe, J.A. 1984. *Astron and Astrophys. Suppl.*, 58, 365-369.
- Ferris, J.P. 2005. *Elements*, 1, 145-149.
- Fich, M., Silkey, M. 1991, *Astrophys. J.*, 366, 107-114.
- Finkbeiner, D. P., Davis, M., Schlegel, D. J. 1999. *Astrophys. J.*, 524, 867-886.
- Franchi, M., Ferris, J.P., Gallori, E. 2003. *Orig. Life Evol. Biosphere*, 33, 1-16.
- Friberg, P., and Hjalmarsen, A. 1990. In *Molecular Astrophysics*, edited by T.W. Harquist, Cambridge University Press, 3-35.
- Friel, E. D., and Janes, K. A. 1993. *Astron. Astrophys.*, 267, 75-91.

- Friel, E. D., Janes, K. A., Tavaréz, M., Scott, J., Katsanis, R., Lotz, J., Hong, L., Miller, N. 2002. *Astron. J.*, 124(5), 2693-2720.
- Gabel, N.W., Ponnampereuma, C. 1967. *Nature*, 216, 453-455.
- Goldreich, P., and Kwan, J. 1974. *Astrophys. J.*, 189, 441-454.
- Goldschmidt, V. M. 1952. *New Biology* 12: 97-105.
- Goldsmith, P. F. 1987. In *Interstellar Processes*, edited by D. J. Hollenbach, and H. A. Thronson, Jr., D. Reidel Publishing Company, 51-71.
- Gonzalez, G., Brownlee, D., and Ward, P. 2001. *Icarus*, 152, 185–200.
- Grabelsky, D. A., Cohen, R. S., Bronfman, L., Thaddeus, P., May, J. 1987. *Astrophys. J.*, 315, 122-141.
- Green, S., Garrison, B.J., Lester, W.A., and Miller, W.H. 1978. *Astrophys. J. Suppl. Ser.*, 37, 321-341.
- Gummersbach, C. A., Kaufer, A., Schaefer, D. R., Szeifert, T., Wolf, B. 1998. *Astron. and Astrophys.*, 338, 891-896.
- Ferris, J.P., and Chen, C.T. 1975. *J. Am. Chem. Soc.*, 97, 2962-2967.
- Few, R. W. 1979. *Mon. Not. Roy. Astron. Soc.*, 187, 161-178.
- Harris, H.C. 1981. *Astron. J.*, 86, 719-729.
- Harris, H. C., Pilachowski, C. A. 1984. *Astrophys. J.*, 282, 655-666.
- Hartley, M., Tritton S.B., Manchester, R.N., Smith, R.M., and Goss, W.M. 1986. *Astron. and Astrophys. Suppl.*, 63, 27-48.
- Harvey, G.R., Mopper, K., Degens, E.T. 1971. *Chem. Geo.* 9, 79-87.
- Hatanaka, H. and Egami, F. 1977a. *Bull. Chem. Soc. Japan*, 50, 1147-1156.
- Hatanaka, H. and Egami, F. 1977b. *J. Biochem.*, 82, 499–502.
- Heithausen, A., Mebold, U., and de Vries, H.W. 1987. *Astron. Astrophys.*, 179, 263–267.
- Hennet, R.J., Holm, N.G., and Engel, M.H. 1992. *Naturwissenschaften*, 79, 361–365.
- Heyer, M.H., Brunt, C., Snell, R.L., Howe, J.E., Schloerb, F.P., and Carpenter, J.M. 1998. *Astrophys. J. Suppl. Ser.*, 115, 241–258.
- Holm, N.G., and Andersson, E. 2005. *Astrobiology*, 5(4), 444-460.

- Hubbard, J.S., Hardy, J.P., and Horowitz, N.H. 1971. Proc.Natl. Acad. Sci. U.S.A., 68, 574–578.
- Kasting, J.F. 1993. Science, 259, 920–926.
- Kasting, J.F. and Catling, D. 2003. Annu. Rev. Astron. Astrophys., 41, 429–463.
- Kerr, F.J. and Lynden-Bell, D. 1986. Mon. Not. R. Astron. Soc., 221, 1023–1038.
- Kerr, F. J., Bowers, P. F., Jackson, P. D., Kerr, M. 1986. Astron. Astrophys. Suppl. Ser., 66(3) 373-504.
- Kobayashi, N. and Tokunaga, A.T. 2000. Astrophys. J., 532, 423–429.
- Kuan, Y.J., Charnley, S.B., Huang, H.-C., Tseng, W.-L., and Kisiel, Z. 2003. Astrophys. J., 593, 848–867.
- Kutner, M.L. and Ulich, B.L. 1981. Astrophys. J., 250, 341–348.
- Kutner, M.L. 1983. In *Surveys of the southern galaxy; Proceedings of the Workshop, Leiden, Netherlands, August 4-6, 1982* (A84-32876 14-89). Dordrecht, D. Reidel Publishing Co., 1983, 143-148.
- Kutner, M.L., and Mead, K. N. 1985. In *Milky Way Galaxy: IAU Symp.106*, Groningen, 209.
- Kvenvolden, K., Lawless, J., Pering, K., Peterson, E., Flores, J., Ponnampereuma, C., Kaplan, R., and Moore, C. 1970. Nature, 228, 923-926.
- Lacy, J.H., Knacke, R., Geballe, T.R., and Tokunaga, A.T. 1994. ApJ, 428, L69-L72.
- Lemasle, B., François, P., Piersimoni, A., Pedicelli, S., Bono, G., Laney, C. D., Primas, F., Romaniello, M. 2008. Astron and Astrophys., 490, 613-623.
- Lin, C.C , and Shu, F. 1964. Astrophys. J., 140, 646-655.
- Lineweaver, C.H., Fenner, Y., and Gibson, B.K. 2004. Science, 303, 59–62.
- Liszt, H. and Lucas, R. 1995. Astron. Astrophys., 299, 847–856.
- Liszt, H., Lucas, R. and Pety, J. 2006. Astron. Astrophys., 448, 253–259.
- Lodish, H., Berk, A., and Zipursky, S.L. 1986. *Molecular Cell Biology*, (New York, W.H. Freeman).
- Loeb. W. 1913. Chem. Ber, 46, 690.
- Low, F.J. et al. 1984. Astrophys. J. 278, L19–L22.

- Lubowich, D.A., Pasachoff, J.M., Millar, T.J., Roberts, H., Brammer, G.B., and Henkel, C. 2001. *Bull. Am. Astron. Soc.*, 33, 1390.
- Luck, R. E., Kovtyukh, V. V., Andrievsky, S. M. 2006. *Astron. J.*, 132, 902-918.
- Lundmark, K. 1926. *Upsala Medd.*, No. 12.
- Lynds, B.T. 1962. *Astrophys. J. Suppl. Ser.*, 7, 1-44.
- Maciel, W.J. and Quireza, C. 1999. *Astron. Astrophys.*, 345, 629-634.
- Maciel, W. J., Quireza, C., Costa, R. D. D. 2007. *Astron. and Astrophys.*, 463, L13-L16.
- Magnani, L.A, Blitz, L., and Mundy, L. 1985. *Astrophys. J.*, 295, 402-421.
- Mangum, J.G. and Wooten, A. 1993. *Astrophys. J. Suppl. Ser.*, 89, 123-153.
- Marochnik, L.S. and Mukhin, L.M. 1986. In *The Problem of the Search for Life in the Universe*, Proc. Conf. SETI, Tallinn, Estonia, USSR, Dec. 7-11, 1981, edited by V.A. Ambartsumyan, N.S. Kardashev, and V.S. Troitskii, Nauka, Moscow, pp. 41-46.
- May, J., Murphy, D. C., Thaddeus, P. 1988. *Astron. Astrophys. Suppl. Ser.*, 73, 51-83.
- Mead, K. N., and Kutner, M.L. 1988. *Astrophys. J.*, 330, 399-414.
- Miller, S.L. 1953. *Science*, 117, 528-529.
- Miller, S.L. 1955. *J. Am. Chem. Soc.*, 77, 2351-2361.
- Miller, S.L. 1957. *Ann. N.Y. Acad. Sci.*, 69, 260-275.
- Miller, S.L. 1992. In *Major Events in the History of Life*, edited by J.W. Schopf, Jones & Bartlett, Boston, pp. 1-28.
- Miller, S.L. and Schlesinger, G. 1984. *Orig. Life*, 14, 83-90.
- Miller, S.L., Urey, H.C and Oro, J. 1976. *J. Mol. Evol.*, 9, 59-72.
- Morgan, W.W., Sharpless, S., and Osterbrock, D. 1952. *Astron. J.*, 57, 3.
- Mundy, L.G., Evans, N.J., II, Snell, R.C., and Goldsmith, P.F. 1987. *Astrophys. J.*, 318, 392-409.
- Nakagawa, M., Onishi, T., Mizuno, A., and Fukai, Y. 2005. *Pub. Astro. Soc. Jap.*, 57, 917-931.
- Narayanan, D., Cox, T. J., Shirley, Y., Davé, R., Hernquist, L., Walker, C. K. 2008. *Astrophys. J.*, 684, 996-1008.

- Nguyen, Q.-R., Jackson, J. M., Henkel, C., Truong, B., and Mauersberger, R. 1992. *Astrophys. J.*, 399, 521-532.
- Oparin, A. I. 1938. *The Origin of Life*, (New York, Macmillan)
- Oro, J., Kimball, A., Fritz, R., and Master, F. 1959. *Arch. Biochem. Biophys.*, 85, 115–130.
- Oro, J., Basile, B., Cortes, S., Shen, C. and Yamrom, T. 1984. *Origin of Life*, 14, 237-242.
- Papadopoulos, P. P., Kovacs, A., Evans, A. S., Barthel, P. 1992. *Astron. Astrophys.*, 491, 483-487.
- Peimbert, M. 1978. In *Planetary nebulae; Proceedings of the Symposium, Ithaca, N.Y., June 6-10, 1977.* (A79-13451 03-90) Dordrecht, D. Reidel Publishing Co., p. 224.
- Pinto, J.P., Gladstone, G.R., and Yung, Y.L. 1980. *Science*, 210, 183–185.
- Quiroza, C., Rood, R. T., Bania, T. M., Balser, D. S., Maciel, W. J. 2006. *Astrophys. J.*, 653, 1226-1240.
- Reid, C., and Orgel, L.E. 1967. *Nature*, 216, 455.
- Ricardo, A., Carrigan, M.A., Olcott, A.N., and Benner, S.A. 2004. *Science*, 303, 196.
- Rodriguez, M.I., Allen, R.J., Loinard, L., and Wiklind, T. 2006. *Astrophys. J.*, 652, 1230–1239.
- Rolleston, W. R. J., Smartt, S. J., Dufton, P. L., Ryans, R. S. I. 2000. *Astron. and Astrophys.*, 363, 537-544.
- Rohlfs, K., and Wilson, T.L. 2006. *Tools of Radio Astronomy*, (Berlin, Springer-Verlag).
- Rudolph, A.L., Fich, M., Bell, G.R., Norsen, T., Simpson, J.P., Haas, M.R., and Erickson, E.F. 2006. *Astrophys. J. Suppl. Ser.* 162, 346–374.
- Sakurai, M and Yanagawa, H. 1984. *Orig. Life*, 14, 171-176.
- Santos, N.C., Yun, J.L., Clemens, D.P., and Agostinho, R.J. 2000. *Astrophys. J.*, 540, L87–L90.
- Scoville, N.Z. and Sanders, D.B. 1987. In *Interstellar Processes*, edited by D.J. Hollenbach and H.A. Thronson, Jr., Reidel, Dordrecht, pp. 21–50.
- Searle, L. 1971. *Astrophys. J.*, 168, 327.
- Shaver, P. A., McGee, R. X., Newton, L. M., Danks, A. C., Pottasch, S. R. 1983. *Mon. Notic. Roy. Astron. Soc.*, 204, 53-112.
- Shen C., Yang, L., Miller, S.L., Oro, J. 1987. *Orig. Life.*, 295-305.

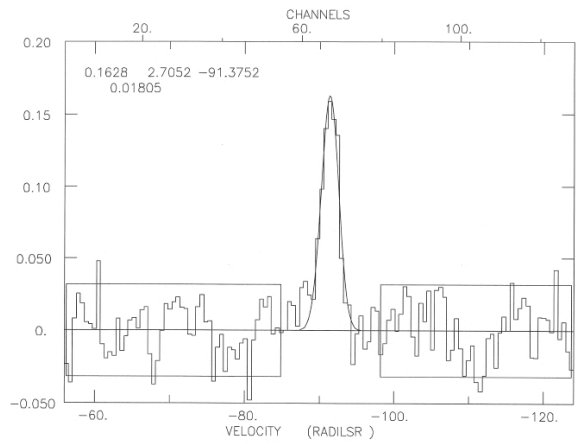
- Shock, E. L. 1990. *Orig. Life.*, 20, 331.
- Smartt, S.J., Dufton, P.L., and Rolleston, W.R.J. 1996. *Astron. Astrophys.*, 305, 164–170.
- Smartt, S. J., Rolleston, W. R. J. 1997. *Astrophys. J.*, 481, L47.
- Snell, R.L., Carpenter, J.M., and Heyer, M.H. 2002. *Astrophys. J.*, 578, 229–244.
- Snyder, L.E., Buhl, D., Zuckerman, B., and Palmer, P. 1969. *Phys. Rev. Lett.*, 22, 679–681.
- Snyder, L.E. Lovas, F.J., Hollis, J.M., Friedel, D.N., Jewell, P.R., Remijan, A., Ilyushin, V.V., Alekseev, E.A., Dyubko, S.F. 2005. *Astrophys. J.*, 619, 914-930.
- Sodroski, T.J. 1991. *Astrophys. J.* 366, 95-106.
- Solomon, P. M., Rivolo, A. R., Barrett, J., Yahil, A. 1987. *Astrophys. J.*, 319, 730-741.
- Stark, A. A., Bally, J., Knapp, G. R., Wilson, R. W. 1988. In *Molecular Clouds in the Milky Way and External Galaxies*, Berlin, Springer, pp. 303-308.
- Szutka, A. 1964. *Nature*, 202, 1231-1232.
- Townes, C.H. and Cheung, A.C. 1969. *Astrophys. J.*, 157, L103 -L108.
- Turner, B.E. 1988. In *Galactic and Extragalactic Radio Astronomy*, 2nd ed., edited by G.L. Verschuur and K.I. Kellermann, Springer-Verlag, Berlin, pp. 154–199.
- Turner, B.E. 1993. *Astrophys. J.*, 410, 140–156.
- Turner, B.E. 1994. *Astrophys. J.*, 437, 658-677.
- Twarog, B. A., Ashman, K. M., Anthony-Twarog, B. J. 1997. *Astron. J.*, 114, 2556.
- Urey, H.C. 1952. *Phys. Rev.*, 88(2), 248-252.
- Vallée, J.P. 2005. *Astron.J.*, 130, 569–575.
- Van Dishoeck, E.F , Blake, G.A., Draine, B.T. and Lunine, J.I. 1993. In *Protostars and Planets III*, edited by E.H Levy and J.I. Lunine, The University of Arizona Press, 245-278.
- Viala, Y.P. 1986. *Astron. Astrophys. Suppl. Ser.*, 64(3), 391-437.
- Vilchez, J.M, and Esteban, C. 1996. 280, 720. *Month. Notic. Royal Astron. Soc.*, 280(3), 720-734.
- Voglesonger, K.M., Holloway, J.R., Dunn, E. E., Dalla-Betta, P.J., and O’Day, P.A. 2001. *Chem. Geo.*, 180. 129-139.

- Ward, P.D., and Brownlee, D. 2000. *Rare Earth: Why Complex Life Is Uncommon in the Universe*, (New York, Copernicus)
- Weber, A.L. 1992. *J. Mol. Evol.*, 35, 1-6.
- Weber, A.L. 1998. *Origins of Life*, 28, 259.
- Weber, A.L. 2000. *Orig. Life Evol. Biosph.*, 30, 33–43.
- Wilson, T.L. and Jaffe, D.T. 1981. *Astrophys. J.*, 246, 866–870.
- Wooten, A., Snell, R., and Evans, N.J., II. 1980. *Astrophys. J.*, 240, 532–546.
- Wouterloot, J.G.A. and Brand, J. 1989. *Astron. Astrophys. Suppl. Ser.*, 80, 149–187.
- Wouterloot, J.G.A., Brand, J., and Henkel, C. 1988. *Astron. Astrophys.*, 191, 323–340.
- Wouterloot, J.G.A., Brand, J., Burton, W.B., and Kwee, K.K. 1990. *Astron. Astrophys.*, 230, 21–36.
- Wouterloot, J.G.A. and Brand, J. 1993. *Astro. Astrophys. Suppl. Ser.*, 98, 589-636.
- Wouterloot, J. G. A., Fiegle, K., Brand, J., Winnewisser, G. 1995. *Astron. Astrophys.*, 301, 236-260.
- Wouterloot, J. G. A., and Brand, J. 1996. *Astron. Astrophys. Suppl. Ser.*, 119, 439-457.
- Xu, Y., Reid, M.J., Zheng, X.W., and Menten, K.M. 2006. *Science*, 311, 54–57.
- Zahnle, K.J. 1986. *J. Geophys. Res.*, 91(D2), 2819-2834.
- Zuckerman, B., Buhl, D., Palmer, P., and Snyder, L.E. 1970. *Astrophys. J.*, 160, 485–506.
- Zylka, R., Güsten, R., Henkel, C., and Batrla, W. 1992. *Astron. Astrophys. Suppl. Ser.* 96, 525–547.

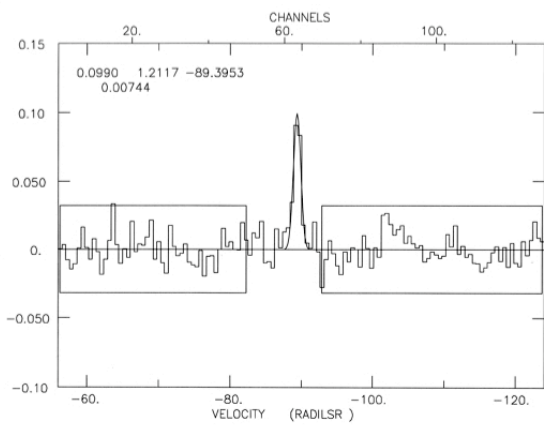
APPENDIX A

SPECTRA OF H₂CO OBSERVATIONS

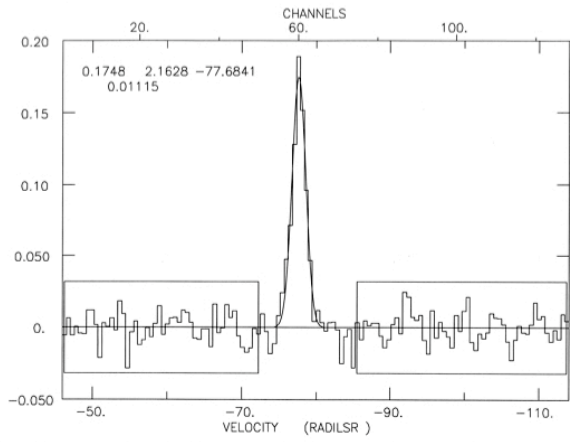
This appendix contains spectra from several of the sources detected in the 140.8 GHz, the 4.83 GHz and the 225.6 GHz transitions of H₂CO. For the first 49 spectra, the boxes indicate the region where a polynomial was fit and removed from the raw data. The numbers in the upper left represent the parameters of the best-fit Gaussian (shown superimposed on the data). From left to right: T_R^* , Δv (FWHM), and centroid velocity with respect to the LSR. The number on the second row is the rms of the fit.



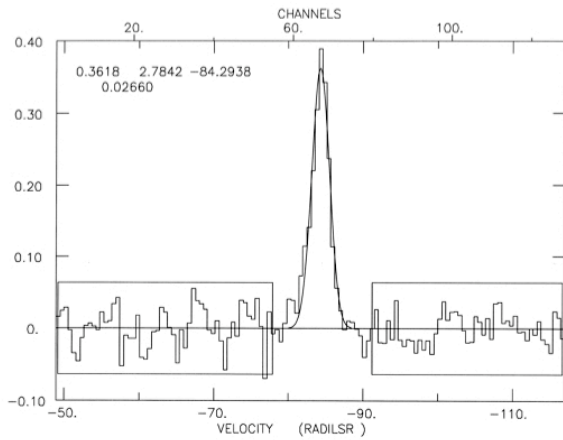
W006 8 SCANS: 108.03- 111.04 INT= 01:20: 0 DATE: 10 NOV 2005
 1950RADC=20:41:19.5 47:24:44 (20:41:19.5 47:24:44) CAL= 431.9 TS= 366.
 FREQ=140839.52 SYN=1.98833136 VEL= -90.0 DV= -0.53 FR= 250 SB=2



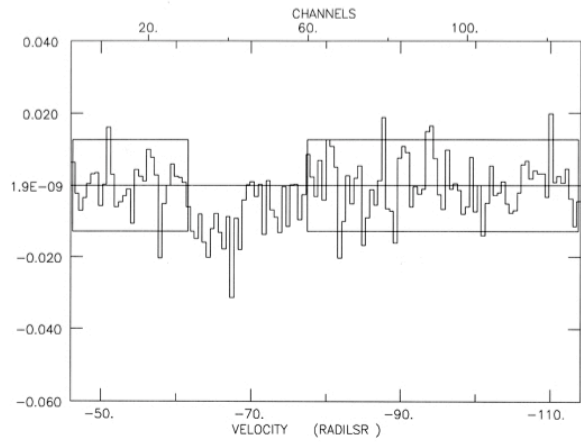
WB031 12 SCANS: 52.03- 57.04 INT= 02:00: 0 DATE: 09 NOV 2005
 1950RADC=21:02:33.6 46:41:12 (21:02:33.6 46:41:12) CAL= 438.9 TS= 326.
 FREQ=140839.52 SYN=1.98832366 VEL= -90.0 DV= -0.53 FR= 250 SB=2



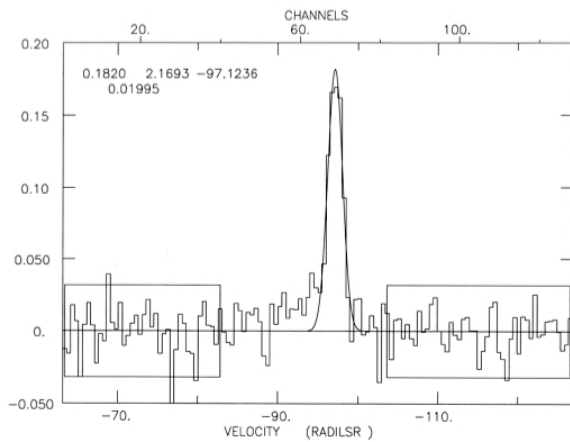
WB035 8 SCANS: 219.03- 222.04 INT= 01:20: 0 DATE: 12 NOV 2005
 1950RADC=21:03:39.4 49:03:57 (21:03:39.4 49:03:57) CAL= 423.0 TS= 232.
 FREQ=140839.52 SYN=1.98826046 VEL= -80.0 DV= -0.53 FR= 250 SB=2



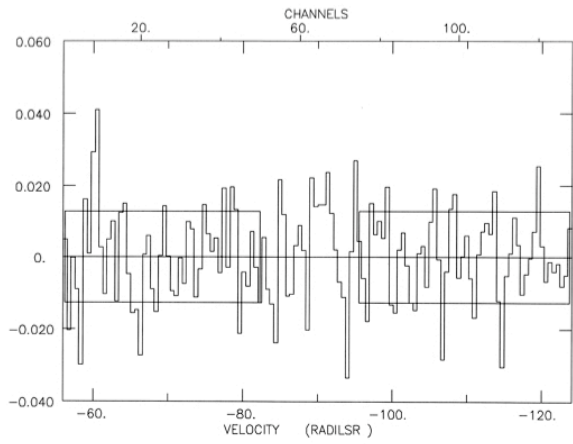
WB060 4 SCANS: 154.03- 155.04 INT= 00:40: 0 DATE: 11 NOV 2005
 1950RADC=21:14:24.1 54:30:57 (21:14:24.1 54:30:57) CAL= 426.2 TS= 318.
 FREQ=140839.52 SYN=1.98829424 VEL= -83.0 DV= -0.53 FR= 250 SB=2



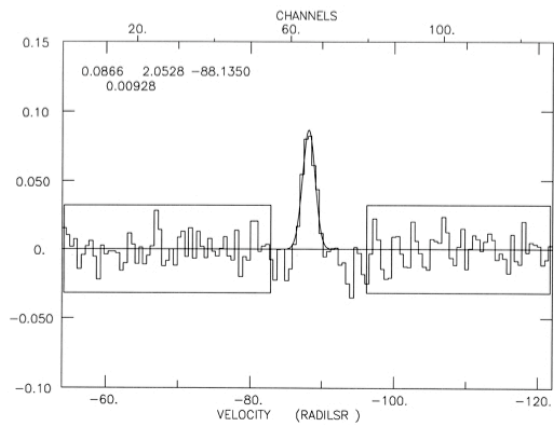
WB066 12 SCANS: 223.03- 228.04 INT= 02:00: 0 DATE: 13 NOV 2005
 1950RADC=21:17:21.2 54:03:19 (21:17:21.2 54:03:19) CAL= 418.7 TS= 223.
 FREQ=140839.52 SYN=1.98827052 VEL= -80.0 DV= -0.53 FR= 250 SB=2



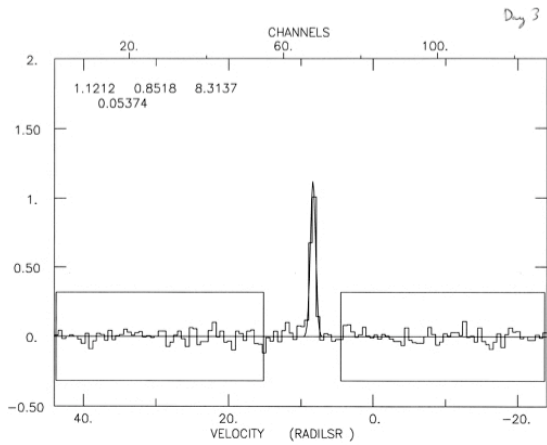
WB076 6 SCANS: 285.03- 287.04 INT= 01:00: 0 DATE: 14 NOV 2005
 1950RADC=21:22:52.5 53:32:36 (21:22:52.5 53:32:36) CAL= 423.3 TS= 240.
 FREQ=150498.34 SYN=1.95852194 VEL= -95.0 DV= -0.50 FR= 250 SB=2



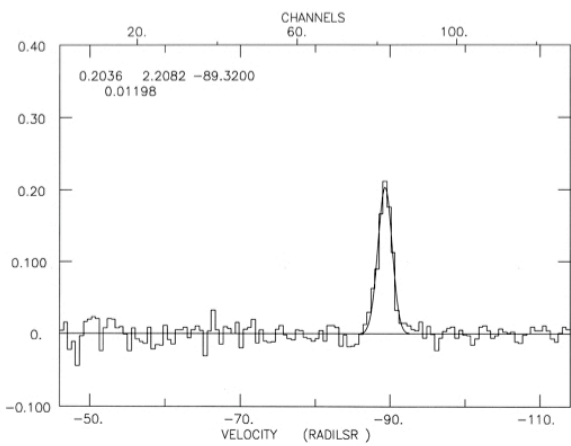
WB098 6 SCANS: 232.03- 234.04 INT= 01:00: 0 DATE: 13 NOV 2005
 1950RADC=21:35:12.0 56:25:26 (21:35:12.0 56:25:26) CAL= 418.8 TS= 221.
 FREQ=140839.52 SYN=1.98833978 VEL= -90.0 DV= -0.53 FR= 250 SB=2



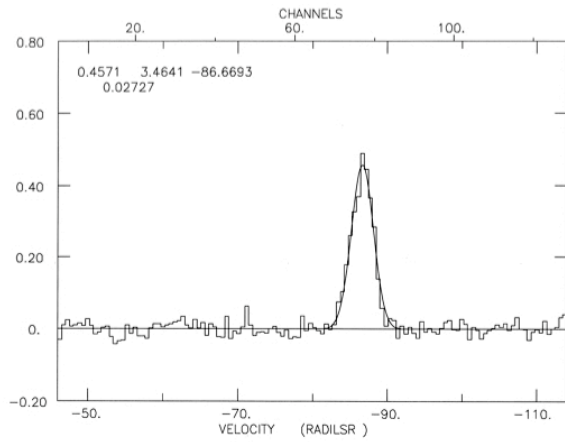
WB152 16 SCANS: 159.03- 166.04 INT= 02:40: 0 DATE: 12 NOV 2005
 1950RADC=22:03:38.8 60:34:04 (22:03:38.8 60:34:04) CAL= 421.9 TS= 308.
 FREQ=140839.52 SYN=1.98833572 VEL= -88.0 DV= -0.53 FR= 250 SB=2



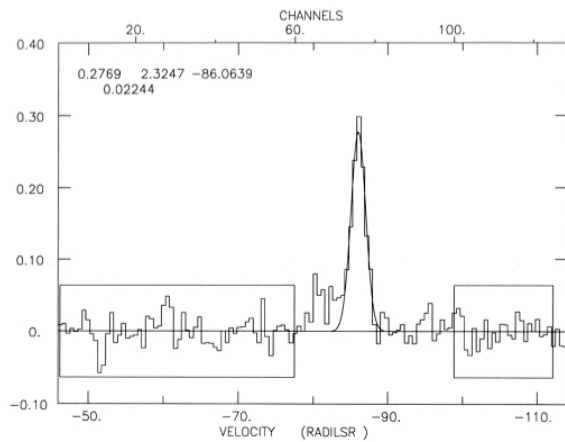
B335 2 SCANS: 107.03- 107.04 INT= 00:20: 0 DATE: 10 NOV 2005
 1950RADC=19:34:34.0 07:27:20 (19:34:34.0 07:27:20) CAL= 434.3 TS= 437.
 FREQ=140839.52 SYN=1.98759092 VEL= 10.0 DV= -0.53 FR= 250 SB=2



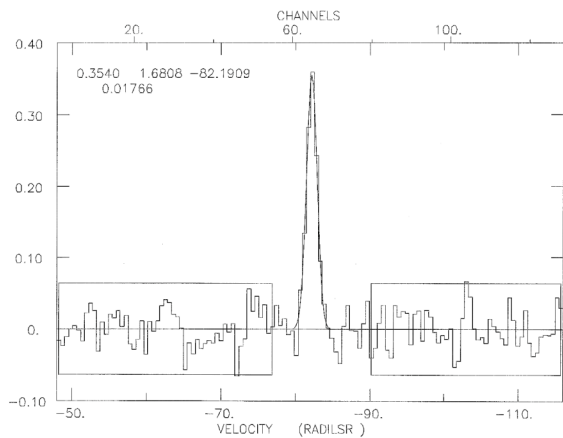
WB379 12 SCANS: 23.03- 28.04 INT= 02:00: 0 DATE: 09 NOV 2005
 1950RADC=01:03:45.2 65:04:52 (01:03:45.2 65:04:52) CAL= 431.2 TS= 327.
 FREQ=140839.52 SYN=1.98829684 VEL= -80.0 DV= -0.53 FR= 250 SB=2



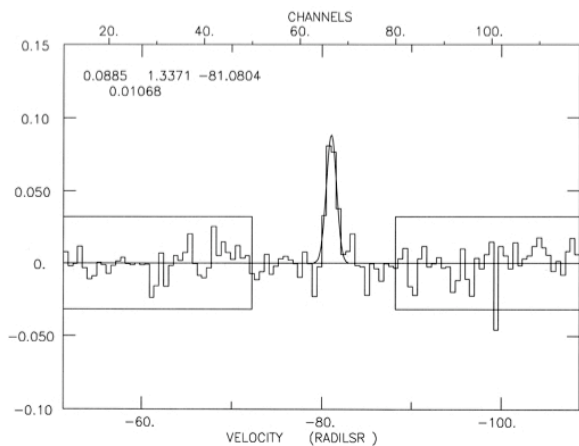
WB380 6 SCANS: 32.03- 34.04 INT= 01:00: 0 DATE: 09 NOV 2005
 1950RADC=01:04:35.7 65:05:21 (01:04:35.7 65:05:21) CAL= 429.9 TS= 323.
 FREQ=140839.52 SYN=1.98829636 VEL= -80.0 DV= -0.53 FR= 250 SB=2



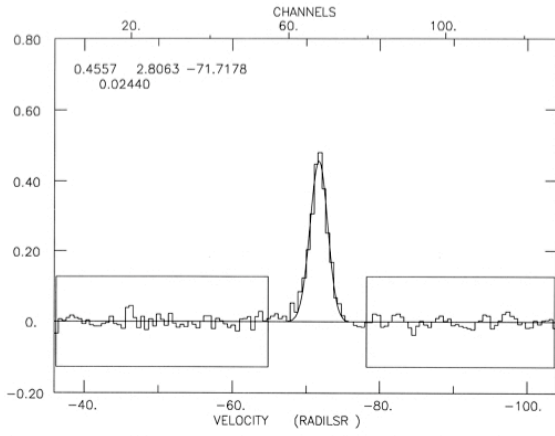
WB391 5 SCANS: 35.03- 37.04 INT= 00:50: 0 DATE: 09 NOV 2005
 1950RADC=01:16: 4.0 65:29:59 (01:16: 4.0 65:29:59) CAL= 431.1 TS= 322.
 FREQ=140839.52 SYN=1.98829856 VEL= -80.0 DV= -0.53 FR= 250 SB=2



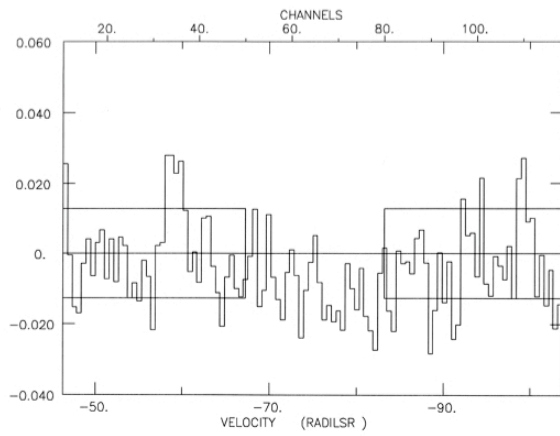
WB399 4 SCANS: 146.03- 147.04 INT= 00:40: 0 DATE: 11 NOV 2005
1950RADC=01:42: 5.1 64:01:01 (01:42: 5.1 64:01:01) CAL= 421.5 TS= 370.
FREQ=140839.52 SYN=1.98830556 VEL= -82.0 DV= -0.53 FR= 250 SB=2



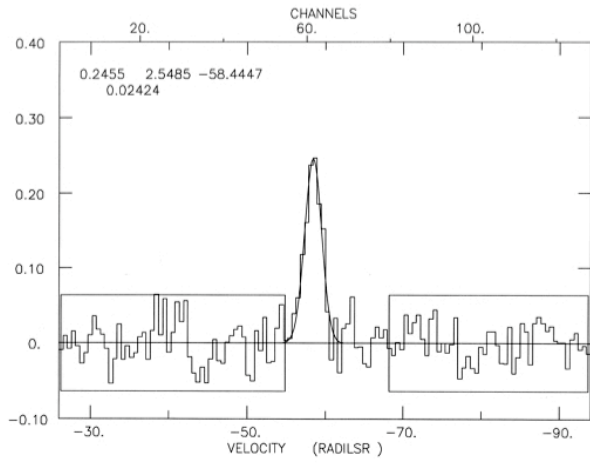
WB401 12 SCANS: 399.03- 404.04 INT= 02:00: 0 DATE: 16 NOV 2005
1950RADC=01:44:54.5 63:54:09 (01:44:54.5 63:54:09) CAL= 418.8 TS= 273.
FREQ=140839.52 SYN=1.98828284 VEL= -80.0 DV= -0.53 FR= 250 SB=2



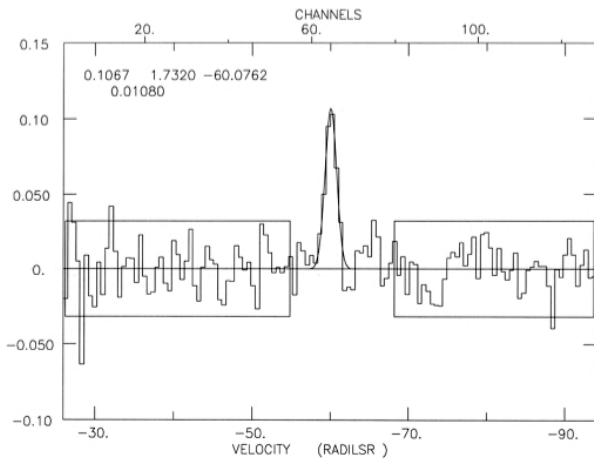
WB437 6 SCANS: 136.03- 138.04 INT= 01:00: 0 DATE: 11 NOV 2005
1950RADC=02:39:30.5 62:44:25 (02:39:30.5 62:44:25) CAL= 423.9 TS= 312.
FREQ=140839.52 SYN=1.98823230 VEL= -70.0 DV= -0.53 FR= 250 SB=2



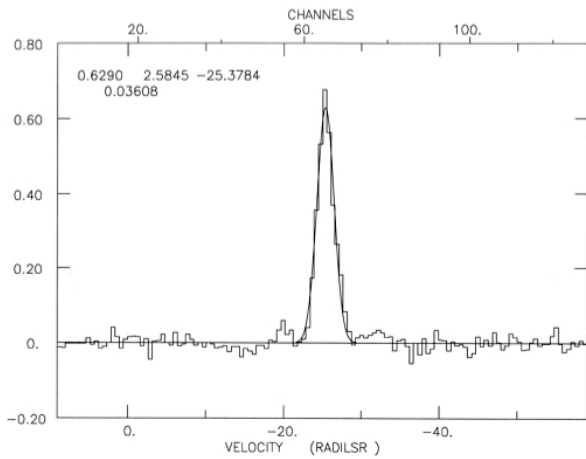
WB438 12 SCANS: 405.03- 410.04 INT= 02:00: 0 DATE: 16 NOV 2005
1950RADC=02:40:48.8 60:29:55 (02:40:48.8 60:29:55) CAL= 418.8 TS= 275.
FREQ=140839.52 SYN=1.98824818 VEL= -75.0 DV= -0.53 FR= 250 SB=2



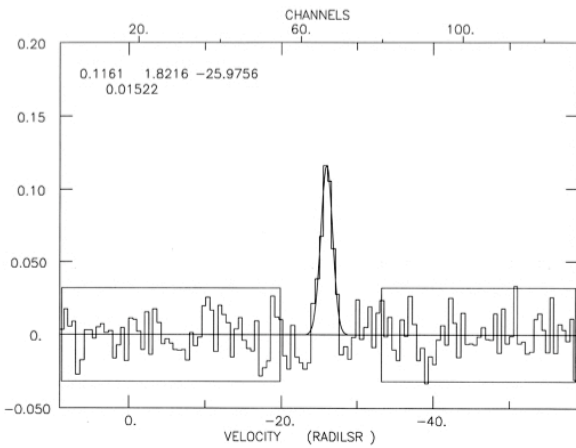
WB501 4 SCANS: 148.03- 149.04 INT= 00:40: 0 DATE: 11 NOV 2005
 1950RADC=03:48:24.4 57:39:36 (03:48:24.4 57:39:36) CAL= 419.3 TS= 329.
 FREQ=140839.52 SYN=1.98816882 VEL= -60.0 DV= -0.53 FR= 250 SB=2



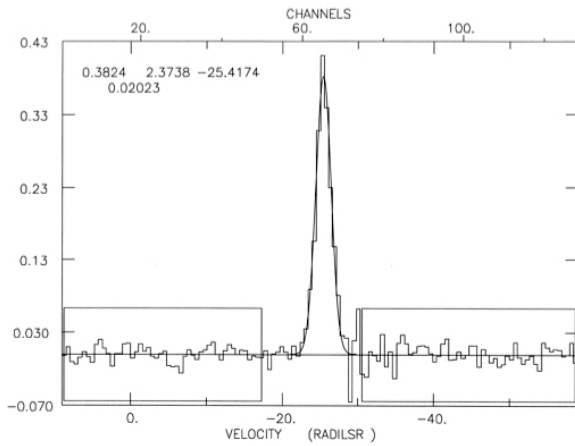
WB529 12 SCANS: 171.03- 176.04 INT= 02:00: 0 DATE: 12 NOV 2005
 1950RADC=04:02:33.3 53:13:46 (04:02:33.3 53:13:46) CAL= 419.3 TS= 363.
 FREQ=140839.52 SYN=1.98816366 VEL= -60.0 DV= -0.53 FR= 250 SB=2



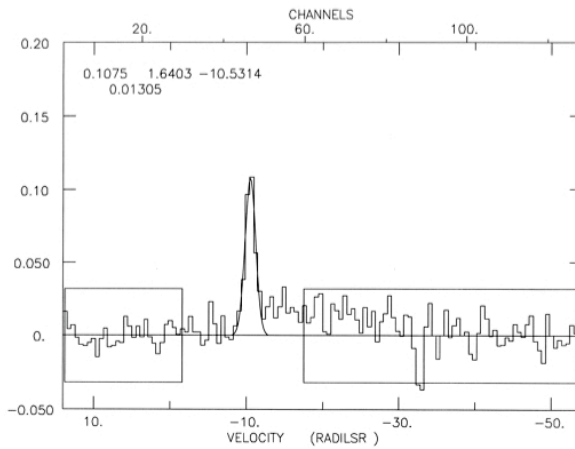
WB621 4 SCANS: 44.03- 45.04 INT= 00:40: 0 DATE: 09 NOV 2005
 1950RADC=05:13:45.8 39:19:01 (05:13:45.8 39:19:01) CAL= 429.3 TS= 280.
 FREQ=140839.52 SYN=1.98793700 VEL= -25.0 DV= -0.53 FR= 250 SB=2



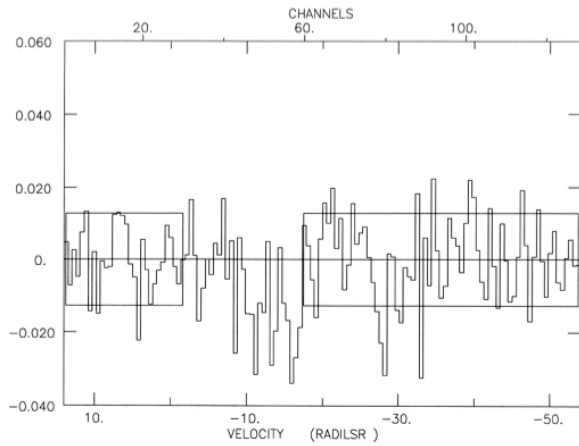
WB625 12 SCANS: 177.03- 182.04 INT= 02:00: 0 DATE: 12 NOV 2005
 1950RADC=05:16:44.1 38:58:19 (05:16:44.1 38:58:19) CAL= 420.0 TS= 376.
 FREQ=140839.52 SYN=1.98793206 VEL= -25.0 DV= -0.53 FR= 250 SB=2



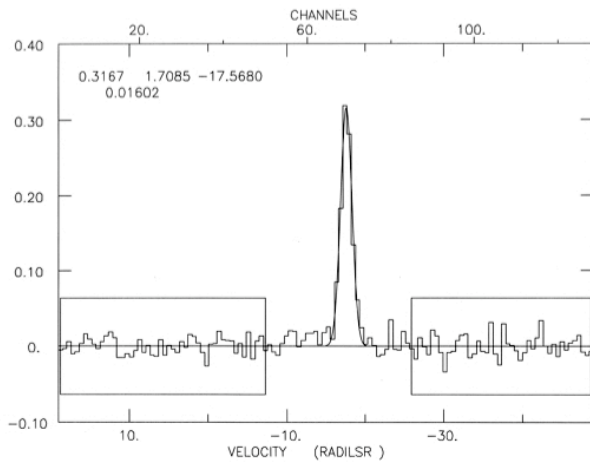
WB640 10 SCANS: 244.03- 248.04 INT= 01:40: 0 DATE: 13 NOV 2005
1950RADC=05:22: 8.1 41:39:17 (05:22: 8.1 41:39:17) CAL= 419.1 TS= 239.
FREQ=140839.52 SYN=1.98793678 VEL= -25.0 DV= -0.53 FR= 250 SB=2



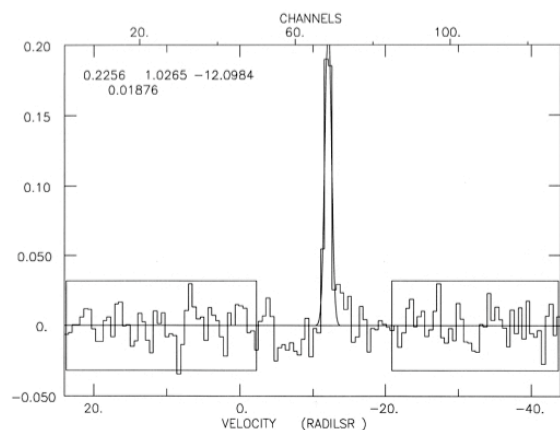
WB656 12 SCANS: 258.03- 263.04 INT= 02:00: 0 DATE: 13 NOV 2005
1950RADC=05:30:15.2 37:39:05 (05:30:15.2 37:39:05) CAL= 417.5 TS= 212.
FREQ=140839.52 SYN=1.98789892 VEL= -20.0 DV= -0.53 FR= 250 SB=2



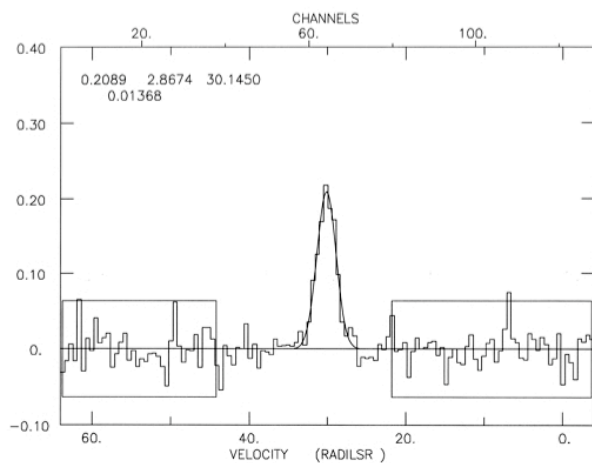
WB658 6 SCANS: 264.03- 266.04 INT= 01:00: 0 DATE: 13 NOV 2005
 195ORADC=05:30:50.1 37:52:07 (05:30:50.1 37:52:07) CAL= 416.4 TS= 211.
 FREQ=140839.52 SYN=1.98789848 VEL= -20.0 DV= -0.53 FR= 250 SB=2



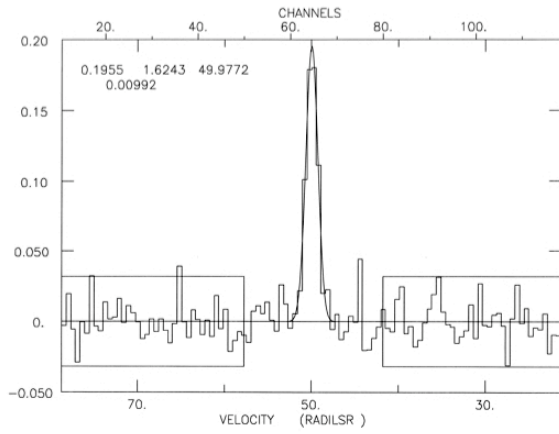
WB670 6 SCANS: 252.03- 254.04 INT= 01:00: 0 DATE: 13 NOV 2005
 195ORADC=05:34:19.6 36:05:36 (05:34:19.6 36:05:36) CAL= 417.6 TS= 217.
 FREQ=140839.52 SYN=1.98786534 VEL= -15.0 DV= -0.53 FR= 250 SB=2



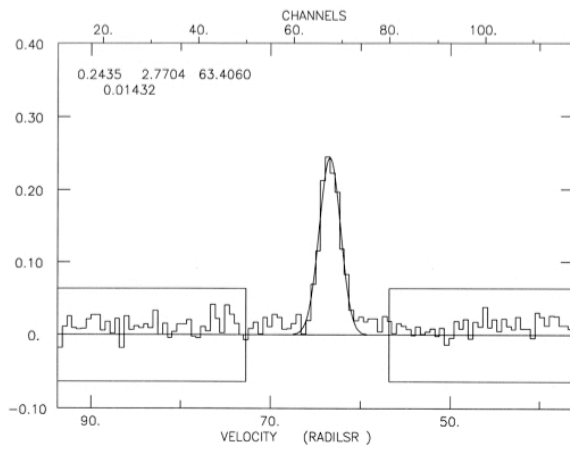
WB705 4 SCANS: 250.03- 251.04 INT= 00:40: 0 DATE: 13 NOV 2005
 1950RADC=05:44:26.5 35:20:58 (05:44:26.5 35:20:58) CAL= 418.4 TS= 223.
 FREQ=140839.52 SYN=1.98783634 VEL= -10.0 DV= -0.53 FR= 250 SB=2



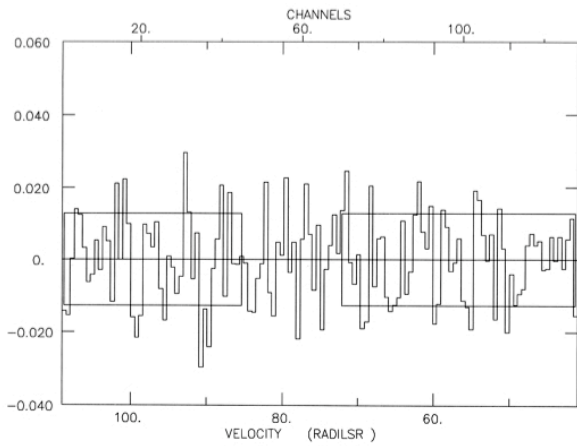
WB794 4 SCANS: 192.03- 193.04 INT= 00:40: 0 DATE: 12 NOV 2005
 1950RADC=06:15:53.6 15:18:07 (06:15:53.6 15:18:07) CAL= 414.7 TS= 305.
 FREQ=140839.52 SYN=1.98755270 VEL= 30.0 DV= -0.53 FR= 250 SB=2



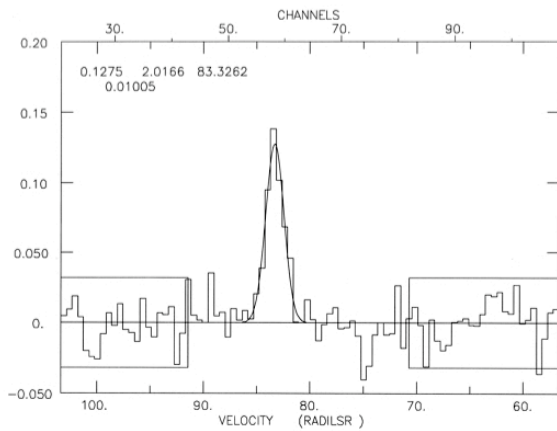
WB847 12 SCANS: 417.03- 422.04 INT= 02:00: 0 DATE: 16 NOV 2005
 1950RADC=06:34:50.9 02:34:47 (06:34:50.9 02:34:47) CAL= 424.2 TS= 336.
 FREQ=140839.52 SYN=1.98739704 VEL= 50.0 DV= -0.53 FR= 250 SB=2



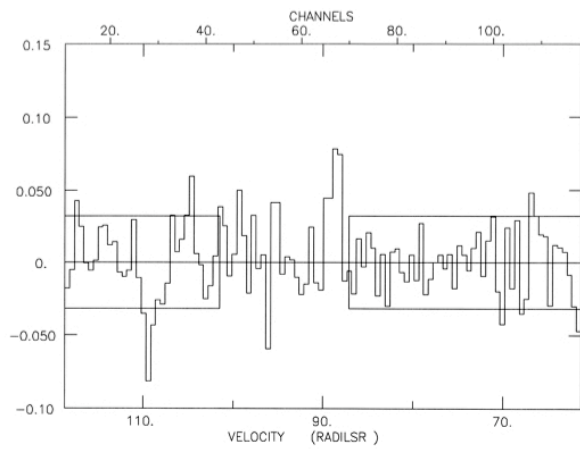
WB898 12 SCANS: 423.03- 428.04 INT= 02:00: 0 DATE: 16 NOV 2005
 1950RADC=06:48: 9.7 -05:17:28 (06:48: 9.7 -05:17:28) CAL= 422.0 TS= 306.
 FREQ=140839.52 SYN=1.98728946 VEL= 65.0 DV= -0.53 FR= 250 SB=2



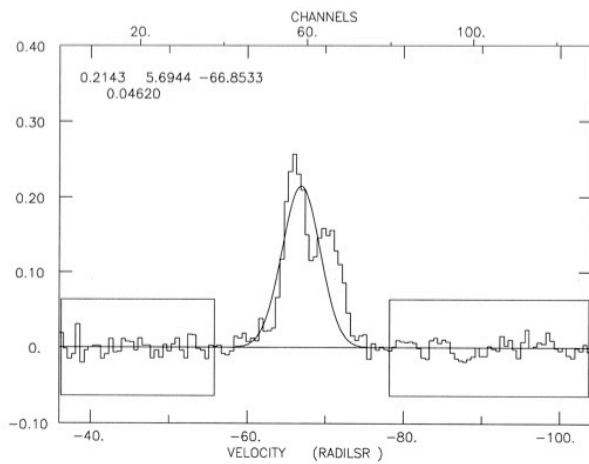
WB1000 12 SCANS: 203.03- 208.04 INT= 02:00: 0 DATE: 12 NOV 2005
 1950RADC=07:27: 9.0 -19:37:16 (07:27: 9.0 -19:37:16) CAL= 417.0 TS= 330.
 FREQ=140839.52 SYN=1.98722228 VEL= 75.0 DV= -0.53 FR= 250 SB=2



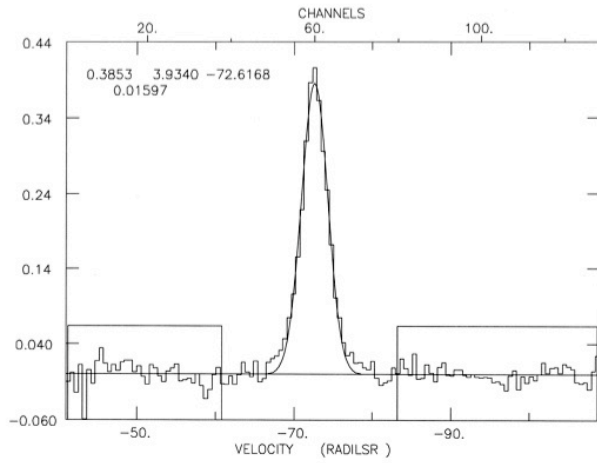
WB1012 10 SCANS: 315.03- 321.04 INT= 01:40: 0 DATE: 14 NOV 2005
 1950RADC=07:29:54.1 -24:32:37 (07:29:54.1 -24:32:37) CAL= 428.3 TS= 352.
 FREQ=140839.52 SYN=1.98717706 VEL= 80.0 DV= -0.53 FR= 250 SB=2



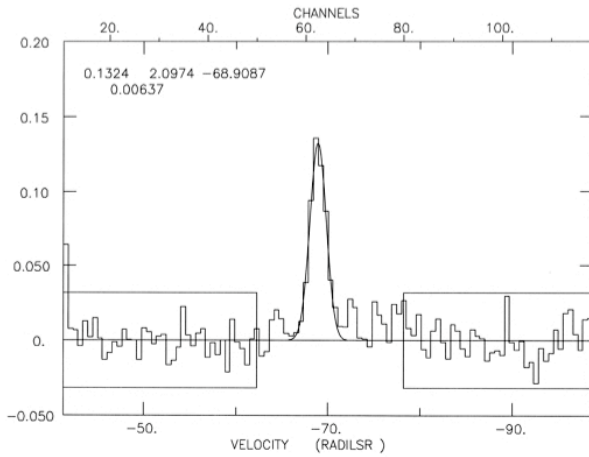
WB1023 12 SCANS: 369.03- 374.04 INT= 02:00: 0 DATE: 15 NOV 2005
 1950RADC=07:32:15.9 -23:36:05 (07:32:15.9 -23:36:05) CAL= 430.8 TS= 491.
 FREQ=140839.52 SYN=1.98711266 VEL= 90.0 DV= -0.53 FR= 250 SB=2



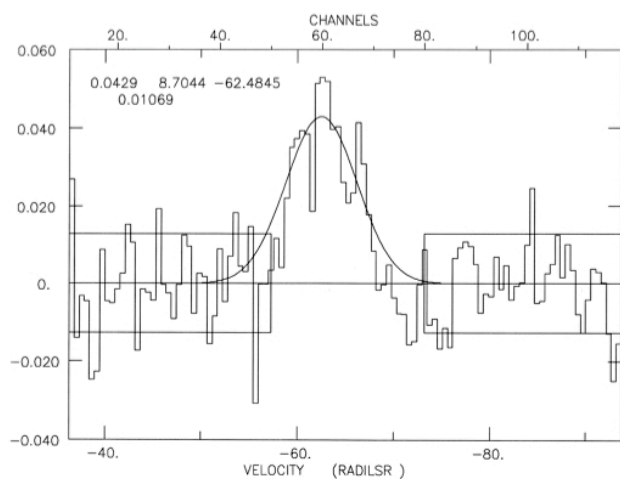
CS3 12 SCANS: 329.03- 334.04 INT= 02:00: 0 DATE: 14 NOV 2005
 1950RADC=19:38:19.5 27:11:33 (19:38:19.5 27:11:33) CAL= 434.2 TS= 262.
 FREQ=140839.52 SYN=1.98817450 VEL= -70.0 DV= -0.53 FR= 250 SB=2



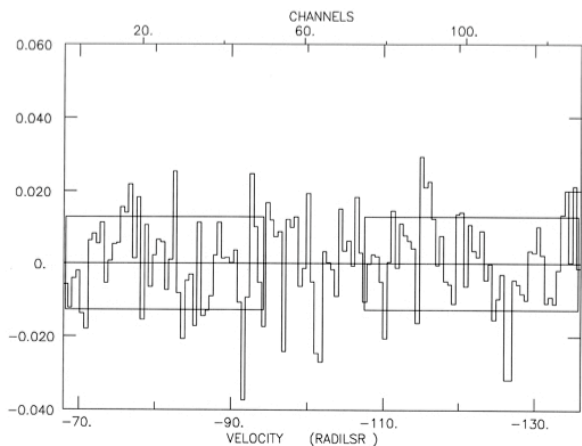
CS4 10 SCANS: 335.03- 339.04 INT= 01:40: 0 DATE: 15 NOV 2005
1950RADC=19:42:18.6 25:41:24 (19:42:18.6 25:41:24) CAL= 427.3 TS= 260.
FREQ=140839.52 SYN=1.98820148 VEL= -75.0 DV= -0.53 FR= 250 SB=2



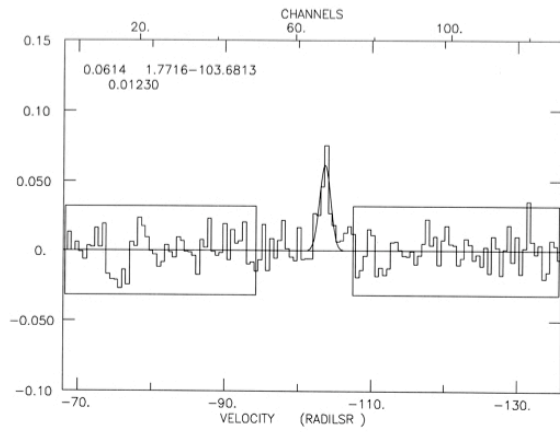
CSS 12 SCANS: 383.03- 389.04 INT= 02:00: 0 DATE: 15 NOV 2005
1950RADC=19:48:54.4 30:30:09 (19:48:54.4 30:30:09) CAL= 429.6 TS= 265.
FREQ=140839.52 SYN=1.98817688 VEL= -70.0 DV= -0.53 FR= 250 SB=2



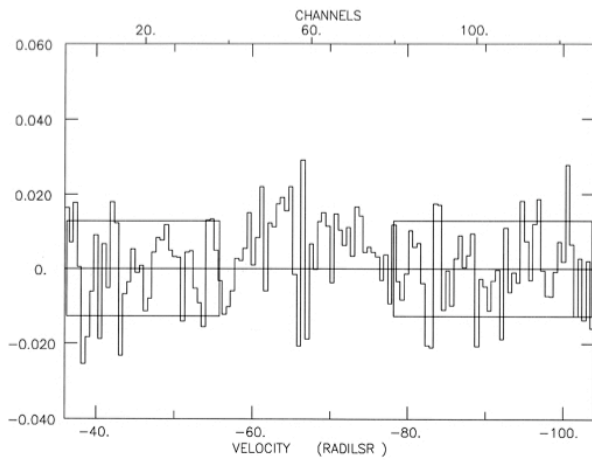
CS6 11 SCANS: 390.03- 390.04 INT= 01:50: 0 DATE: 16 NOV 2005
 1950RADC=19:57:10.1 31:13:33 (19:57:10.1 31:13:33) CAL= 420.4 TS= 251.
 FREQ=140839.52 SYN=1.98813956 VEL= -65.0 DV= -0.53 FR= 250 SB=2



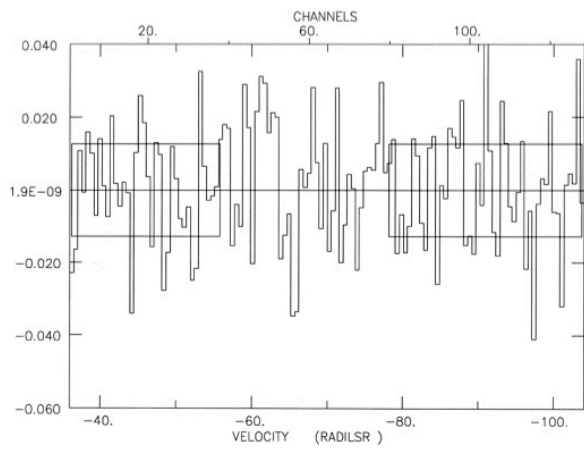
DGT01 12 SCANS: 80.03- 85.04 INT= 02:00: 0 DATE: 10 NOV 2005
 GALACTIC= 30.3212 62.8862 (30.3212 62.8862) CAL= 429.0 TS= 312.
 FREQ=140839.52 SYN=1.98844332 VEL= -102.0 DV= -0.53 FR= 250 SB=2



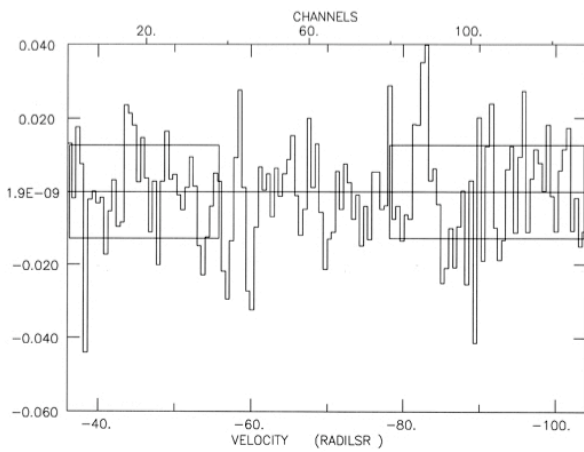
DGT02a 10 SCANS: 97.03- 101.04 INT= 01:40: 0 DATE: 10 NOV 2005
 1950RADC=02:44:52.6 58:16:00 (02:44:52.6 58:16:00) CAL= 427.4 TS= 299.
 FREQ=140839.52 SYN=1.98843770 VEL= -102.0 DV= -0.53 FR= 250 SB=2



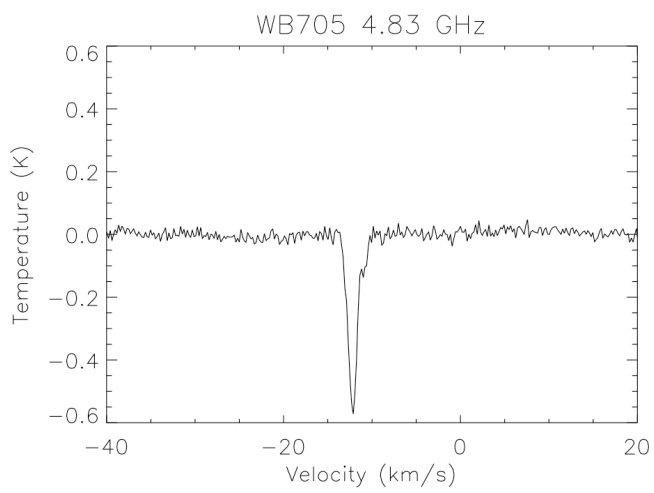
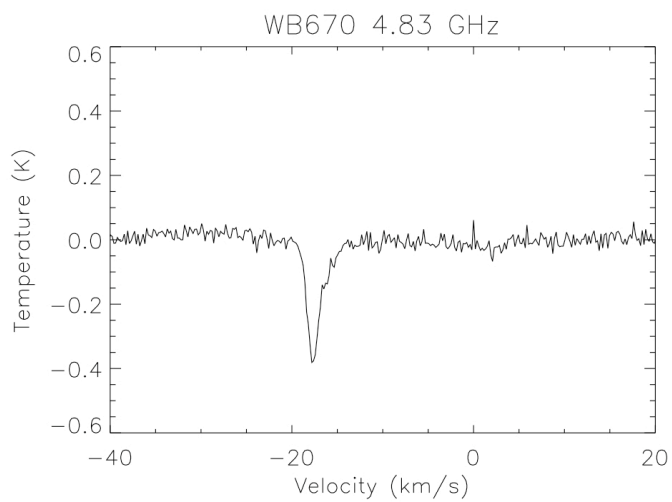
DGT04a 10 SCANS: 343.03- 347.04 INT= 01:40: 0 DATE: 15 NOV 2005
 GALACTIC= 53.4994 55.2929 (53.4994 55.2929) CAL= 424.2 TS= 289.
 FREQ=140839.52 SYN=1.98821748 VEL= -70.0 DV= -0.53 FR= 250 SB=2

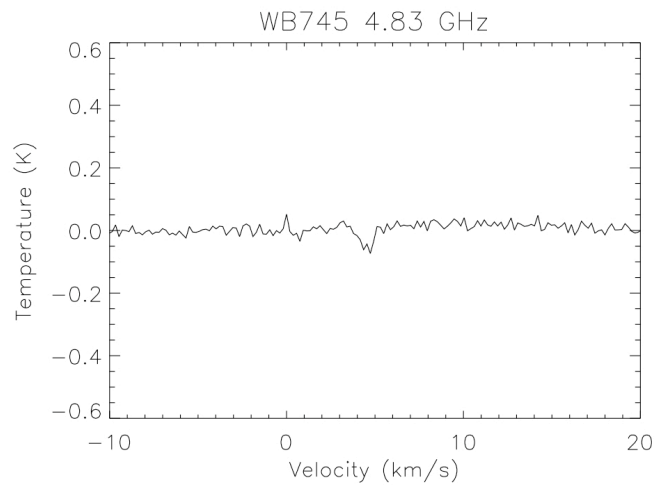
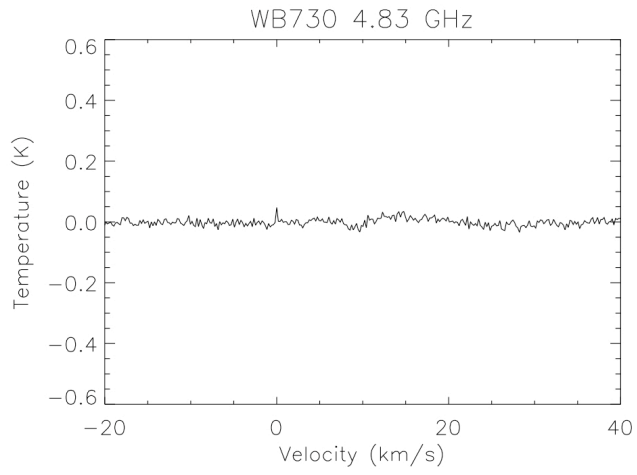


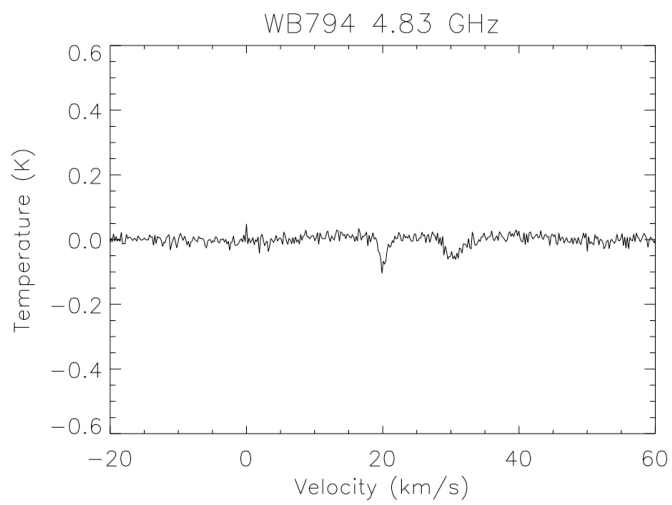
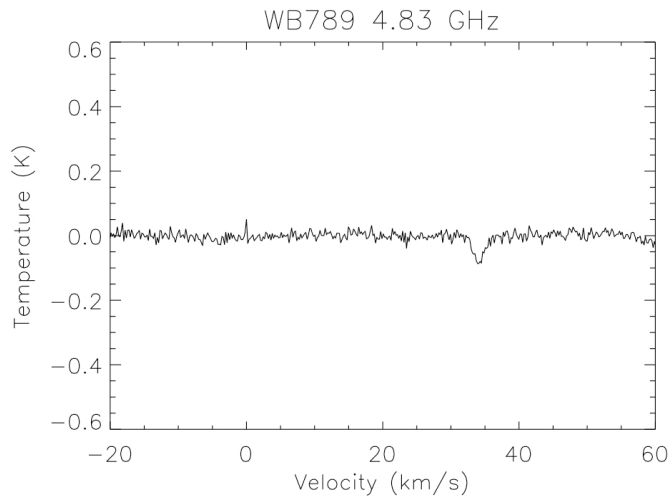
DGT04b 6 SCANS: 348.03- 350.04 INT= 01:00: 0 DATE: 15 NOV 2005
 GALACTIC= 53.9952 55.0870 (53.9952 55.0870) CAL= 423.7 TS= 279.
 FREQ=140839.52 SYN=1.98821722 VEL= -70.0 DV= -0.53 FR= 250 SB=2

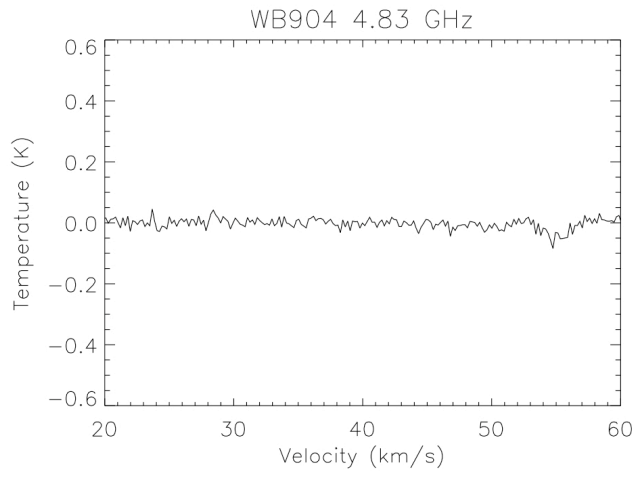


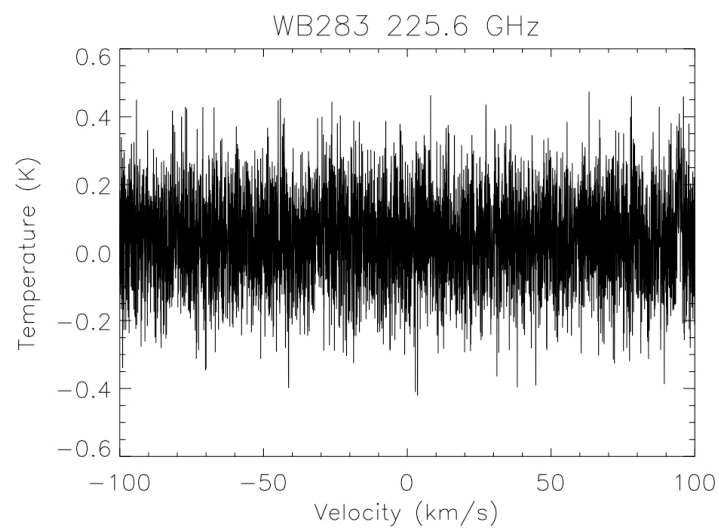
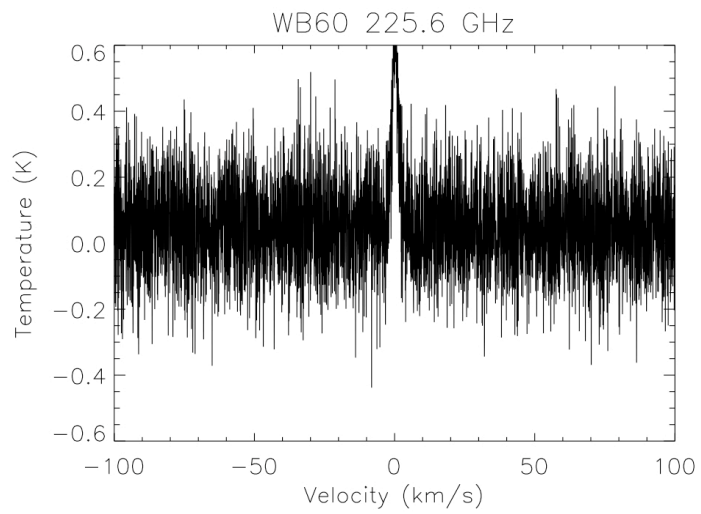
DGT05 8 SCANS: 351.03- 354.04 INT= 01:20: 0 DATE: 15 NOV 2005
 GALACTIC= 53.6998 55.0247 (53.6998 55.0247) CAL= 423.3 TS= 277.
 FREQ=140839.52 SYN=1.98821644 VEL= -70.0 DV= -0.53 FR= 250 SB=2

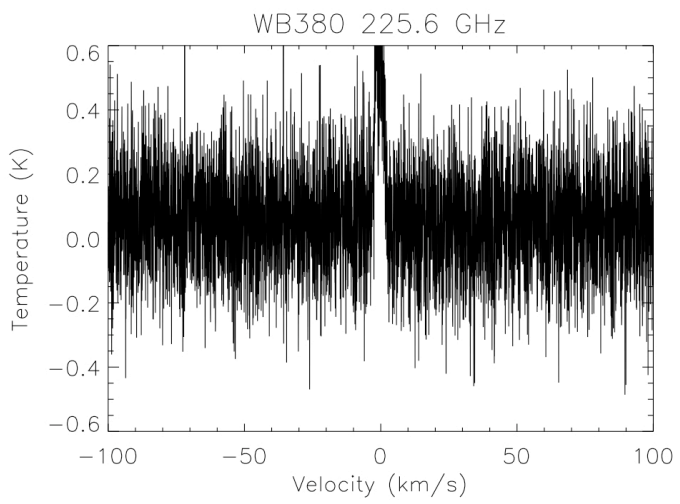
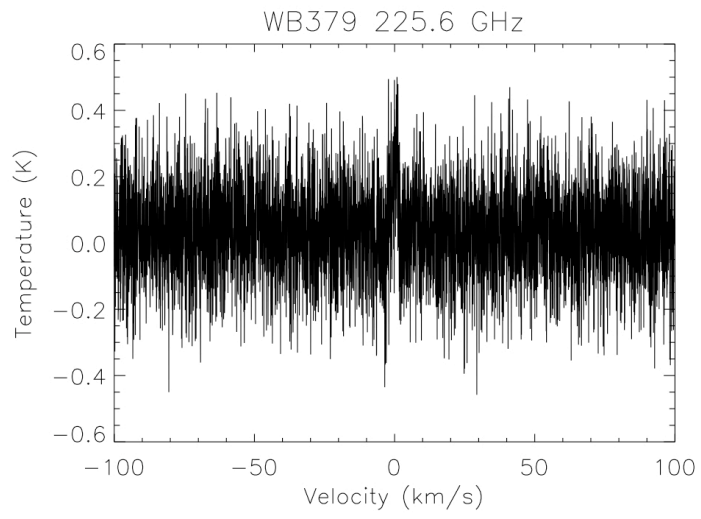


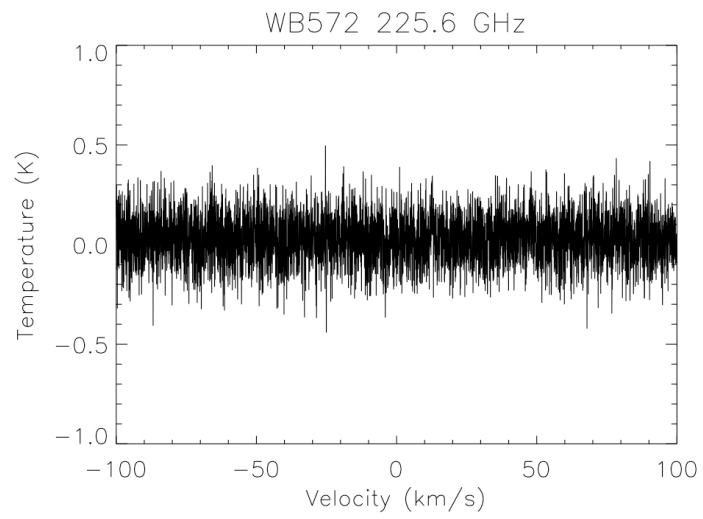
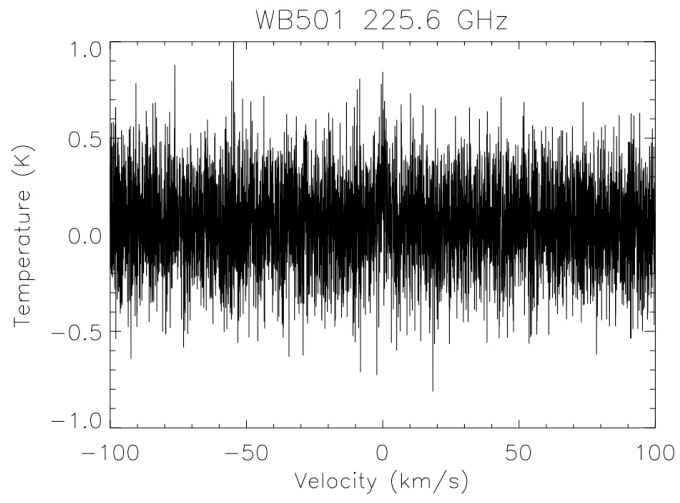


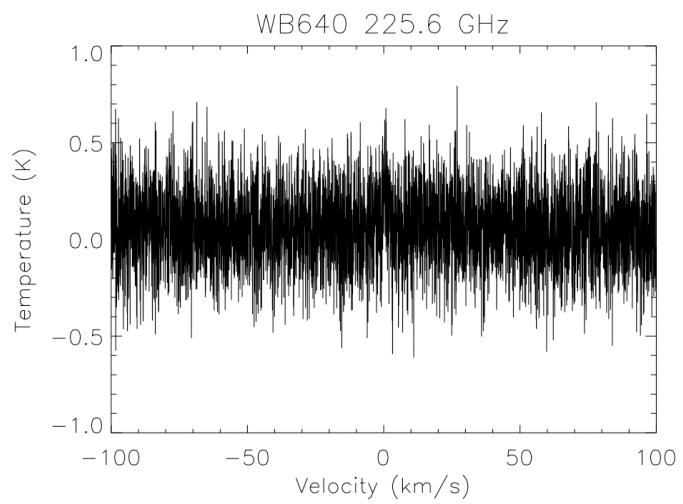
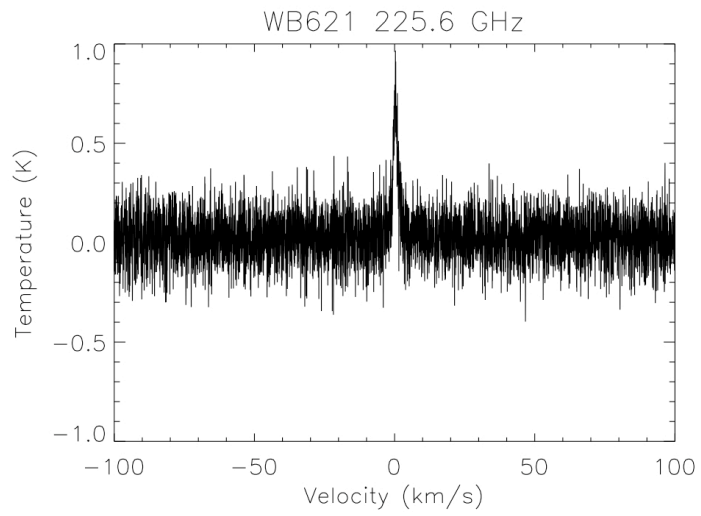


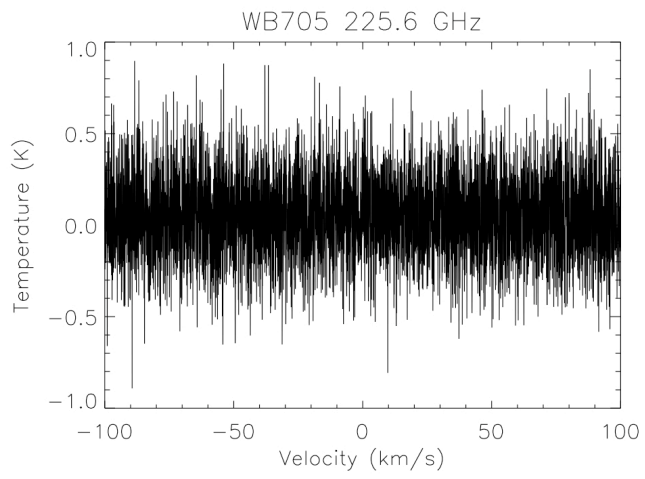
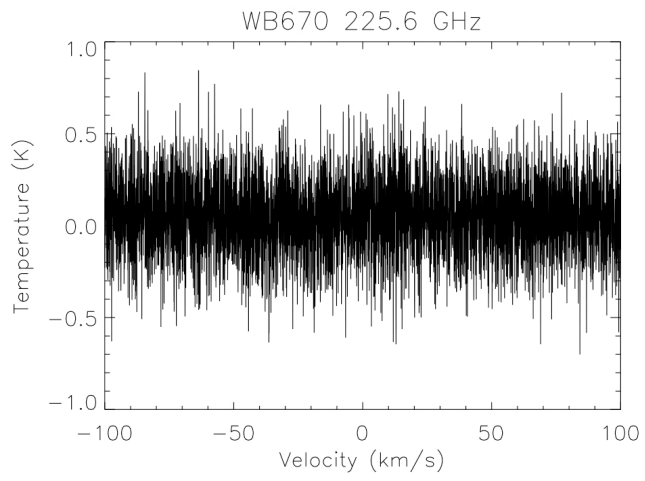


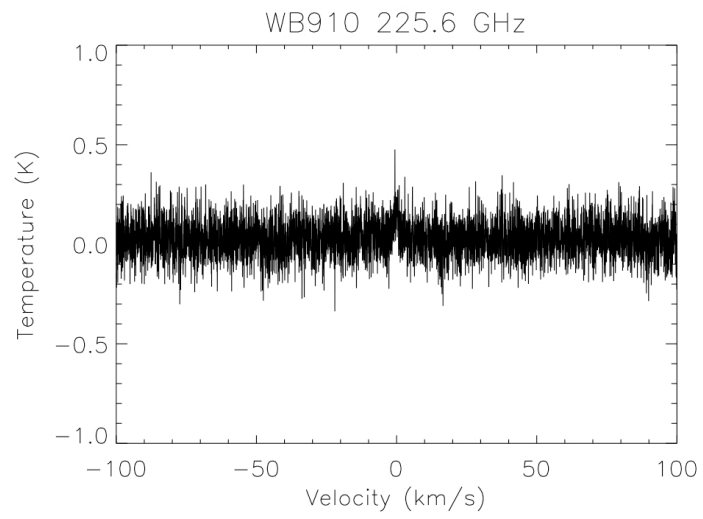
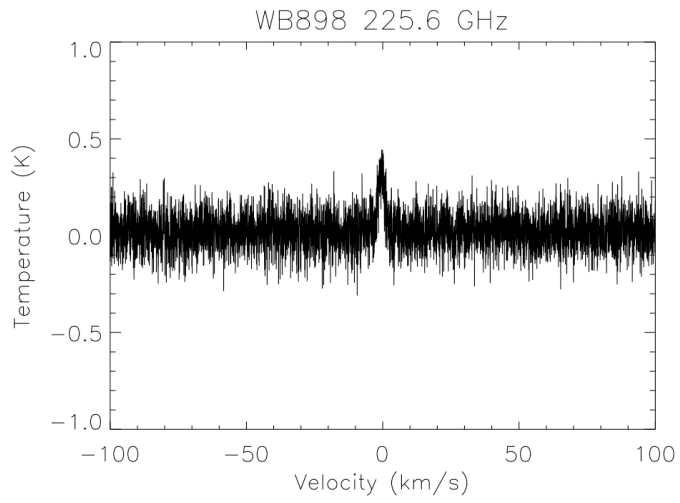












APPENDIX B

SPECTRA OF HCN OBSERVATIONS

This appendix contains the spectra from the HCN observations. For each source, T_R^* (K) is shown on the y-axis and velocity (km/s) on the x-axis.

